

Spring 5-15-2015

Genetic and Cellular Studies of The Podocyte in Focal Segmental Glomerulosclerosis

Haiyang Yu

Washington University in St. Louis

Follow this and additional works at: https://openscholarship.wustl.edu/art_sci_etds



Part of the [Biology Commons](#)

Recommended Citation

Yu, Haiyang, "Genetic and Cellular Studies of The Podocyte in Focal Segmental Glomerulosclerosis" (2015). *Arts & Sciences Electronic Theses and Dissertations*. 431.

https://openscholarship.wustl.edu/art_sci_etds/431

This Dissertation is brought to you for free and open access by the Arts & Sciences at Washington University Open Scholarship. It has been accepted for inclusion in Arts & Sciences Electronic Theses and Dissertations by an authorized administrator of Washington University Open Scholarship. For more information, please contact digital@wumail.wustl.edu.

WASHINGTON UNIVERSITY IN ST. LOUIS
Division of Biology and Biomedical Sciences
Molecular and Cell Biology

Dissertation Examination Committee:

Andrey Shaw, Chair
Kendall Blumer
Phyllis Hanson
Gregory Longmore
Jeffrey Miner
David Ornitz

Genetic and Cellular Studies of The Podocyte in Focal Segmental
Glomerulosclerosis

by
Haiyang Yu

A dissertation presented to the
Graduate School of Arts & Sciences
of Washington University in
partial fulfillment of the
requirements for the degree
of Doctor of Philosophy

May 2015
St. Louis, Missouri

© 2015, Haiyang Yu

Table of Contents

List of Figures.....	iii
List of Tables.....	v
Acknowledgements.....	vi
Abstract.....	ix
Chapter 1. Introduction.....	1
1.1 Podocytes form the outer layer of the kidney filtration barrier.....	1
1.2 Focal Segmental Glomerulosclerosis.....	2
1.3 The actin cytoskeleton supports the morphology and function of podocytes.....	4
1.4 Rho Family GTPases are the main regulators of Actin cytoskeleton.....	6
1.5 Regulators of Rho GTPases.....	7
1.6 Large-scale genetic studies discover FSGS susceptibility genes.....	9
1.7 Current mouse genetic models of podocyte diseases.....	10
1.8 Intravital imaging by multi-photon microscopy.....	11
1.9 Conclusions.....	12
1.10 Figures.....	14
Chapter 2. Arhgap24 Inactivates Rac1 in Mouse Podocytes, and a Mutant Form is Associated with Familial Focal Segmental Glomerulosclerosis.....	19
2.1 Abstract.....	19
2.2 Introduction.....	19
2.3 Methods.....	21
2.4 Results.....	27
2.5 Discussions.....	35
2.6 Tables and Figures.....	41
Chapter 3. Rac1 Activation in Podocytes Induces Rapid Foot Process Effacement and Proteinuria.....	51
3.1 Abstract.....	51
3.2 Introduction.....	51
3.3 Methods.....	54
3.4 Results.....	58
3.5 Discussions.....	65
3.6 Figures.....	69
Chapter 4. A Role for Genetic Susceptibility in Sporadic Focal Segmental Glomerulosclerosis.....	79
4.1 Abstract.....	79
4.2 Introduction.....	80
4.3 Methods.....	82
4.4 Results.....	87
4.5 Discussions.....	95

4.6 Tables and Figures.....	97
Chapter 5. Conclusions and Future Directions.	110
5.1 Conclusions	110
5.2 Future Directions	114
References.....	116
Curriculum Vitae.....	127

List of Figures

Figure 1.1 The structure of the glomerulus.....	14
Figure 1.2 The podocyte and the slit diaphragm	15
Figure 1.3 Foot process effacement.....	15
Figure 1.4 Histology of FSGS.....	16
Figure 1.5 The actin cytoskeleton in the podocyte foot processes.....	16
Figure 1.6 Rho Family GTPases: regulation and function.....	17
Figure 1.7 The mechanism and advantage of multi-photon microscopy (MPM).....	18
Figure 2.1 Differentiated podocytes show reduced membrane ruffling	43
Figure 2.2 <i>Arhgap24</i> transcript and <i>Arhgap24</i> protein are specifically expressed in podocytes	44
Figure 2.3 <i>Arhgap24</i> is expressed in kidney podocytes <i>in vivo</i>	45
Figure 2.4 <i>Arhgap24</i> knockdown in differentiated podocytes increases membrane ruffling	46
Figure 2.5 <i>Arhgap24</i> knockdown in differentiated podocytes increases active Rac1 and Cdc42 levels and accelerates epithelial monolayer wound closure.....	47
Figure 2.6 Pedigree information for T97I and P417A variations.....	48
Figure 2.7 Individuals with end-stage kidney disease are denoted by black symbols	49
Figure 2.8 <i>Arhgap24</i> Q158R has defective Rac1-GAP activity and dimerizes with the wild-type protein.....	50
Figure 3.1 Constitutively active Rho family GTPases exert opposing effects on the actin cytoskeleton of podocytes	69
Figure 3.2 Generation of inducible EGFP_CA-Rac1 transgenic mice.....	70
Figure 3.3 Podocyte specific expression of CA-Rac1 causes proteinuria.....	71
Figure 3.4 EGFP_CA-Rac1 expression driven by <i>Nphs1</i> -rtTA induces more robust transgene expression and transient proteinuria	72
Figure 3.5 No obvious pathological changes were detected in histological analysis, and the transgene positive podocytes were lost after prolonged DOX treatment	73
Figure 3.6 EGFP_CA-Rac1 expression in podocytes is associated with foot process effacement <i>in vivo</i>	74
Figure 3.7 EGFP_CA-Rac1 expression correlates with reduced expression of podocin and nephrin.....	75
Figure 3.8 Time-lapse intravital MPM imaging of DOX induced NEFxRac1 mice.....	76
Figure 3.9 Z-stack images of EGFP_CA-Rac1+ podocyte that attach to the epithelium of the renal tubules	77
Figure 3.10 EGFP_CA-Rac1+ podocytes extended protrusions that penetrates the tubular epithelium and touched the basal side of the interstitial endothelial cells	78
Figure 4.1 Comparability of variant calls between cases and controls.....	101
Figure 4.2 Supplementary figure for Figure 4.1	102
Figure 4.3 Generating an ES cell line with an FSGS susceptibility genetic background.....	103

Figure 4.4 Generating a system to validate candidate FSGS genes.....	104
Figure 4.5 Supplemental figure for Figure 4.4	106
Figure 4.6 Validation of five FSGS candidate disease genes	107
Figure 4.7 Supplemental figure for Figure 4.6	109

List of Tables

Table 2.1 Incidence of ARHGAP24 nonsynonymous sequence variations in patients with biopsy-proven FSGS (n=310) and controls (n=180).....	41
Table 2.2 Non-synonymous SNPs in ARHGAP24	42
Table 2.3 Q158 is a conserved residue.....	42
Table 4.1 Distribution of single and rare variants in FSGS subjects and controls.....	97
Table 4.2 Potential FSGS susceptibility genes identified by common variant analyses	98
Table 4.3 Potential FSGS susceptibility genes identified by rare variant analyses	99
Table 4.4 The list of 20 known FSGS genes	99
Table 4.5 The list of rare deleterious variants identified in 20 known FSGS genes in the FSGS subjects that we sequenced	100

Acknowledgements

First, I would like to express my sincere gratitude to Dr. Andrey Shaw for his mentorship. During my thesis research, he gives me generous support, guidance, advice and inspiration. He always encourages me to try new ideas, to attend important conferences and most importantly, to think as an independent investigator. This work would not have been possible without his mentorship. His passion and curiosity about science also motivates me to devote my career in basic science.

I would also like to thank Drs. Jeffrey Miner, Raphael Kopan, Kendal Blumer, Gregory Longmore, Phyllis Hanson, and David Ornitz for serving as my thesis committee members. They give me many good advices not only on my research but also on my career development. I would like to appreciate the help and guidance from Drs. John Cooper, Zhongsheng You, Jianghui Hou, Eynav Klechevsky, and Adish Dani.

I appreciate the opportunities to interact with and to learn from my colleagues. I would like to thank Drs. Jiancheng Hu, Shreeram Akilesh, Alfred Kim, Hani Suleiman, Sebastian Braehler, and Bernd Zinselmeyer for their generous help in my thesis research. They helped me with the research techniques and gave me valuable suggestions on designing experiments. I also appreciate the discussions with former and current Shaw lab members. Their view of science has been inspiring me since I joined Shaw lab.

I would like to thank the technical assistance from the core facilities in Washington University. I want to thank Michael White and Terri Sherlinsky from Transgenic Knockout Micro-injection Core for over 40 microinjection experiments they performed for this work. I want

also thank Jacqueline Mudd and Nicole Havey from the Murine Embryonic Stem Cell Core for their assistance on the embryonic stem cell targeting experiments, Robyn Roth from Heuser lab, Jaclynn Lett from Research Center for Auditory and Vestibular Studies, and Jeanette Cunningham from Miner lab for their assistance on the electron microscopy sample preparation and imaging.

I would also like to acknowledge many members of the Molecular Cell Biology program, with particular acknowledgement to the program directors, Drs. Phyllis Hanson, Maurine Linder, Heather True and Jason Weber for their guidance and advice, and acknowledge Stacy Kiel and Sharon Smith for their assistance in processing documentary works.

Finally, I would like to thank my classmates in DBBS program and postdoctoral fellows that I met in Cell Biology Department, Pathology and Immunology Department, and Renal Division in Washington University School of Medicine for their support, valuable discussions, and friendship.

This work was supported by funding from NIDDK and HHMI.

Haiyang Yu

Washington University in St. Louis

May 2015

Dedicated to my parents and my wife.

ABSTRACT OF THE DISSERTATION

Genetic and Cellular Studies of the Podocyte in Focal Segmental Glomerulosclerosis

by

Haiyang Yu

Doctor of Philosophy in Biology and Biomedical Sciences

Molecular and Cellular Biology

Washington University in St. Louis, 2015

Professor Andrey Shaw, Chair

The podocyte forms the outer layer of the filtration barrier in the glomerulus to prevent albumin leakage. Podocyte damage leads to focal segmental glomerulosclerosis (FSGS), a leading cause of chronic kidney disease. The cause of the majority of FSGS cases is unknown and referred to as sporadic FSGS. Genetic studies have identified genes as monogenic causes of FSGS in patients with a strong family history, but these cases account for only a small proportion of the FSGS population. Whether genetic susceptibility contributes to sporadic FSGS and which cellular process in the podocyte initiates the pathogenesis of FSGS are important questions that remain to be elucidated. To answer these questions, my research followed two different lines of inquiry. I performed a genetic analysis of both familial and sporadic FSGS patients, and I investigated the role of the actin cytoskeleton in podocytes. Based on expression analysis, we identified a new FSGS susceptibility gene, *ARHGAP24*, and showed that it was mutated in a family with FSGS. Since *ARHGAP24* functions to maintain high Rho and low Rac levels, my work suggested that this balance might be important in FSGS. Using an inducible transgenic

mouse model and multi-photon intravital microscopy, we validated that high activity of Rac1, one of the Rho family GTPases, is responsible for podocyte foot process effacement, increased membrane dynamics, and podocyte shedding into the urine, three important processes that lead to proteinuria and FSGS. By sequencing a large cohort of sporadic FSGS patients, I identified 16 potential FSGS susceptibility genes that were novel. Using a novel podocyte-specific inducible RNAi mouse model that I developed, four of these genes were validated. Some of these genes function as regulators of the actin cytoskeleton. Our genetic study further reinforces the role of actin cytoskeletal regulation in the pathogenesis of FSGS.

Chapter 1. Introduction

1.1 Podocytes form the outer layer of the kidney filtration barrier

The kidney is the organ where the urine forms. In adults, each kidney has 0.33~1.4 million glomeruli [1]. The primary function of the glomerulus is to filter small solutes in the blood and to generate the primary urine. During the filtration process, the blood flows into a tuft of capillaries from the afferent arteriole. Molecules that are smaller than 40 kilodaltons (kD), including glucose, urea, inorganic ions and water, pass through the filtration barrier, and enter the Bowman's space (Figure 1.1A). The filtration barrier is a three-layer structure: the inner layer is the fenestrated endothelium; the middle layer is glomerular basement membrane (GBM), which is formed by negative-charged and glycosylated extracellular matrix proteins; the outer layer is formed by a kind of visceral epithelial cells, the podocyte (Figure 1.1B) [2].

Podocytes are unique-shaped epithelial cells that wrap around the glomerular capillaries. They extend major (primary and secondary) processes from the cell body. The tertiary processes (foot processes) interdigitate with those from neighboring podocytes to form a mesh-like network (Figure 1.1B and 1.2A). The foot processes are connected by an electron-dense, ~40nm-wide structure, the slit diaphragm, which composed of many adhesion proteins such as nephrin, NEPH1, P-cadherin, and FAT (Figure 1.2B). As terminal-differentiated cells, podocytes rarely proliferate post developmental period.

Pathological changes usually cause foot processes and the slit diaphragm to disappear.

The interface between two neighboring podocytes is flattened (Figure 1.3). This morphological abnormality is usually referred to as “foot process effacement”. The loss of the organized foot process–slit diaphragm meshwork is accompanied by the loss of the barrier function, and thus large size proteins in plasma could leak into the Bowman’s space, which further results in proteinuria. Albumin (MW ~70kD) leakage is measured as an indicator for the barrier function.

1.2 Focal Segmental Glomerulosclerosis

Focal Segmental Glomerulosclerosis (FSGS) is a glomerular disease that causes end stage renal disease. As one of the leading causes, FSGS accounts for about 4% of the patients who developed ESRD, and 40% of adult patients with nephrotic syndrome [3]. About ninety years ago, Theodor Fahr, a German pathologist, published the first drawing of FSGS glomerulus with great details [4]. Later, in 1957, A. Rich described that the cardinal characteristic of FSGS is progressive scarring in some glomeruli [5]. In the early stage of this disease, sclerotic tissue (scar) is found in a portion of the glomerulus (segmental), which only occurs in a subset of glomeruli (focal) (Figure 1.4). The scarred glomerulus often exhibits other pathological features such as mesangial hypercellularity and accumulation of foam cells in the capillaries [6]. Global sclerosis can be diagnosed as FSGS progresses [7]. Recent studies suggest that the incidence of FSGS has been increasing since the first clinical-pathological study in 1970s [3]. The major cell type that is affected in this disease is the podocyte. At electron microscopic level, the cardinal feature of FSGS is the effacement of podocyte foot processes. FSGS can be classified into familial FSGS and sporadic FSGS base on the patient family history of this disease. Sporadic FSGS is

more common in the patient population.

Although the details of the pathogenesis of FSGS are not fully uncovered, genetic studies of familial FSGS and animal models show that both genetic and environmental factors are important in this disease. Genetic approaches have identified 8 genes, which are all specifically expressed in the podocytes, as FSGS susceptibility genes: *ACTN4* [8], *ANLN* [9], *CD2AP* [10–12], *INF2* [13], *MYH9* [14, 15], *NPHS2* [16], and *TRPC6* [17, 18]. In African American population, *APOL1*-G1 and -G2 alleles cause susceptibility to HIV-associated FSGS and hypertension-associated kidney disease [19, 20]. The combined heterozygosity of *Cd2ap* and *Synpo* induces FSGS in mice with incomplete penetrance: in 25% of the mice after 6 months of age [21]. This result suggests that genetic background could contribute to the susceptibility to FSGS. A nephrotoxic drug-induced FSGS model also supports this hypothesis. Adriamycin induces severe glomerular injury and FSGS in BALB/cJ, 129X1/SvJ and 129SvlmJ mouse strains, but C57BL/6J strain is relatively resistant to this drug [22]. Recently Papeta *et al* discovered the genetic cause of this phenomenon, C6418T SNP in *Prkdc* gene, by meiotic mapping and genome sequencing [23]. This variant protects podocyte from mitochondria DNA depletion during Adriamycin treatment. Thus, there could be other triggers, like drug treatment or virus infection, which initiate the pathogenesis of FSGS.

Aging is also an important factor that contributes to the susceptibility of FSGS. Since podocytes are terminal differentiated and they do not undergo mitosis to generate new podocytes, the capacity of healthy podocytes to cover extra space is limited [24]. Each day, hundreds of podocytes are shed into the urine, and capillary surface left will be covered by the

remaining healthy podocytes through a process called podocyte hypertrophy [25]. Diseases and environmental factors that dramatically reduce podocyte number will be an important aspect of FSGS pathogenesis, because when the capillary surface exceeds the capacity of the remaining podocytes, the barrier system is permanently damaged and the damaged glomerulus will undergo sclerosis. Studies that use diphtheria toxin induced podocyte depletion in transgenic rats show that >40% of podocyte depletion induces segmental to global glomerulosclerosis [26].

1.3 The actin cytoskeleton supports the morphology and function of podocytes

Actin cytoskeleton is a dynamic cytoskeleton network in all eukaryotic cells. The polymerization and depolymerization of actin filament networks allow the cell to form dynamic structures that facilitate migration, cytokinesis, endocytosis, and other biological processes that are essential to maintain the normal functions of a cell. Actin filaments can also form stable bundles, which are named stress fibers, to facilitate the adhesion between cells and the extracellular matrix. Actin network is responsible for generating and transmitting force. Transverse arches and dorsal stress fibers are the structures that are involved in generating force on the cell body and transmit them to stress fibers and branched actin networks [27].

The fine structure of podocyte foot processes is supported by actin cytoskeleton network [28]. Transmission Electron Microscopy (TEM) shows that there electron dense actin bundles are enriched in the center of the foot processes, which are surrounded by loose cortical actin networks (Figure 1.5A,B). These actin bundles initiate from the major processes. Curved actin

bundles connect the straight bundles of two neighbor foot processes that initiate from the same major process [29] (Figure 1.5C). Details about how these structures form during podocyte differentiation are still not known. The actin cytoskeleton network in the foot processes connects the adhesive complex in the slit diaphragm, the focal contacts near the basement membrane, and the apical cell membrane of the foot processes.

Slit diaphragm is an adhesive complex that maintains interaction between adjacent podocytes. It connects to the actin cytoskeleton network inside the foot processes [30] (Figure 1.2B). Nephrin and Neph1 are transmembrane proteins that form the “zipper” like structure in the slit diaphragm. They have large extracellular domains that bind to another Nephrin or Neph1 molecules from the adjacent podocyte. Nephrin has a small intracellular domain that binds to several other cytoplasmic proteins like CD2AP and Nck [31–33]. Cd2ap directly bind to actin filaments, cortactin, and capping proteins [34–37]. Nck recruit WASp, another nucleation factor of actin filaments [38]. These proteins regulate branched actin network, and are believed to form a signal hub that maintains the normal morphology of foot processes.

Other actin-associated proteins also play important roles in podocytes. Alpha-actinin4 (encoded by *ACTN4*) connects between actin fibers to form stable bundles [39]. *INF2* (Inverted formin 2) antagonizes the Rho-activated formin mediated actin polymerization and also the localization of formin in cultured podocytes [40]. Non-muscle myosin IIA is responsible for tension generation in response to the upstream signaling on the actin bundles, and regulates podocyte adhesion and migration [41]. Synaptopodin also functions to facilitate the polymerization of G-actin [42]. It rescues the tropomyosin defects in drosophila and human cells [43].

The focal complexes that mediate the podocyte-GBM interaction also connect to actin network in the foot processes. Focal complexes transmit the force that is generated by the cytoskeleton networks inside the cell to the extracellular matrix. They also can sense the force change outside the cell and convert it into intracellular signals. Integrin complexes are the transmembrane proteins mediating the inside-out and outside-in signals [44]. In podocytes, the most common integrin isoforms are $\alpha3\beta1$ and $\alpha v\beta3$ [45, 46]. The extracellular domain of $\alpha3\beta1$ and $\alpha v\beta3$ recognize laminin and collagen. The intracellular domains of multiple integrin heterodimers assemble the platform of the focal complexes. Focal adhesion molecules, including talin, zyxin, paxilin and vinculin form layers and connect to actin stress fibers. Kinases such as FAK, SRC and ILK are regulated by the focal complex proteins and regulate the actin cytoskeleton structure *in vivo* [47].

1.4 Rho Family GTPases are the main regulators of Actin cytoskeleton

Rho family guanosine triphosphatases (hereafter called Rho GTPases) are a family of molecular switches that mainly regulate actin cytoskeleton structures [48]. The most studied members are Rac1, RhoA and Cdc42. Rho GTPases cycles between GTP-bound, active conformation and GDP-bound, inactive conformation. GTP-bound Rho GTPases activate the downstream pathway by interacting with their effector molecules (Figure 1.6A). The C-terminus of most Rho GTPases is modified by farnesyl or geranylgeranyl isoprenoid lipid, which is required for membrane targeting. Active Rac1 recruits WAVE complex to the plasma membrane and induces actin polymerization into branched network. Cells with high Rac activity forms large

lamellipodia (Figure 1.6B,C). GTP-bound RhoA, on the other hand, activates formin mediated actin polymerization, resulting in long linear actin fibers and bundles (Figure 1.6B,C). Active RhoA induces the assembly of stress fibers. Active Cdc42 induces finger-like extensions through recruiting Wiskott–Aldrich Syndrome protein (WASp) to the plasma membrane and release its auto-inhibitory conformation (Figure 1.6B,C). WASp further recruits Arp2/3 complex and assembles thin, linear actin filaments, which protrude from the plasma membrane, and form finger-like structures.

Direct modulation of the activity of Rho GTPases affects podocyte morphology and function [49–51]. Podocyte-specific expression of CA-RhoA induced late onset of proteinuria and FSGS [49]. Podocyte specific deletion of Cdc42 in mice causes congenital nephrotic syndrome and foot process effacement [50]. However, deletion of either Rac1 or RhoA in podocytes does not induce any defects in mice. Podocyte specific deletion of Rac1 in mice causes resistance to protamine sulfate perfusion-mediated transient podocyte damage and foot process effacement, but susceptibility to a chronic model of podocyte injury in UNX/DOCA-salt-hypertensive mouse model [52].

1.5 Regulators of Rho GTPases

Three families of regulators mainly control the activity of Rho GTPases. Two classes of Rho GTPase regulators control the processes of cycling between GTP- and GDP-bound states: Guanine nucleotide exchange factors (GEFs) and GTPase-activating proteins (GAPs) (Figure 1.6A) [53]. The Rho GTPases are slow GTPases by themselves. The exchange between

GDP-bound and GTP-bound forms is also ineffective. GEFs facilitate GTP loading, and increase the level of active Rho GTPases. GAPs enhance the catalytic activity of Rho GTPases, converting the active Rho family GTPases to the inactive state. A third family of regulatory proteins are the guanine nucleotide dissociation inhibitors (RhoGDIs) (Figure 1.6A), which sequester Rho GTPases at GDP-bound state, and pull it out of the cycling pool. RhoGDIs are shown as “chaperones” for small GTPases because they stabilize GDP-bound state, and also mediate the translocation of Rho GTPases between different membrane compartments [54, 55].

Although the exact physiological function of the Rho GTPase regulators has not been extensively studied in podocytes, several studies indicate their crucial roles in regulating podocyte morphology and function. RhoGDI-alpha knockout mice (*Arhgdia*^{-/-}) exhibit congenital nephrotic syndrome, and the knockout mice have high Rac activity in the kidney [56]. Tyrosine phosphorylation on nephrin endoplasmic tail could also regulate p190RhoGAP through Rac [57]. Human protein atlas project has also identified GAPs and GEFs that are highly expressed in podocytes, including ARHGAP12, ARHGAP28, ARHGAP35, SRGAP2, ARHGEF11, and ARHGEF12 [58].

Some podocyte specific and/or FSGS susceptibility genes also regulate the activity of Rho GTPases. Nephrin controls the Rac activity through PI3K-p85 signaling pathway [57]. Synaptopodin, another podocyte-specific protein, protects Rho from degradation by Smurf-mediated ubiquitination, and inhibit the Cdc42-IRSp53 interaction [59, 60]. Mutations in *TRPC6*, encoding a calcium channel, are associated with familial FSGS [17, 18]. Recently studies showed that TRPC6 forms complex with RhoA, and TRPC5 forms complex with Rac1

[61]. Calcium influx through TRPC6 increases active RhoA, while through TRPC5 increases active Rac1. PLCE1, a risk gene for steroid resistant nephrotic syndrome and FSGS, is responsible for efficient activation of Rac1 [62].

1.6 Large-scale genetic studies discover FSGS susceptibility genes

Next-generation sequencing (NGS) technologies, revolutionary sequencing methods developed in early 2000s, allow researchers to access to personal genome in a faster and more economic than traditional sanger sequencing method [63]. These methods read millions of sequencing reactions simultaneously by high throughput monitoring approaches [64]. Using NGS methods, researchers can identify specific genetic variants in a large cohort of patients. These methods have been applied to investigate cancer genomes [65], to identify susceptibility variants that associate with diseases such as autism and diabetes [66, 67], and to map the epigenetic modification loci in the genome. Since the cost of whole genome sequencing for each patient is still high, Hildebrandt's group combines linkage analysis of familial nephrotic syndrome with NGS recently identified several new genes that could cause FSGS, including *ADCK4* [68], *ARHGDI1* [69], and *EMP2* [70].

Genome-wide association studies (GWAS) have been widely used to identify the linkage between common variants that associate with diseases before NGS technologies became popular. This method scan hundreds of thousands common DNA variant in human. Several GWAS have identified 24 susceptible loci for chronic kidney disease, including *SHROOM3*, *UMOD*, and *DACH1* [71, 72]. GWAS method was also applied to study HIV-associated FSGS in

African American population, and identified genetic locus between *APOL1* and *MYH9* that are strongly associated with HIV-associated FSGS [14]. G1 and G2 variants of *APOL1* are the coding variants for FSGS susceptibility [19, 20].

1.7 Current mouse genetic models of podocyte diseases

Using *in vitro* models such as podocyte cell culture to study the function of podocytes is limited since cultured podocytes do not generate foot processes. Thus *in vivo* models are necessary to investigate and truly understand podocyte functions. Currently, transgenic and knockout mouse models are the most widely used *in vivo* models for podocyte diseases. Rat models are also commonly used and they are more susceptible to kidney damage than mouse models. However, rats require more space and longer breeding period, and also the transgenic/knockout tools in rat models are not as efficient as in mouse models. Knockout mouse models have shown that many podocyte-specific genes and FSGS disease genes are essential for maintaining the podocyte foot process structure *in vivo*, including *Nphs1* [73], *Nphs2* [74], *Neph1* [75], *Actn4* [76], and *Cd2ap* [77]. Loss of function of some other genes in mice does not cause any podocyte dysfunction, but increases the susceptibility to artificial kidney injury models, such as *Synpo* [21], *Trpc6* [78], and *Myh9* [79]. The combinations of heterozygosity in *Cd2ap/Synpo* and *Cd2ap/Fyn* also induce proteinuria and podocyte foot process effacement, the early signs of FSGS in aged mice, indicating there could be genetic complexity in FSGS patients [21].

1.8 Intravital imaging by multi-photon microscopy

Since podocyte cell culture cannot recapitulate the foot process architecture in petri dishes, intravital imaging is the only option to investigate the podocyte cell dynamics at the physiological conditions. Currently multi-photon microscopy (MPM) is the best method to perform non-invasive live imaging *in vivo*. This method based on a theory that multiple low-energy, long wavelength photons can excite a fluorophore simultaneously (Figure 1.7A). The interaction between multiple photons and the fluorophore will induce sequential electronic transition that equals to a single high-energy photon [80]. The first MPM microscope was invented by Denk *et al* in 1990 [81]. Since low-energy, long-wave length photon is the source of excitation, MPM achieves three following advantages: first, it penetrates tissue up to several hundred micrometers, which is much deeper than another microscopy system; second, it reduces phototoxicity and bleaching of the fluorophores; third, it reduces out-of-focus background signal because fluorophores are excited only at the laser beam focus (Figure 1.7B) [82, 83]. Since the excitation is not linear, second harmonic signal can be generated to visualize membrane structures like kidney capsule and fascia by visualize their native fluorescence [84].

All the features make MPM an excellent approach to track podocytes *in vivo*. Using MPM, Hackl *et al* showed podocyte migration in response to kidney injuries in podocin-GFP and podocin-CRE confetti mice [85]. Endlich *et al* observed podocyte migration during the development of zebrafish glomeruli. They also observed that zebra fish podocytes and their

branch patterns are stationary at physiological conditions [86]. Peti-Peterdi's group also reported increased calcium waves in podocyte during unilateral ureteral obstruction induced kidney injury by using podocyte specific GCaMP mice [87].

1.9 Conclusions

The cell body of podocytes and the slit diaphragm between the interdigitating foot processes from adjacent podocytes form the outer layer of the filtration barrier to prevent albumin leakage into the primary urine. The organized structures of foot process and the slit diaphragm are the indicators of the intact barrier function. In podocyte diseases, the effacement of foot processes and the loss of slit diaphragm are often observed. These pathological changes are also correlated with albuminuria. Actin network is the major cytoskeleton structure inside the foot processes. Cortical Actin network connects the cell-cell adhesion of adjacent podocytes (slit diaphragm) to the actin bundles in the center of the foot processes, which is thought to be the cytoskeletal support of the foot process. Actin bundles are also connected to the focal complexes that mediate the interaction between the podocytes and GBM. As the major regulators of actin cytoskeleton, Rho family small GTPases are very important in maintaining foot processes and slit diaphragm. Previous studies have indicated that dysregulation of the activities of Rho GTPases could cause foot process effacement and glomerulosclerosis. However, it is not fully understood about which small GTPase play the most important role in the podocyte damage.

FSGS, a leading cause of end stage renal failure, is one of the diseases that caused by podocyte damage. It remains unknown about how much genetic risk causes susceptibility to

FSGS. FSGS can be classified as familial FSGS and sporadic FSGS based on whether another family member is diagnosed with the same disease or not. Genetic studies of familial FSGS cases have identified many FSGS causing genes, most of which are components of the slit diaphragm, and/or regulate the actin cytoskeleton structure. Gain or loss of function mutations of FSGS genes could cause actin cytoskeleton remodeling in the podocytes, which could be the reason of foot process effacement. However, FSGS genes do not explain the sporadic form of this disease, because they are rarely mutated in sporadic cases. Whether there is a genetic factor and how much of the genetic risk is in the sporadic FSGS remain to be investigated.

1.10 Figures

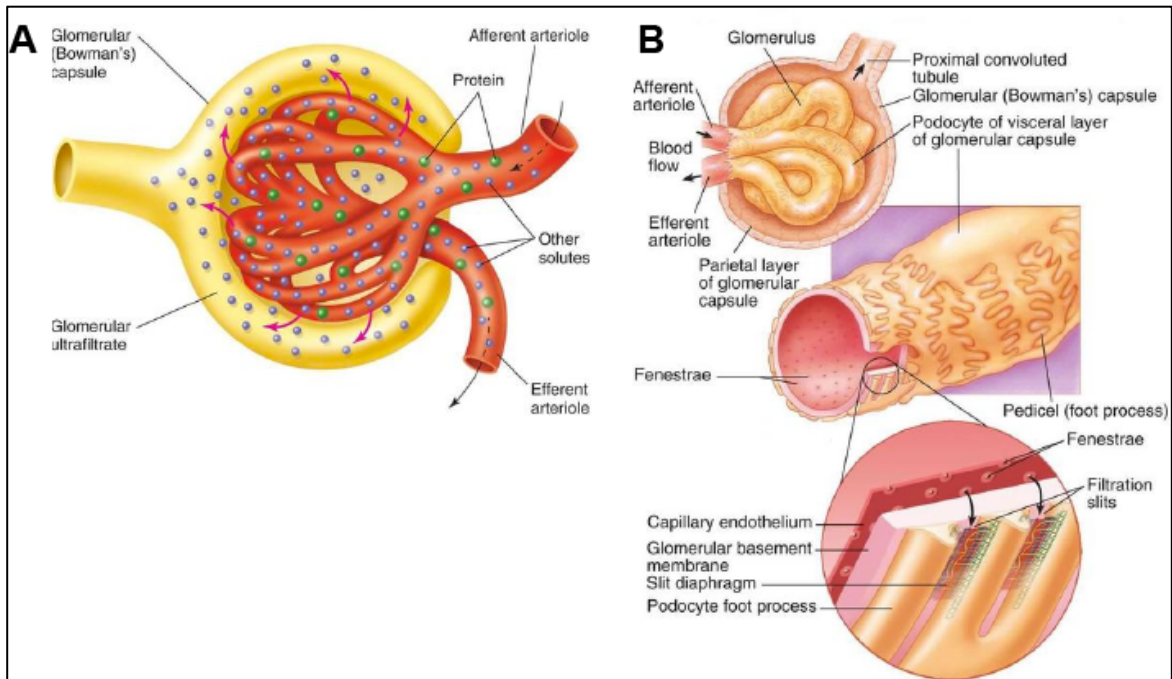


Figure 1.1 The structure of the glomerulus

(A) The image showed the composition of the glomerulus. Afferent arteriole branched into capillaries ball inside the Bowman's capsule. During the filtration process, water and small solutes can penetrate through the filtration barrier and become the glomerular ultrafiltrate. The rest of the blood including blood cells and proteins remain in the capillary loops, which combine to form the efferent arteriole. (B) The structure of the filtration barrier. The capillaries inside the Bowman's capsule are fenestrated. They are covered by podocytes. Between foot processes of the podocyte, big transmembrane proteins form an adhesive structure called slit diaphragm (filtration slits). (Adjusted from *Human Physiology*, Chapter 12, <https://humanphysiology2011.wikispaces.com/12.+Urology>, by Rausch A and Kortlever C)

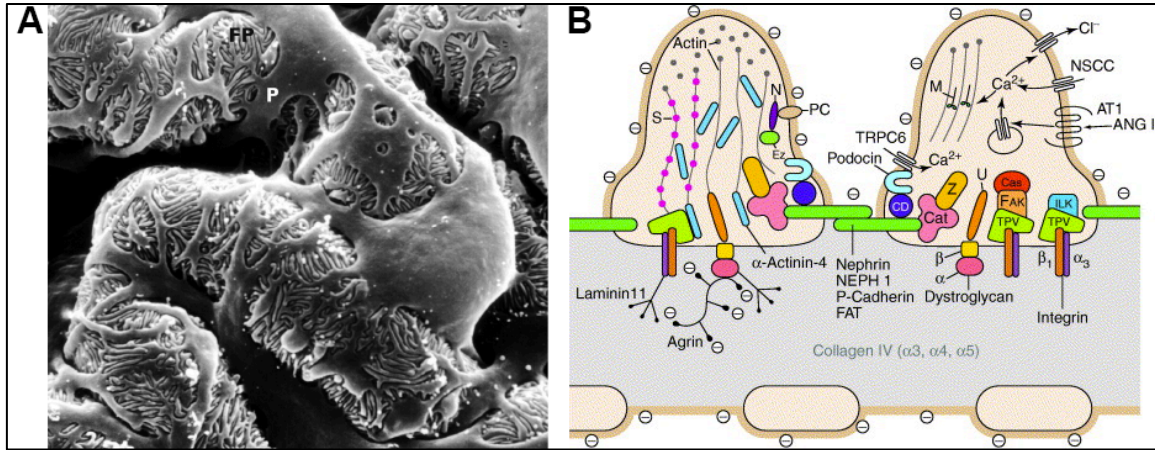


Figure 1.2 The podocyte and the slit diaphragm

(A) Scanning microscopy of the podocyte. FP: foot processes; P: primary processes. (B) A cartoon of the cross-section view of foot processes and slit diaphragm. Important proteins and their locations are also shown [88, 89].

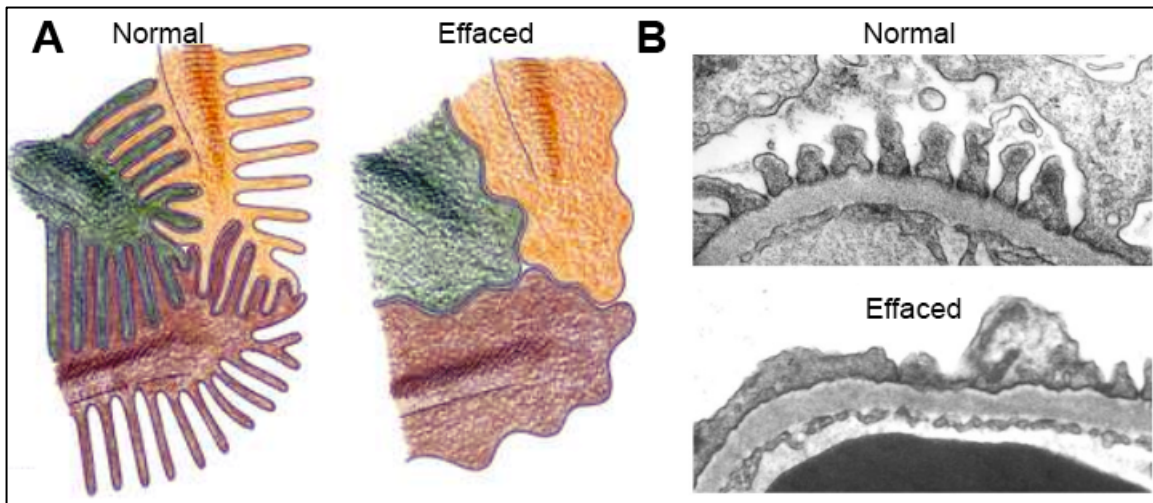


Figure 1.3 Foot process effacement

(A) A cartoon showed the effaced podocytes lose their foot processes. The effaced area looks like lamellipodia. (B) Transmission electron microscopy shows normal and effaced foot processes.

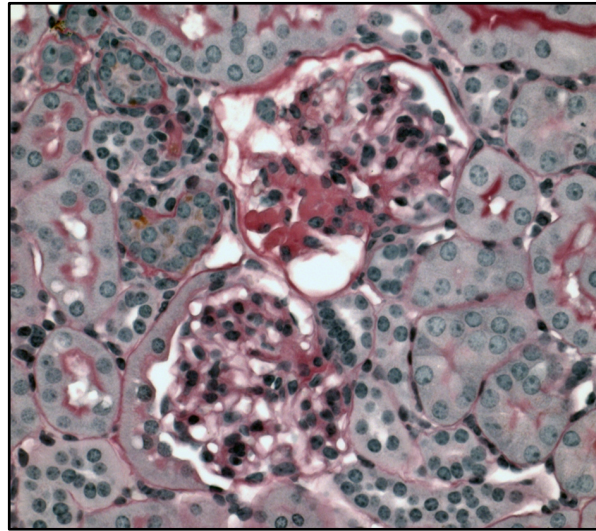


Figure 1.4 Histology of FSGS

The upper glomerulus shows features of glomerulosclerosis on the left lobe. The lower glomerulus is normal. The red-staining area on the left lobe of the upper glomerulus shows sign of scarring (sclerosis). (A mouse kidney was stained by a method called periodic acid-Schiff stain)

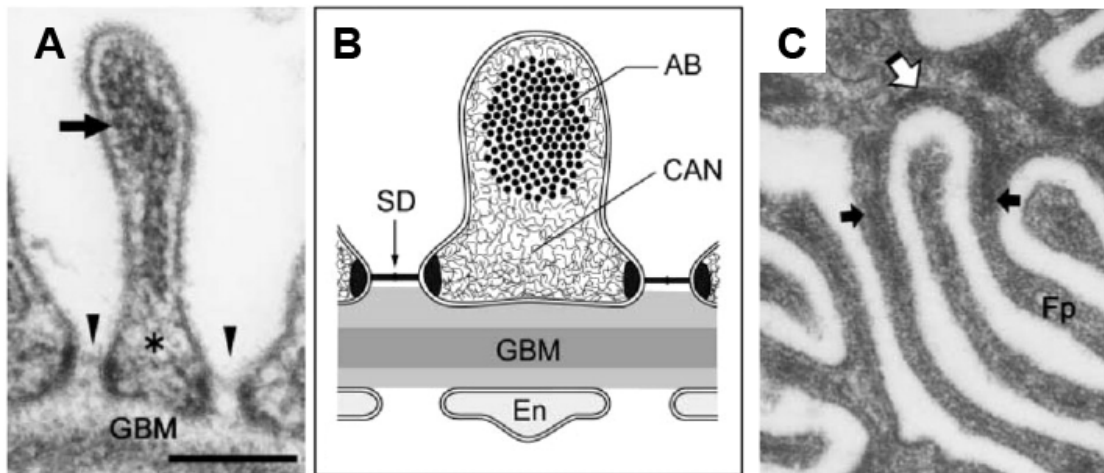


Figure 1.5 The actin cytoskeleton in the podocyte foot processes

(A) An cross-section image of a foot process imaged by transmission electron microscopy. The arrow showed the actin bundle in the center of the foot processes, the star showed the loose actin network at the bottom of the foot processes and surrounding the actin bundle. The arrowheads show the slit diaphragm. (B) A cartoon of a foot process. AB: Actin bundles, CAN: cortical actin network, SD: slit diaphragm, GBM: glomerular basement membrane, and En: endothelial cells. (C) A bird view image of foot processes. The open arrow shows curved actin bundles that connects adjacent foot processes extended from the same podocyte; the closed arrows show the straight actin bundles inside the foot processes. This figure is adapted from Sakai et al [29].

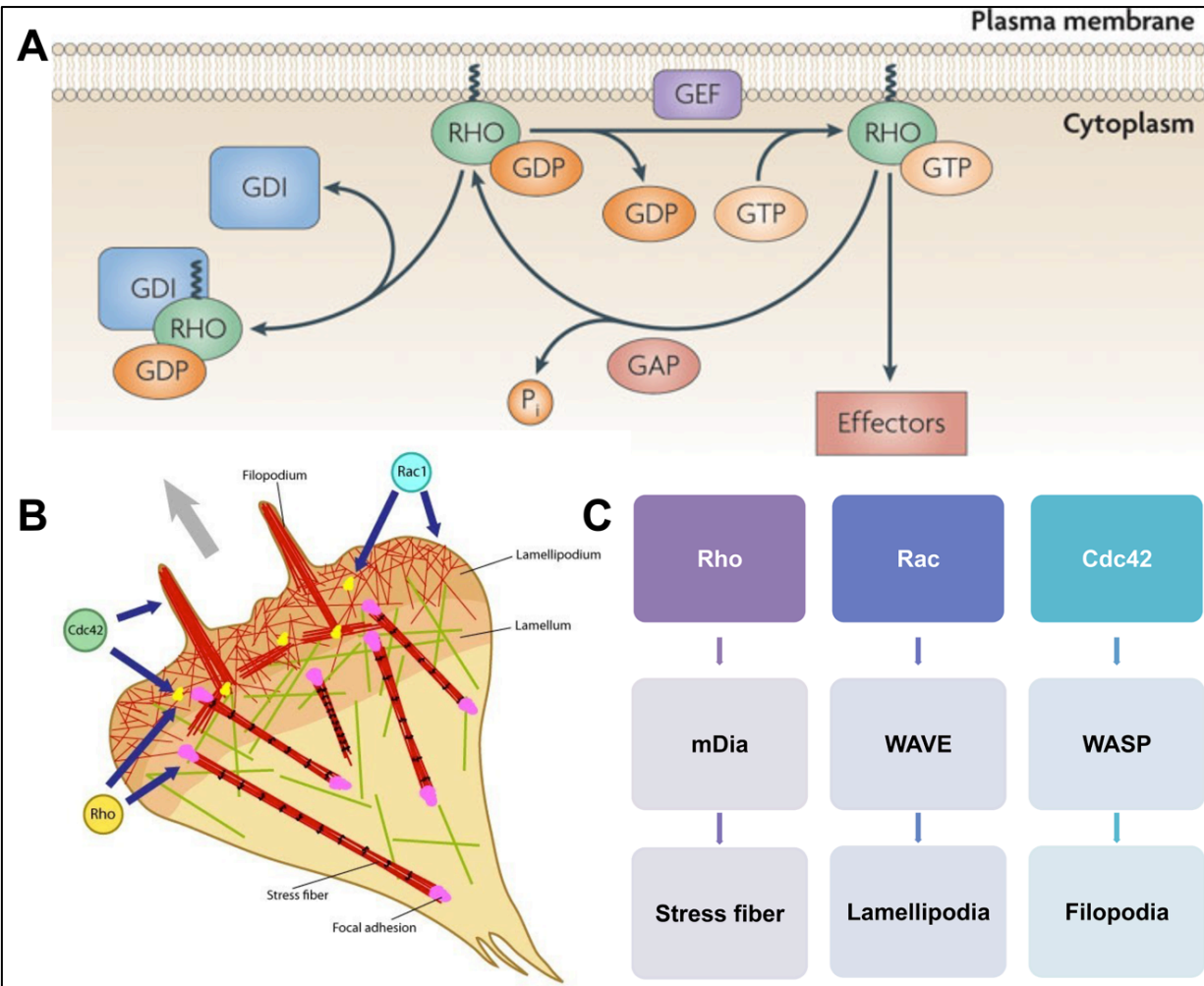


Figure 1.6 Rho Family GTPases: regulation and function

(A) The regulated catalytic cycle of Rho family GTPases. Lipid modification allows Rho GTPases attach to the membrane structures in the cell. GEFs facilitate the exchange of GDP to GTP and convert GDP-bound Rho GTPases to GTP-bound form. GTP-bound Rho GTPases activate the downstream effectors through allosteric mechanisms. GAPs stimulate the GTPase activity of Rho family GTPases and convert the GDP-bound form to GDP bound form. RhoGDI proteins bind the GDP-bound form, and pull it out from the membrane structure. (B, C) Active Rho stimulates stress fiber formation through mDia, activate Rac stimulates lamellipodia formation through WAVE complexes, and active Cdc42 stimulates filopodia formation through WASP. This figure is adapted from Tubulewicz *et al* [90] and <http://www.mechanobio.info/modules/go-0051893>

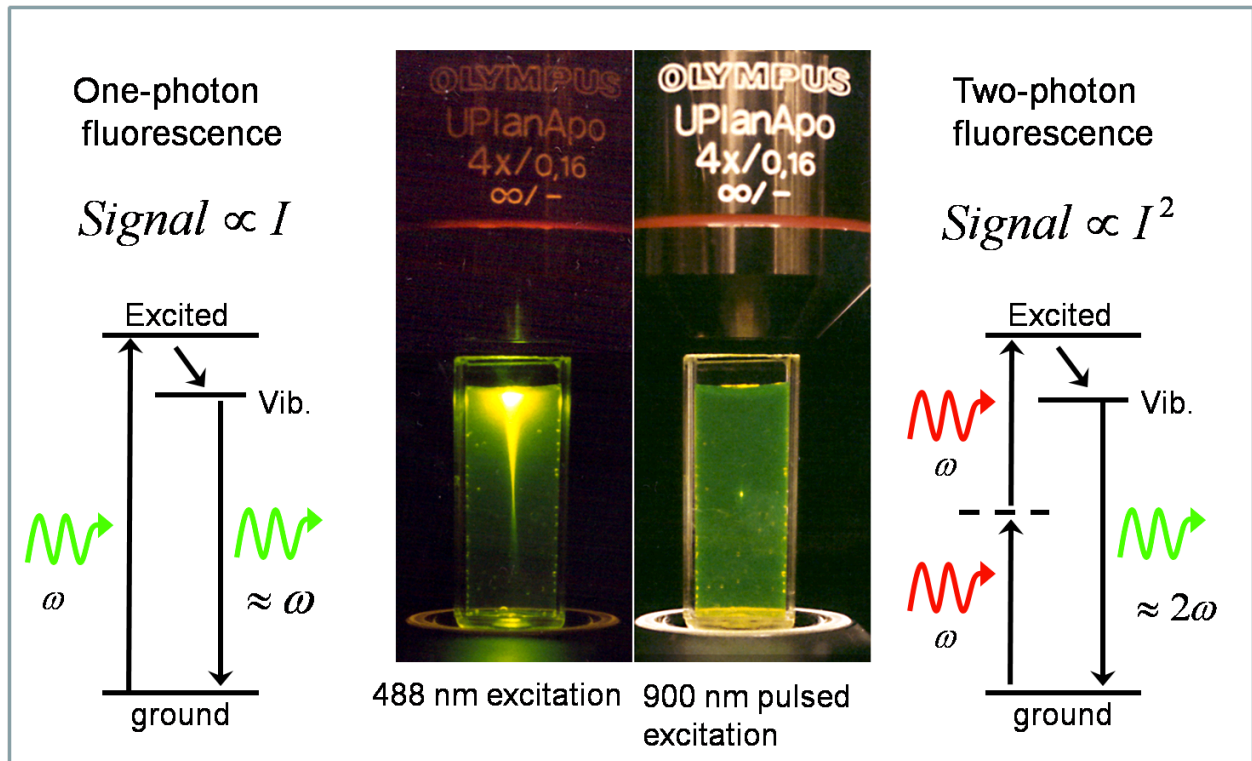


Figure 1.7 The mechanism and advantage of multi-photon microscopy (MPM)

MPM reduces the fluorescent background compare to single photon microscopy. This figure is adapted from

<http://cleoqels2010.blogspot.com/2010/05/expo-idea-generation-and-multiphoton.html>

Chapter 2. Arhgap24 Inactivates Rac1 In mouse Podocytes, and A mutant Form is Associated with Familial Focal Segmental Glomerulosclerosis

2.1 Abstract

Podocyte has a complex actin-based cytoskeleton that maintains efficient barrier function of glomeruli. Disruption of components of the actin cytoskeleton results in podocyte damage and cell loss, which may lead to a prototypic injury response called focal segmental glomerulosclerosis (FSGS). From genes that are highly expressed in mouse podocytes, we identified a RhoA-activated Rac1 GTPase-activating protein, *Arhgap24*, which was upregulated in podocytes as they differentiated, both *in vitro* and *in vivo*. Decreased *Arhgap24* expression results in high level of active Rac1 and Cdc42, which influenced the cell shape and membrane dynamics. Consistent with a role for *Arhgap24* in maintaining normal podocyte functions *in vivo*, we identified a mutation in *Arhgap24* that impaired its Rac1-GAP activity by sequencing FSGS patients and that was associated with disease in a family. Thus, *Arhgap24* contributes to the careful balancing of RhoA and Rac1 signaling in podocytes, the disruption of which may lead to kidney disease.

2.2 Introduction

The kidney filters plasma and reabsorb salts and nutrients to maintain the appropriate extracellular environment. The proximal component of the nephron, the glomerulus, is the primary filtration barrier that prevents the loss of serum proteins into the primary filtrate. The

glomerular filtration barrier consists of fenestrated endothelial cells, a thick glomerular basement membrane (GBM), and specialized epithelial cells (podocytes) arranged in series. Diseases affecting the filtration barrier, especially of the GBM or the podocyte, result in the leakage of serum proteins into the urine, progressive damage to the glomerulus, and loss in renal function [91].

The podocyte has a complex cellular architecture composed of an octopus-like cell body that attaches to the GBM through actin-based foot processes [88]. In kidney diseases that are associated with proteinuria, such as focal segmental glomerulosclerosis (FSGS) and minimal change disease, podocytes rearrange their actin cytoskeleton network, which results in retraction or effacement of foot processes [92]. While it is unclear how this change leads to the leakage of serum proteins, foot process effacement appears to be a key step in the breakdown of the filtration barrier. Studies to understand the molecular basis of foot process effacement *in vitro* have shown that, in response to stress, podocytes switch from a RhoA-dependent stationary state to a Cdc42- and Rac1-dependent migratory state [28, 93]. These studies suggest the intriguing possibility that altered membrane dynamics and increased cell motility are the mechanisms underlying foot process effacement *in vivo*.

Since podocyte membrane reorganization is a common feature of proteinuric kidney diseases, we sought to understand the regulation of membrane dynamics of these cells. Using an *in vitro* model of podocyte differentiation, we found that podocytes reduced their membrane ruffling activity as they were differentiated. We found that decreased membrane ruffling in differentiated podocytes was dependent on the presence of a GTPase-activating protein (GAP),

Arhgap24. Previous works from Stossel and colleagues have shown that Arhgap24 (also known as Filamin A-binding RhoGAP [FilGAP]) is a GAP for Rac1, and it binds to branched actin network and suppresses lamellipodia formation and cell spreading downstream of RhoA signaling [94]. Their work also shows that the highest level of *Arhgap24* transcript is in the kidney. Here we show that *Arhgap24* was specifically expressed in podocytes in the kidney. Its expression increased as these cells differentiate *in vivo*. The *ARHGAP24* gene is highly conserved, implying an important role for the gene product. We sequenced the DNA from patients with FSGS, and identified a loss-of-function mutation in the *ARHGAP24* gene in kindred with familial kidney disease. Taken together, these results suggest that Arhgap24 controls the RhoA-Rac1 signaling balance in podocytes that could be dysregulated in proteinuric kidney diseases, such as FSGS.

2.3 Methods

2.3.1 Podocyte cell culture

Generation and propagation of conditionally immortalized murine podocyte cell lines has been described previously [95, 96]. Briefly, podocytes were propagated on collagen I-coated dishes at 33°C (permissive temperature) in RPMI supplemented with 10% fetal bovine serum (FBS) and 10 U/ml of recombinant mouse interferon- γ (IFN- γ , a gift from Robert Schreiber, Washington University School of Medicine). To induce differentiation, the medium was changed to RPMI with 5% FBS without IFN- γ , and the cells were shifted to 37°C (nonpermissive temperature) for 7 to 14 days. Under these conditions, cells underwent growth arrest, increased

in size, and developed elongated cell processes.

For live cell imaging experiments, podocytes were stably transduced with YFP-actin by lentivirus transduction, and purified by automated cell sorting. Control and knockdown cell lines were generated using a bicistronic lentiviral vector incorporating the targeting shRNA and YFP-actin expressed downstream of an internal ribosomal entry site. The control knockdown sequence targeted the firefly luciferase gene (Fluc). The 2 Arhgap24 knockdown constructs targeted the sequences 5'-TTAAGGAGCTAATGAAACA-3' (line 451) and 5'-TAACGATGGTCATAAGAAA-3' (line 756), respectively. Stably transduced cell lines were generated by automated cell sorting for YFP expression.

2.3.2 RNA isolation

Isolation of primary mouse podocytes using Dynabead perfusion and flow cytometric cell sorting has been described previously [97, 98]. RNA was extracted from 6,000 primary podocytes and from cultured podocytes grown at the permissive or nonpermissive temperatures using an RNeasy Kit (Qiagen) following the manufacturer's protocol. RNA quality was verified by gel electrophoresis and to ensure that the 260/280 nm absorbance ratio was greater than 1.8.

2.3.3 Arhgap24 antiserum production

Amino acids 390–604 of isoform 1 (NCBI accession no. NP_083546) of mouse Arhgap24 were cloned downstream of glutathione-S-transferase (GST) in the pGEX4T-1 expression vector. This portion of Arhgap24 is well conserved across species and lies downstream of the GAP domain in both isoforms of Arhgap24. GST-tagged Arhgap24 was expressed in BL21 (DE3) pLysS *E. coli*. After induction with IPTG and sonication of bacteria, soluble GST-Arhgap24 was

batch purified using glutathione-agarose beads. GST-Arhgap24 was eluted with reduced glutathione and dialyzed against PBS to remove excess glutathione. This antigen was emulsified in complete Freund's adjuvant (Sigma-Aldrich) and was used to immunize rabbits and Armenian hamsters. Hamster handling and immunization were performed by the Washington University School of Medicine Hybridoma Center. Specificity for Arhgap24 was confirmed by immunoblotting FLAG-tagged Arhgap24 transfected into HEK293 cells. Specific signal in immunoblotting and staining experiments was confirmed by quenching of signal with antiserum preincubated with antigen.

2.3.4 Confocal imaging

Podocytes grown on sterilized collagen I-coated coverslips at 33°C or 37°C were fixed with 4% PFA in PBS for 10 minutes. Cells were then blocked and permeabilized for 1 hour with PBS with 2.5% FBS and 0.1% saponin. Primary rabbit anti-Arhgap24 antiserum (1:300) in blocking buffer was applied to the cells for 1 hour at room temperature. After four 5-minute washes with blocking buffer, coverslips were mounted using ProLong Antifade mounting medium (Invitrogen) according to the manufacturer's protocol. Images were captured with confocal settings using an Olympus FluoView FV1000 microscope. A similar protocol was used to stain Arhgap24 in formalin-fixed paraffin-embedded mouse kidney after antigen retrieval. Podocytes were stained using a mouse anti-synaptopodin monoclonal antibody (a gift from Peter Mundel, Massachusetts General Hospital, Boston, Massachusetts, USA) [99]. For wound healing experiments, differentiated knockdown podocytes were plated to confluence on collagen I-coated coverslips. A scratch was created using a sterile 200 µl pipette tip. Loosely adherent cells were washed

away by 3 vigorous washes with PBS. The cells were transferred to culture medium, and, at various time points, coverslips were harvested and fixed in 4% PFA in PBS. Cells were identified by nuclear staining with DAPI (4',6-diamidino-2-phenylindole).

2.3.5 Tissue isolation and immunoblotting

Whole mouse tissues (~200 mg) were snap frozen on dry ice and homogenized in cold lysis buffer containing 1% NP-40 and protease inhibitors using a dounce homogenizer. Post nuclear supernatants were loaded to equalize actin levels by immunoblotting. Glomerular isolation/enrichment experiments using magnetic particles were performed as described previously [97].

2.3.6 Live cell imaging and kymograph analysis

Podocytes that were lentivirally transduced with YFP-actin were cultured in glass bottom dishes at 33°C or differentiated at 37°C (nonpermissive condition) for 7 to 14 days and then imaged. Similarly, YFP-actin transduced Arhgap24 knockdown (lines 451 and 756) and control knockdown (Fluc) cell lines were differentiated on glass bottom dishes for 7 to 14 days before imaging experiments. Sequential images were captured every 15 seconds for a 20-minute duration using an Olympus FluoView FV1000 microscope. Movies were assembled using Olympus Fluoview software. The Multiple Kymograph plug-in of ImageJ (<http://rsbweb.nih.gov/ij/>) was used to generate kymographs at 3 different locations of maximal membrane ruffling for each cell imaged [100]. For each kymograph, up to 13 actin spikes were measured, and the average length was computed as described previously [101]. A value of 1 was assigned to kymographs without a measurable actin spike. Ruffling movies were generated by H. Suleiman, and the

kymographic analysis was performed in a blinded fashion by S. Akilesh. Images were assembled in Adobe Photoshop.

2.3.7 Sequencing

DNA was obtained from affected ($n = 310$) and control ($n = 180$) individuals. DNA from 96 of the control individuals was purchased from the Coriell Institute. PCR primer pairs were designed to completely sequence exons and exon-intron junctions of *ARHGAP24*. Bidirectional sequencing using ABI Big Dye 3.1 sequencing chemistry on an ABI PRISM 3730 sequencing platform (Applied Biosystems) was performed. Sequences were aligned using Sequencher software (Gene Codes) and manually verified. The Q158R variation was determined by A.S. Shaw's laboratory and verified by M.P. Winn's laboratory. In addition, the exon incorporating this variation was sequenced in an additional 554 control chromosomes to rule out the possibility that it represented a low-frequency noncausal variation.

2.3.8 Haplotype analysis

MSM primer sequences for markers D4S1538, D4S1534, D4S2409, and D4S2460 were obtained from UniSTS (<http://www.ncbi.nlm.nih.gov/unists>) or designed with Primer3 software (<http://frodo.wi.mit.edu/primer3/>). Carboxyfluorescein succinimidyl ester-labeled (FAM-labeled) oligonucleotides were synthesized by Invitrogen Life Technologies and were run on the 3730 DNA Analyzer (Applied Biosystems) and analyzed using GeneMapper Software v4.0 (Applied Biosystems). The analysis was carried out by visual inspection, assigning the most likely linkage phase by minimizing the number of recombinants in the pedigree.

2.3.9 Arhgap24 dimerization assay

FLAG- or GFP-tagged wild type or Q156R Arhgap24 were cotransfected into HEK293 cells. Cell lysates were immunoprecipitated with M2 mouse anti-FLAG antibody (Sigma-Aldrich) with protein A conjugated to sepharose beads. The immunoprecipitates were resolved by SDS-PAGE and then immunoblotted with JL-8 mouse anti-GFP antibody (Invitrogen).

2.3.10 Rac1, Cdc42, and RhoA pull-down assays

The GST-tagged Pak1-PBD used for the pull-down assays was expressed in BL21(DE3) *E. coli*. The recombinant protein was bound to glutathione-agarose beads stored at -80°C until use. For the active Rac1 pull-down assay, HEK293T cells were seeded in 6-cm dishes and transfected at 80%–90% confluence using Lipofectamine 2000 reagent according to the manufacturer's protocol (GIBCO BRL). Cells were transfected with FLAG-tagged wild-type or mutant Q156R Arhgap24 or a titration of the 2 constructs, keeping the total DNA transfected constant. Twenty-four hours after transfection, the cells were lysed, and a sample of the lysate was retained for measurement of total Rac1 and FLAG-Arhgap24 levels. Equal volumes of the remaining lysates were incubated with GST-PBD bound to glutathione-agarose beads. Rac1-GTP bound to the beads (active Rac1) was eluted with Laemmli sample buffer and separated on a 12% polyacrylamide gel. After transfer to a nitrocellulose membrane, active and total Rac1 were detected with the 23A8 mouse anti-Rac1 monoclonal antibody (Upstate Biotechnology). FLAG-tagged Arhgap24 was detected with the M2 mouse anti-FLAG antibody. For Cdc42 activity assays, active Cdc42 was immunoprecipitated with GST-PBD bound to glutathione-agarose beads and detected with B-8 mouse anti-Cdc42 (Santa Cruz Biotechnology Inc.). For RhoA activity assays, active RhoA was immunoprecipitated with GST-Rhotekin bound

to glutathione-agarose beads and detected with 26C4 mouse anti-RhoA (Santa Cruz Biotechnology Inc.). The immunoblot signal was detected using a LI-COR Odyssey Imaging System using their infrared dye-labeled secondary reagents. Data are representative of at least 3 independent experiments.

2.3.11 Statistics

Data are represented as mean \pm SD. In all cases, group differences were assessed by ANOVA with post-test correction (Bonferroni-Holm). A *P* value of less than 0.05 was considered significant.

2.3.12 Study approval

Patient and control DNA samples were obtained after written informed consent and with local Institutional Review Board approval (Washington University School of Medicine, Duke University Medical Center, Université René Descartes, Brigham and Women's Hospital, and the NIDDK). All animal experiments were conducted with approval of the Washington University Animal Care and Use Committee

2.4 Results

2.4.1 Differentiated podocytes reduce ruffling of their cell membranes

Podocytes can be propagated *in vitro* by conditional expression of a temperature-sensitive SV40 large T antigen at the permissive temperature of 33°C. Shifting the cells to the nonpermissive temperature (37°C) induces destabilization of the large T antigen, growth arrest, and morphologic changes that mimic podocyte differentiation *in vivo* [95]. During development,

podocytes reorganize their cell membranes from broad sheets into sieve-like foot processes [88]. Conversely, in proteinuric diseases, podocytes lose this membrane complexity and exhibit effacement of their foot processes [92]. Therefore, we hypothesized that the membrane dynamics of podocytes would be regulated in this *in vitro* model of cell differentiation. When undifferentiated podocytes were cultured at the permissive temperature, they exhibited highly ruffled plasma membranes (Figure 2.1A). In contrast, the plasma membranes of the differentiated podocytes had a very smooth, flat appearance. In order to quantitate these membrane dynamics, we performed time-lapse imaging of live podocytes transduced with yellow fluorescent protein–actin (YFP-actin). While undifferentiated podocytes rapidly ruffled their membranes, differentiated podocytes had reduced membrane motility, correlating with the reduced frequency of ruffled cell membranes (Supplemental Videos 1 and 2; supplemental material available online with this article; doi: 10.1172/JCI46458DS1). This difference is also apparent by kymographic analysis (Figure 2.1A and 2.1B).

2.4.2 Podocytes upregulate Arhgap24 when they differentiate

Next, we evaluated the expression of the small G proteins and their regulators that might control membrane motility in this *in vitro* model of podocyte differentiation. We isolated RNA from undifferentiated and differentiated mouse podocytes and performed gene expression analysis using microarrays. Our cultured podocytes expressed genes for several known podocyte-specific proteins, such as Wilms tumor protein 1 (*Wt1*), podocin (*Nphs2*), CD2-associated protein (*Cd2ap*), podocalyxin (*Podxl*), synaptopodin (*Synpo*), α -actinin-4 (*Actn4*), and to a lower extent nephrin (*Nphs1*). We focused our analysis on the expression patterns of known regulators of the

actin cytoskeleton and membrane dynamics, such as GAPs and guanine nucleotide exchange factors (GEFs) for Rac1, RhoA, and Cdc42 (a list of these genes is available as a supplemental data table in the Gene Expression Omnibus (GEO) database, series GSE23856; <http://www.ncbi.nlm.nih.gov/gds/>). Of these known GAPs and GEFs, the message for *Arhgap24* was highly upregulated when podocytes were differentiated *in vitro*. *Arhgap24* was an intriguing gene, because previous work from Stossel and colleagues had shown high transcript levels in the kidney [94]. However, the cell expressing *Arhgap24* within the kidney was unknown. We found that RNA from *in vivo*-isolated podocytes also had a high level of *Arhgap24* transcript [96]. Next, we examined *Arhgap24* gene expression in publicly available microarray data (the GenitoUrinary Molecular Anatomy Project; www.gudmap.org) generated from microdissected glomeruli isolated at various stages of kidney development. The *Arhgap24* message was upregulated as glomeruli progressed from the E12.5 renal vesicle stage to the E15.5 S-shaped body to the almost mature E15.5 renal corpuscle (Figure 2.2A).

We confirmed the microarray results by quantitative RT-PCR. *Arhgap24* transcript levels increased ~70 fold when podocytes were differentiated (Figure 2.2B). To confirm upregulation at the protein level, we generated *Arhgap24*-specific antiserum in Armenian hamsters and rabbits. Preabsorption of these antisera with *Arhgap24* antigen abolished specific signal (Supplemental Figure 2.1). Podocytes upregulated a 95-kDa band corresponding to the *Arhgap24* protein when they were differentiated *in vitro* (Figure 2.2C). The lower band seen in the undifferentiated podocytes (at approximately 50 kDa) did not correspond to the predicted molecular weight of known splice isoforms of *Arhgap24*. This 50kDa band likely represents a specific degradation

product of Arhgap24, perhaps due to increased turnover of the protein in undifferentiated podocytes. Confocal imaging of podocytes showed that Arhgap24 was enriched in structures at the base of the cell, and the staining intensity at these sites increased with differentiation (Figure 2.2D). Since Arhgap24 has been described to localize to focal adhesions [94], we verified that these structures were in fact focal adhesions by co-labeling with vinculin (Figure 2.2E). These experiments showed that Arhgap24 is highly expressed in the focal adhesions of cultured podocytes and is upregulated as these cells are differentiated.

2.4.3 Arhgap24 is expressed in kidney podocytes *in vivo*

Next, we tested Arhgap24 expression and localization in murine tissues and its specific localization within the kidney. Immunoblotting of lysates from several tissues showed that the highest level of full-length Arhgap24 protein (95-kDa band) was in the kidney. Again, the approximately 50-kDa putative breakdown product was seen in lysates from the brain, kidney, and liver. We then evaluated whether Arhgap24 was expressed in the glomeruli of the kidney. We trapped magnetic particles within the glomeruli by beating heart perfusion and then used magnetic separation to isolate whole glomeruli to more than 95% purity (Figure 2.3B). Arhgap24 was enriched in the glomerular fraction (verified by podocin immunoblotting) compared with the flow through fraction that contained mostly tubule fragments (Figure 2.3C). Next, we stained sections of mouse kidney and detected the greatest signal within glomeruli (Figure 2.3D). This signal was specific since it was completely abolished by preabsorption of the antiserum with Arhgap24 antigen (Data not shown). Within the glomeruli, the Arhgap24 signal colocalized with the podocyte marker synaptopodin, confirming that Arhgap24 is expressed in podocytes *in vivo*

(Figure 2.3E).

2.4.4 Arhgap24 knockdown restores membrane ruffling in differentiated podocytes

Having established that Arhgap24 is expressed in podocytes *in vitro* and *in vivo*, we next asked whether it was responsible for the dramatic decrease in membrane ruffling that we observed in differentiated podocytes (Figure 2.1). Membrane ruffling is dependent on the activity of the small G protein Rac1 [102]. Rac1 cycles between an active, GTP-bound state and an inactive, GDP-bound state. When activated by GEFs, Rac1 interacts with multiple downstream effectors to stimulate actin nucleation and branching required for lamellipodia formation and membrane ruffling. Subsequently, Rac1 can be inactivated by GAPs that stimulate the intrinsic GTPase activity of Rac1, resulting in the hydrolysis of GTP to GDP. Previous work has shown that Arhgap24 is a GAP protein that inactivates Rac1 [94]. Since Arhgap24 is upregulated in podocytes as they differentiate, it was a logical candidate to inactivate Rac1 and thereby slow membrane ruffling in differentiated podocytes.

We investigated whether Arhgap24 upregulation was responsible for the reduced Rac1 activity and membrane motility of differentiated podocytes. We generated podocyte cell lines (lines 451 and 756) with 2 different Arhgap24 lentiviral knockdown constructs that coexpressed the YFP-actin reporter. Compared with that of the control vector (Fluc), the podocyte cell lines transduced with the 2 knockdown constructs resulted in approximately 85% (line 451) or 60% (line 756) downregulation of the Arhgap24 protein in differentiated podocytes (Figure 2.4A). After differentiation, the control and 2 Arhgap24 knockdown cell lines were assayed for their membrane motility as before. Compared with that of the control knockdown, Arhgap24

knockdown resulted in increased membrane motility in differentiated podocytes (Figure 2.4B and Supplemental Videos 3–5). Kymograph analysis showed that Arhgap24 knockdown significantly increased membrane motility (Figure 2.4C).

Since Arhgap24 inhibits Rac1 and Cdc42 activity, we asked whether Arhgap24 knockdown resulted in increased levels of active Rac1 and Cdc42 in differentiated podocytes. We measured active Rac1, Cdc42, and RhoA by standard pull-down assays and found that the Arhgap24 knockdown cell lines had higher levels of active Rac1 and Cdc42 compared with those of the control knockdown cell line (Figure 2.5A). Interestingly, Arhgap24 knockdown did not affect RhoA activity. Another assay of Rac1 activity is epithelial monolayer wound closure. When a confluent monolayer of differentiated control knockdown podocytes was scratched/wounded, the cells migrated into the gap but did not completely close the wound in 24 hours. In contrast, both Arhgap24 knockdown cell lines showed accelerated wound closure kinetics, consistent with higher Rac1 activity (Figure 2.5B). Thus, Arhgap24 knockdown increases levels of active Rac1 and Cdc42. Two measures of increased Rac1 activity, membrane ruffling and epithelial wound closure, are enhanced when Arhgap24 levels are reduced in podocytes, consistent with its function as a Rac1-GAP.

2.4.5 Sequencing ARHGAP24 in patients with FSGS identifies several nonsynonymous changes in a highly conserved gene

Given the podocyte-specific pattern of expression of Arhgap24 and its effects on membrane dynamics and epithelial wound healing, we next asked whether variations in *ARHGAP24* were associated with kidney disease. The *ARHGAP24* gene consists of at least 8

exons (depending on the splice isoform) that span approximately 500 kilobases on the long arm of human chromosome 4. Complete exon sequencing of the *ARHGAP24* gene in 310 patients (620 chromosomes) with biopsy-proven FSGS and 180 controls (360 chromosomes) identified 13 nonsynonymous sequence variations in the 2 main splice isoforms of Arhgap24 (Table 2.1). Two of these (P417A and F539L) were found in both patients and controls and also in the 1000 genomes database (www.1000genomes.org) (Table 2.2). However, seven of the nonsynonymous changes were only found in patients and not in any of the controls. These results suggest that variation in the *ARHGAP24* gene may be linked with susceptibility to FSGS.

2.4.6 Identification of an ARHGAP24 variation in familial FSGS

Most of the nonsynonymous changes that we detected in patients with FSGS were in the uncharacterized portions of the Arhgap24 protein. However, 1 of the sequence variations (Q158R) is located in the GAP domain of Arhgap24 close to the catalytic arginine (residue 175). This variation is predicted to result in a coding change that would substitute a positively charged arginine for a neutral polar glutamine at position 158 (isoform 1; NCBI accession no. NP_001020787) or position 65 (isoform 2; NCBI accession no. NP_112595). Remarkably, this residue is conserved in the *ARHGAP24* gene across several model organisms that have been sequenced (Table 2.3). Of the other 2 nonsynonymous variations for which pedigree DNA was available (T97I and P417A), neither variation reliably correlated with disease status (Figure 2.6).

We first identified the Q158R variation in a Hispanic proband and explored the association of this variation with kidney disease in his family (Figure 2.7). The proband (patient number 1) had elevated serum creatinine levels (16 mg/dl), and a biopsy that was performed at age 20 that

showed FSGS. His sister (patient number 101) also had biopsy-proven FSGS that had progressed to end-stage kidney disease by age 12. The mother (patient number 1001) presented at a late stage and died at age 29 of renal failure. Sequencing showed that the patient's affected sister and his mother both had the Q158R variation in the *ARHGAP24* gene. In contrast, the proband's 2 other siblings did not possess this variation. The brother (patient number 100) remains healthy, but the sister (patient number 102) had pregnancy-related proteinuria and hypertension. A biopsy was not performed on this individual, and she was lost to follow-up. However, an extended haplotype consisting of 4 flanking microsatellite markers (MSMs) showed that the haplotype of this sister was similar to that of the unaffected brother, making a disease-contributing rearrangement in this region of the genome unlikely (Figure 2.7).

In addition, the exon incorporating this variation was sequenced in an additional 554 control chromosomes (for a total of 914 control chromosomes) to decrease the probability that it represented a low-frequency noncausal variation. Altogether, we had sequenced over 900 control chromosomes across this span and did not detect the Q158R change. We also sequenced members of the affected kindred for mutations in genes known to cause hereditary FSGS and nephrotic syndrome, such as *NPHS1*, *NPHS2*, *ACTN4*, transient receptor potential cation channel, subfamily C, member 6 (*TRPC6*), phospholipase C, e1 (*PLCE1*), and *WT1* (exons 8 and 9) and inverted formin, FH2 and WH2 domain containing (*INF2*) (data not shown). There were no suggestive mutations in any of these genes, ruling out known monogenic causes of FSGS in this family. Therefore, in kindred with familial FSGS, the Q158R variation of the *ARHGAP24* gene tracked with severe, early-onset kidney disease.

2.4.7 Arhgap24 Q158R has reduced Rac1-GAP activity

Another possibility was that a cosegregating mutation closely linked to the *ARHGAP24* gene was responsible for early-onset kidney disease. We therefore tested whether the Q158R variation produced a defective form of the Arhgap24 protein. The Q158R variation is located close to the catalytically active site arginine residue of the GAP domain, and so we evaluated whether this change affected the Rac1-GAP activity of Arhgap24. For these experiments, we used the mouse Q156R protein, which corresponds to Q158R in human Arhgap24. As expected, wild type Arhgap24 reduced the level of active Rac1 in cell lysates, showing again that it has GAP activity against Rac1 (Figure 2.8A). In contrast, transfection of the Q156R-mutated Arhgap24 resulted in a marked increase in the level of active Rac1. Titrating increasing levels of Q156R Arhgap24 against the wild-type protein confirmed that the Q156R mutation impairs the GAP activity of Arhgap24. Next, we tested whether the Q156R variant Arhgap24 could homodimerize and/or heterodimerize with the wild-type protein. FLAG- and GFP-tagged wild-type and Q156R versions of murine Arhgap24 were cotransfected into HEK293 cells. In bidirectional pull-down assays, we detected that both wild type and Q156R Arhgap24 homodimerized and heterodimerized (Figure 2.8B). These experiments showed that the Q158R mutation reduces the enzymatic activity Arhgap24. The fact that Arhgap24 dimerizes may explain the observed dominant effect of this mutation in our family with inherited kidney disease.

2.5 Discussions

Arhgap24, also known as FilGAP and p73RhoGAP, is the protein product of a highly

conserved gene encoded on human chromosome 4. The longer isoform of Arhgap24, which we have used exclusively in this report, is highly expressed in the kidney [94]. GAPs such as Arhgap24 and GEFs for small G proteins comprise a large family of proteins that have diverse patterns of spatial and temporal expression [103]. Such a restricted pattern of expression may allow GAPs and GEFs to behave as cell-type specific effectors for ubiquitously expressed actin regulatory proteins. Here, we show that Arhgap24 is one such candidate for cytoskeletal regulation of the kidney podocyte.

The small G proteins, Rac1, Cdc42, and RhoA, control cell shape and motility through their effects on the actin cytoskeleton. In many systems, RhoA and Rac1 are mutually antagonistic [104, 105]. However, the molecular basis of this counterregulation had been unclear until the discovery of Arhgap24. Stossel and colleagues showed that, in response to RhoA activation, Arhgap24 is phosphorylated by the RhoA effector kinase, ROCK, and this modification stimulates its GAP activity for Rac1 and Cdc42 [94]. By catalyzing the conversion of Rac1 and Cdc42 to their inactive GDP-bound state, Arhgap24 inhibits cell spreading and cell motility. Recently, a similar mechanism was demonstrated for the closely related family member, Arhgap22, in melanoma cells [106]. The diversity of GAPs likely ensures that specific ones may play a role in Rac1-RhoA counterregulation in different cell types and tissues.

Recent work from several groups has shown that the balance of RhoA and Rac1 signaling is carefully regulated in podocytes. Normally, the podocyte appears to be a stationary cell with predominantly active RhoA signaling. The podocyte-enriched adaptor protein synaptopodin controls a signaling module that promotes RhoA activity via 2 different mechanisms.

Synaptopodin blocks Smurf1-mediated ubiquitination and subsequent proteasomal degradation of RhoA [59]. Synaptopodin also disrupts IRSp53 binding to the Cdc42-Mena complex, interrupting Cdc42 signaling that opposes RhoA-mediated stress fiber formation [60]. Synaptopodin itself is phosphorylated and protected from degradation by binding to 14-3-3 [107]. Conversely, when it is dephosphorylated by calcineurin, synaptopodin is degraded by cathepsin L [107]. The net result is that reduced synaptopodin levels lead to decreased RhoA levels and activity [59].

The RhoA-Rac1 signaling balance in podocytes is also responsive to hormonal stimulation. Binding of the vasoactive hormone angiotensin II to its receptor, angiotensin receptor type I (AT1R), leads to a calcium flux through the channels Trpc5 and Trpc6. Recent work by Tian et al. has shown that Trpc5 associates with Rac1 in membrane microdomains, while Trpc6 has a separate association with RhoA [61]. In response to AT1R stimulation, Trpc5 activation leads to Rac1 activation and RhoA inactivation. Triggering Trpc6 has the opposite response, with increased RhoA activity and reduced Rac1 activity. Of note, mutations in the *TRPC6* gene have already been associated with human FSGS [17]. Therefore, this recent study by Tian et al. provides new insights into how signaling events downstream of the angiotensin receptor may lead to dynamic cytoskeletal reorganization in podocytes via selective modulation of RhoA and Rac1 activity through calcium signaling.

Decreased RhoA activity and increased Rac1 activity is associated with proteinuric kidney disease, consistent with the idea that an imbalance in the RhoA-Rac1 signaling balance is harmful to the podocyte. HIV infects podocytes and modulates the cytoskeleton of the cell such

that patients with HIV are susceptible to collapsing FSGS [108]. In podocytes, the HIV adaptor protein nef interacts with p190RhoGAP that then inactivates RhoA [109]. In addition, nef binds to diaphanous interacting protein and the Rac1-GEF vav2, resulting in Rac1 activation [110]. Nef also downregulates synaptopodin expression [111] and may further destabilize RhoA signaling via the synaptopodin pathway outlined above. The net effect of HIV infection is a downregulation of RhoA signaling activity and a shift toward Rac1 signaling with consequent podocyte injury.

There is further evidence from mouse models that disrupting the RhoA-Rac1 signaling balance in podocytes can cause kidney disease. Studies on mice deficient for the Rho-guanine nucleotide dissociation inhibitor, RhoGDI α (*Arhgdia*), demonstrate that Rac1 activation in podocytes is harmful. RhoGDI α binds to and stabilizes Rac1 and RhoA, and, in its absence, levels of these small G proteins and their activity levels are dysregulated [112]. In particular, Rac1 is relatively overactivated, leading to podocyte foot process effacement and proteinuria [56, 113]. Interestingly, treatment with a Rac1 inhibitor reduced proteinuria and the severity of the kidney damage in this model.

Taken together, these studies highlight that the careful control of relative RhoA and Rac1 activity is critical for the proper functioning of podocytes. However, we believe that until this report a direct regulator of Rac1 activity in response to RhoA signaling had not been described in podocytes. Here, we show that *Arhgap24* is highly expressed in podocytes and inhibits Rac1-dependent membrane ruffling and epithelial wound healing. Our work predicts that *Arhgap24* would enforce the normal RhoA-dependent nonmotile podocyte phenotype by inactivating Rac1. Consistent with a role for *Arhgap24* *in vivo*, we identified a mutation in the

GAP domain of Arhgap24 in kindred with familial FSGS. This mutation reduces the Rac1-GAP activity of Arhgap24. We also show that Arhgap24 dimerizes, and this may explain the dominant pattern of inheritance of the Q158R mutation [114, 115]. Our studies show that *Arhgap24* is a potential candidate gene to explain a subset of inherited FSGS. Perhaps, more informatively, Arhgap24 adds to the emerging model that aberrant Rac1 activation is a key step in podocyte dysfunction, leading to proteinuric kidney disease. Since Arhgap24 is selectively expressed in podocytes, modulating its function can alter relative RhoA/Rac1 activity, with potentially minimal systemic side effects, and provides an intriguing pathway for the therapy of proteinuric kidney disease.

Acknowledgements

We are grateful for the support of Washington University George M. O'Brien Center for Kidney Disease Research (P30 DK079333) for some of the patient specimens. We would like to thank Jeffrey Miner for helpful discussions and Jiancheng Hu for technical assistance and reagents for the GTPase activity pull-down assays. This work was supported in part by the NIDDK Intramural (to J.B. Kopp) and Extramural Research Programs (RO1DK058366, to A.S. Shaw), Howard Hughes Medical Institute, and the Medical Scientist Training Program Grant to Washington University School of Medicine.

* This chapter is adapted from Akilesh S., *et al.* Arhgap24 (FilGAP) inhibits Rac1 activity in mouse podocytes and is associated with familial focal segmental glomerulosclerosis. *J Clin Invest.* 2011; 121(10): 4127-37.

2.6 Tables and Figures

Table 2.1 Incidence of ARHGAP24 nonsynonymous sequence variations in patients with biopsy-proven FSGS (n=310) and controls (n=180)

Variation	No. affected	No. controls
Isoform 1		
T97I	1	0
R142C	1	0
Q158R	2	0
L215V	0	1
Q359R	0	1
S396L	1	0
P417A	9	2
T451I	1	0
T481M	2	0
F539L	5	5
N587I	0	1
Isoform 2		
P2L	3	1
R5L	1	0

The isoform 1 protein reference sequence is NCBI accession no. NP_001020787, and the isoform 2 reference sequence is NCBI accession no. NP_112595.

Table 2.2 Non-synonymous SNPs in ARHGAP24

Non-synonymous SNPs identified in the transcript of isoform 1 of ARHGAP24 from over 1000 human genomes sequenced. (www.1000genomes.org) SNPs in bold are known polymorphisms in the gene.

<u>Residue</u>		
<u>Variation</u>	<u>SNP ID</u>	<u>Alleles</u>
R142H	rs36067390	G/A
Q359R	LWK_P3:4:87134907:G	A/G
D368G	YRI_P3:4:87134934:G	A/G
P417A	rs35521695	C/G
V420I	LWK_P3:4:87135089:A	G/A
K421Q	YRI_P3:4:87135092:C	A/C
G473V	YRI_P3:4:87135249:T	G/T
R483H	LWK_P3:4:87135279:A	G/A
R499Q	TSI_P3:4:87135327:A	G/A
F539L	YRI_P1:4:87135446:C	T/C
G618S	CEU_P3:4:87135683:A	G/A
R622H	JPT_P3:4:87135696:A	G/A
M696K	JPT_P3:4:87140739:A	T/A
E721*	rs13292	G/T

Table 2.3 Q158 is a conserved residue

Sequence alignment of the Arhgap24 protein across various species in the region of the patient variation (Q158) shows complete conservation of the glutamine residue.

Species	aa	Sequence	aa	Accession no.
<i>Homo sapiens</i>	141	vryekrygnr lapmlve Q cv dfirqrglke	170	NP_001020787
<i>Pan troglodytes</i>	330	vryekrygnr lapmlve Q cv dfirqrglke	359	XP_001144292
<i>Mus musculus</i>	139	vryekrygnr lapmlve Q cv dfirqrglke	168	NP_083546
<i>Rattus norvegicus</i>	140	vryekrygnr lapmlve Q cv dfirqrglke	169	Q5U2Z7
<i>Callithrix jacchus</i>	141	vryekrygnr lapmlve Q cv dfirqrglke	170	XP_002745675
<i>Equus caballus</i>	140	vryekrygnr lapmlve Q cv dfirqrglke	169	XP_001495166
<i>Bos taurus</i>	46	vryekrygnr lapmlve Q cv dfirqrglke	75	DAA28474
<i>Canis familiaris</i>	58	vryekrygnr lapmlve Q cv dfirqrglke	87	XP_849790
<i>Gallus gallus</i>	141	vryekrygnr lapmlve Q cv dfirqrglke	170	XP_420552
<i>Monodelphis domestica</i>	156	vsfekryrnc lapmlve Q cv dfirqrglke	185	XP_001371013
<i>Danio rerio</i>	144	vryerrygnk mapmlve Q cv dfirnwglre	173	XP_001339010

The location of the region of interest in each protein is designated by the amino acid start and finish positions. The glutamine residue is shown in bold. NCBI accession numbers are shown.

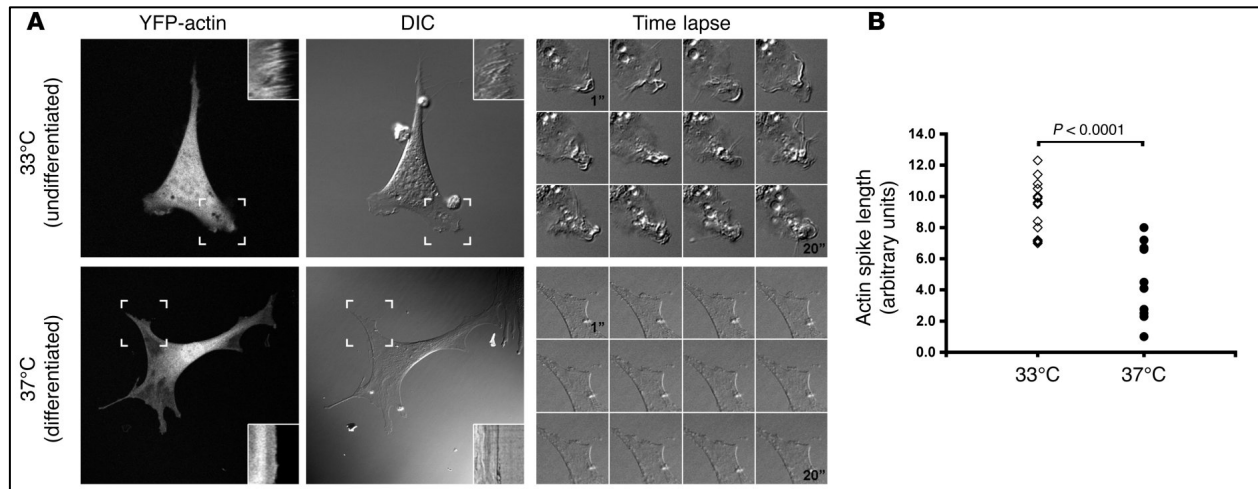


Figure 2.1 Differentiated podocytes show reduced membrane ruffling

(A) YFP-actin–transduced podocytes were cultured at the permissive temperature (33°C) or differentiated for 7 to 14 days at the nonpermissive temperature (37°C). Kymographs (insets) obtained at the sites of active ruffling (hatched boxes) show prominent ruffling at 33°C that is reduced at 37°C (also see Supplemental Videos 1 and 2). DIC, differential interference contrast. Original magnification, $\times 400$; approximately $\times 1,000$ (insets and time-lapse panels). (B) Quantification of actin spike lengths in kymographs shows that differentiated podocytes ($n = 11$) have a significant decrease in ruffling activity compared with that of undifferentiated podocytes ($n = 15$). Individual symbols represent data from individual podocytes. $P = 3.29 \times 10^{-6}$ by ANOVA with post-test correction.

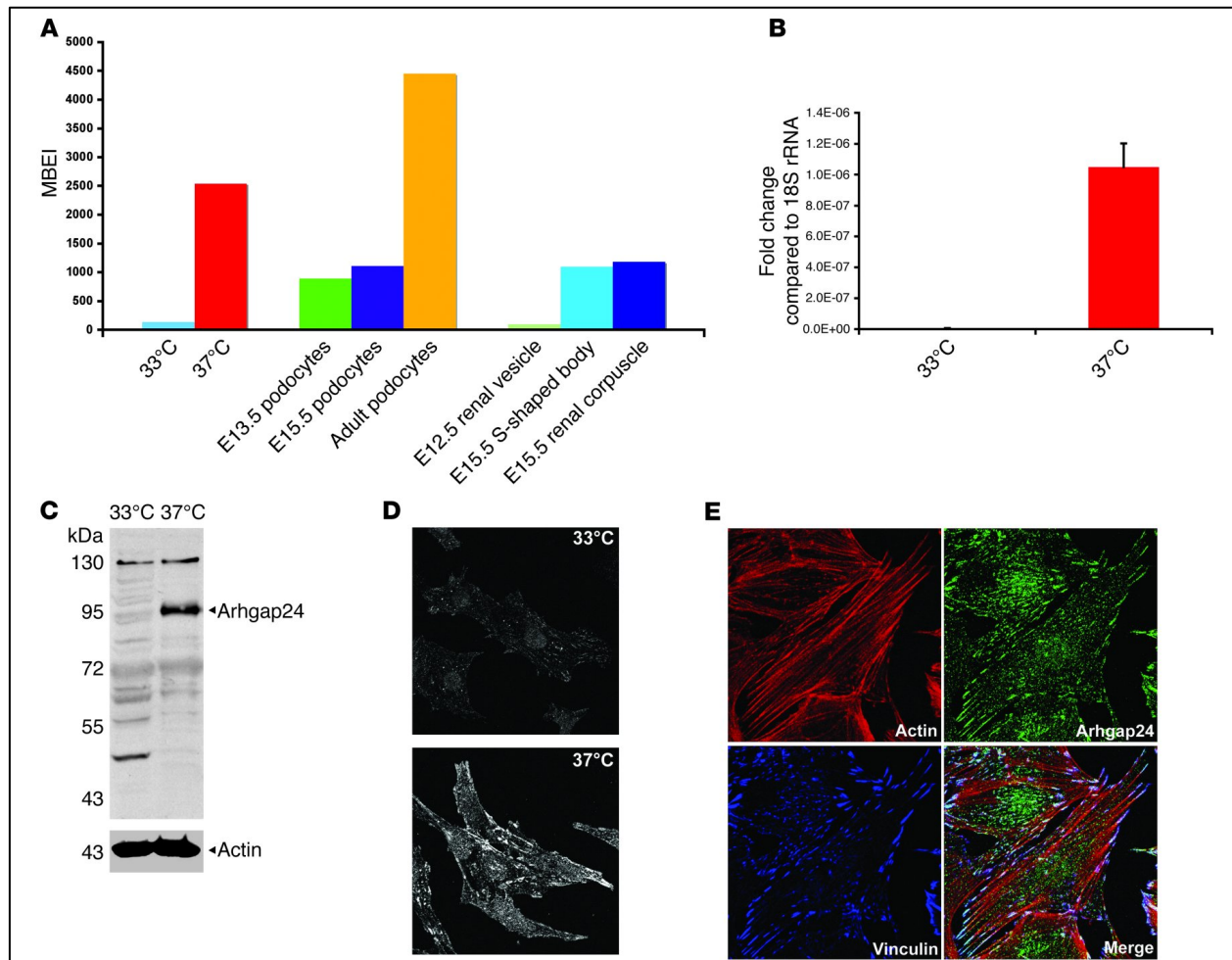


Figure 2.2 *Arhgap24* transcript and *Arhgap24* protein are specifically expressed in podocytes

(A) MBEI values for microarray data for *in vitro*-cultured podocytes (33°C, 37°C), ex vivo-isolated podocytes (E13.5, E15.5, and adult), and laser-capture-microdissected glomeruli (E12.5 renal vesicle, E15.5 S-shaped body, and E15.5 renal corpuscle) show an increase in the *Arhgap24* transcript with differentiation *in vitro* and *in vivo*. (B) By quantitative RT-PCR, differentiated podocytes have higher *Arhgap24* mRNA levels compared with those of undifferentiated podocytes, after normalization to 18S rRNA. (C) Immunoblotting shows that differentiated podocytes have higher levels of *Arhgap24* protein than undifferentiated podocytes. (D) Confocal imaging of cultured podocytes also shows an increase in levels of *Arhgap24* in differentiated podocytes, concentrated in punctate structures at the base of the cell. (E) *Arhgap24* colocalizes with the focal adhesion marker vinculin at the tips of actin stress fibers. Original magnification, $\times 600$ (D and E).

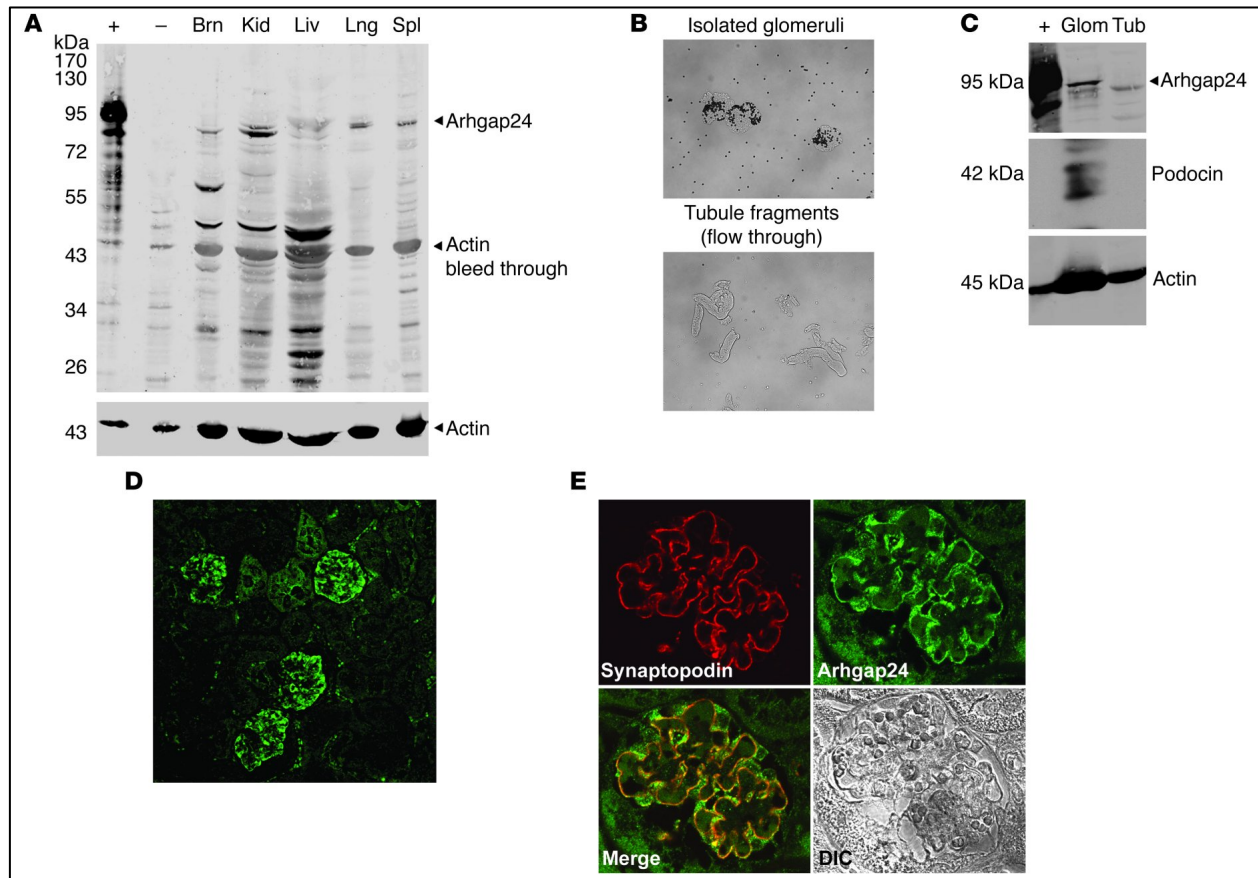


Figure 2.3 Arhgap24 is expressed in kidney podocytes *in vivo*

(A) Immunoblotting of tissue lysates shows that Arhgap24 is expressed in the kidney (expected size ~95 kD). Smaller bands likely represent specific degradation products. The positive control (+) is a lysate from HEK293 cells transfected with FLAG-tagged Arhgap24. The negative control (-) is HEK293 cell lysate. Brn, brain; Kid, kidney; Liv, liver; Lng, lung; Spl, spleen. (B) Magnetic separation of glomeruli after beating heart perfusion of mice with magnetic beads results in more than 95% pure isolated glomeruli (top). The flow through consists of tubule fragments (bottom). Original magnification, $\times 100$. (C) Arhgap24 is enriched in the glomerular (Glom) fraction that also contains the podocyte protein, podocin. Tub, tubule. (D) A low-magnification view (original magnification, $\times 200$) of a mouse kidney stained for Arhgap24 shows that the highest signal is detected in the glomeruli. (E) Within mouse glomeruli, the Arhgap24 signal colocalizes with that of the podocyte marker synaptopodin. Original magnification, $\times 600$.

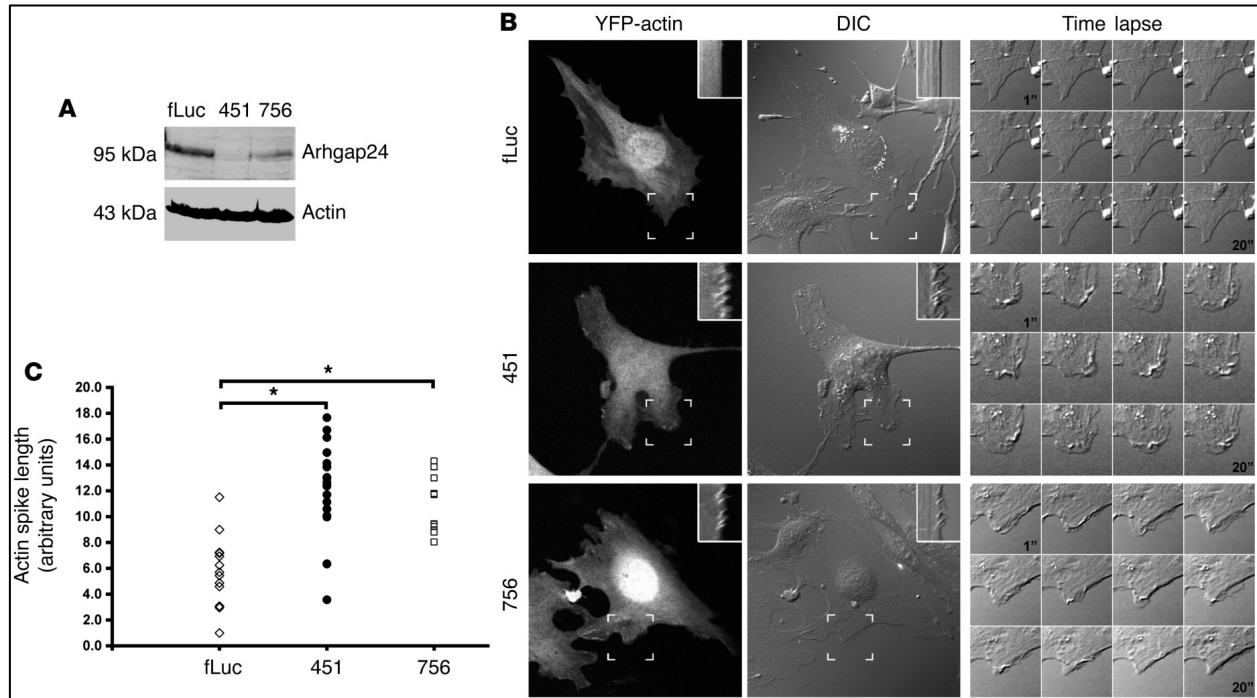


Figure 2.4 Arhgap24 knockdown in differentiated podocytes increases membrane ruffling

(A) Two lentivirally transduced cell lines targeting different portions of the *Arhgap24* transcript show marked reduction of Arhgap24 protein compared with that of an irrelevant knockdown (Fluc, 100%; line 451, 15%; line 756, 40%). Results are representative of at least 3 independent experiments. (B) Representative images of the 3 knockdown cell lines after differentiation at 37°C for 7 to 10 days. Kymographs (insets) generated from the hatched box area and time-lapse sequences show that the 2 knockdown cell lines have increased membrane ruffling compared with that of the control (also see Supplemental Videos 3–5). Original magnification, $\times 400$; approximately $\times 1,000$ (insets and time-lapse panels). (C) Quantitation of actin spikes in kymographs shows that both the 451 ($n = 19$) and 756 ($n = 11$) Arhgap24 cell lines have significantly greater membrane ruffling activity compared with that of the control knockdown Fluc cell line ($n = 18$) ($*P < 0.00001$). The ruffling activity is not significantly different between the 2 knockdown cell lines ($P = 0.57$). Group differences were analyzed by ANOVA with post-test correction.

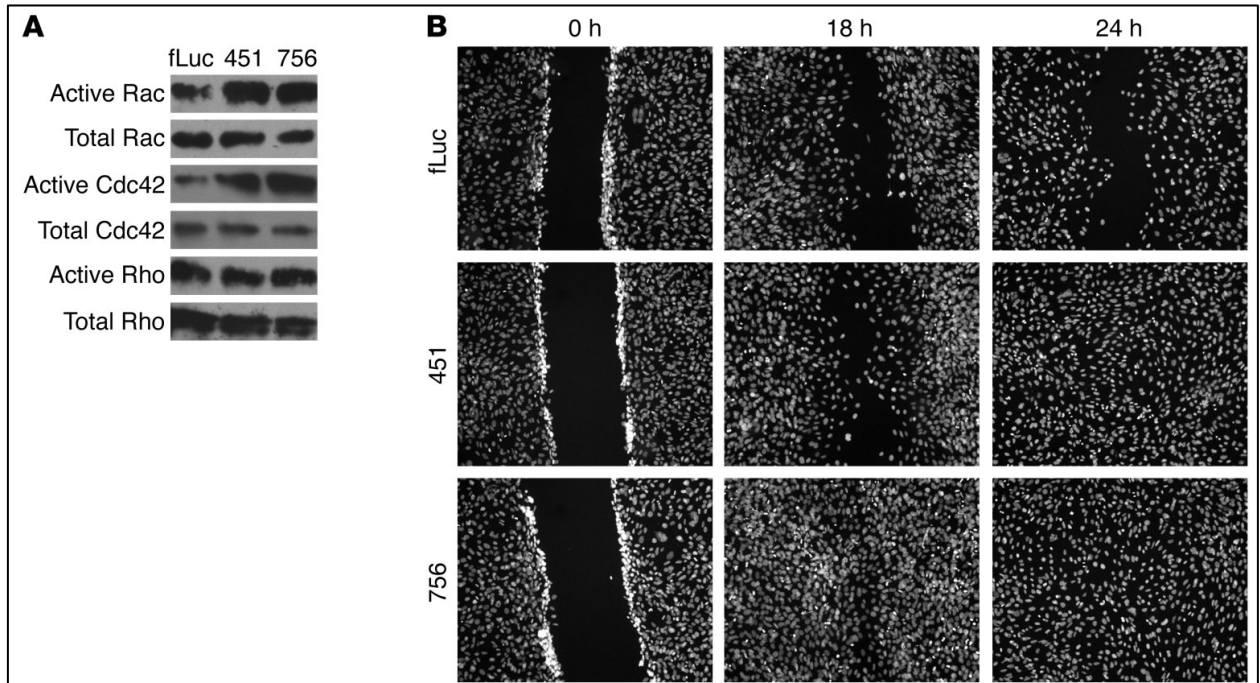


Figure 2.5 Arhgap24 knockdown in differentiated podocytes increases active Rac1 and Cdc42 levels and accelerates epithelial monolayer wound closure

(A) Pull down of active (GTP-bound) Rac1, Cdc42, and RhoA shows that the Arhgap24 knockdown cell lines (lines 451 and 756) have increased levels of active Rac1 and Cdc42 compared with those of the control (Fluc). However, active RhoA levels are similar across all 3 cell lines. Results are representative of 3 independent experiments. (B) Arhgap24 knockdown cells migrate and close a scratch made in a confluent monolayer faster than the control knockdown cell line. Cell nuclei were stained with Hoechst dye. Original magnification $\times 100$.

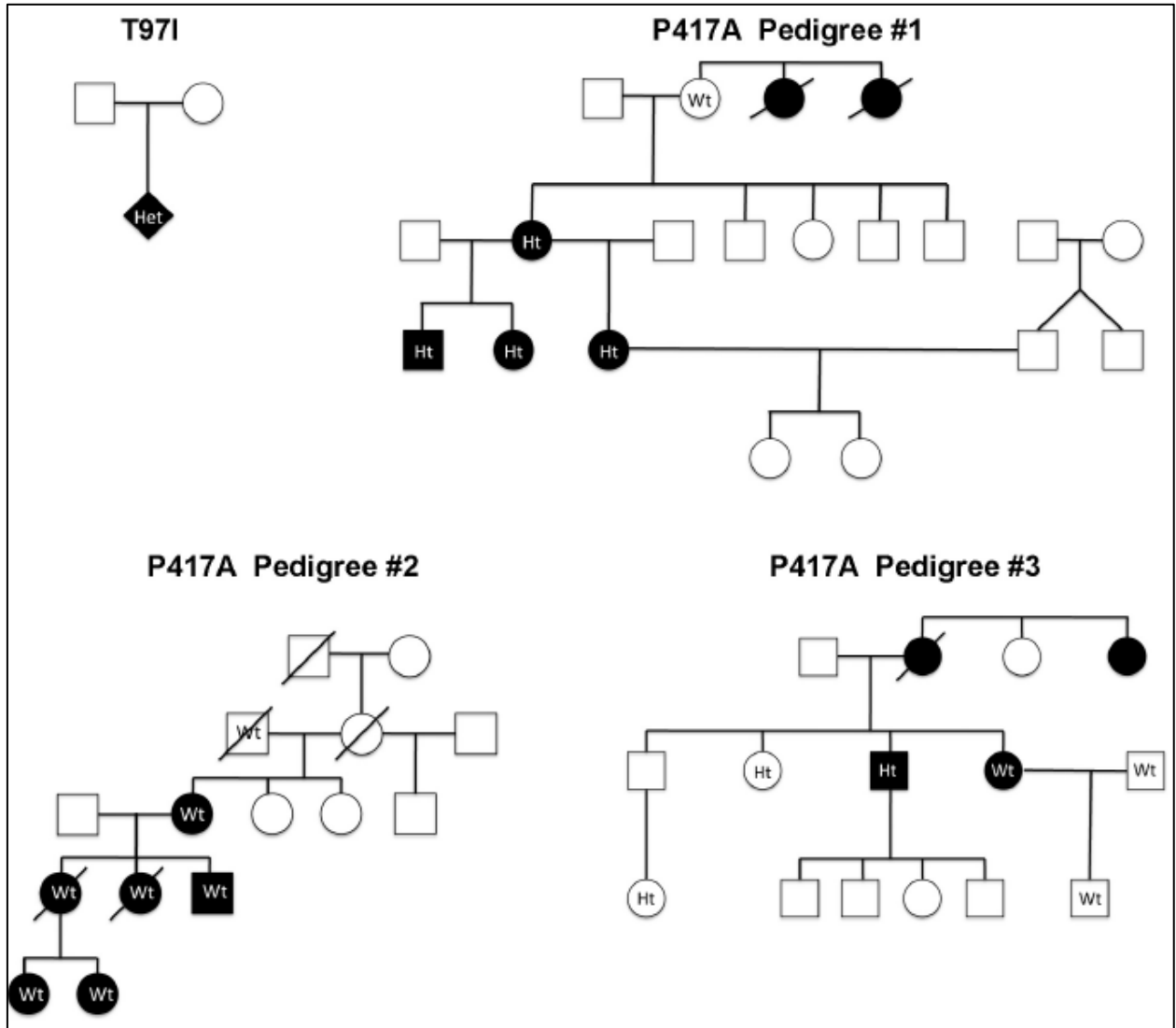


Figure 2.6 Pedigree information for T97I and P417A variations

DNAs from one family for the T97I variation and three families for the P417A variation were available for sequence analysis. The presence of kidney disease (clinical and/or biopsy proven) is denoted by the filled-in symbols. If DNA was analyzed for sequence variation, the result of a non-synonymous variation is denoted within the individual symbol (Wt =wildtype; Ht = heterozygous). The reference protein sequence (NP_001020787) was considered wildtype. In no instance did the variation consistently correlate with kidney disease.

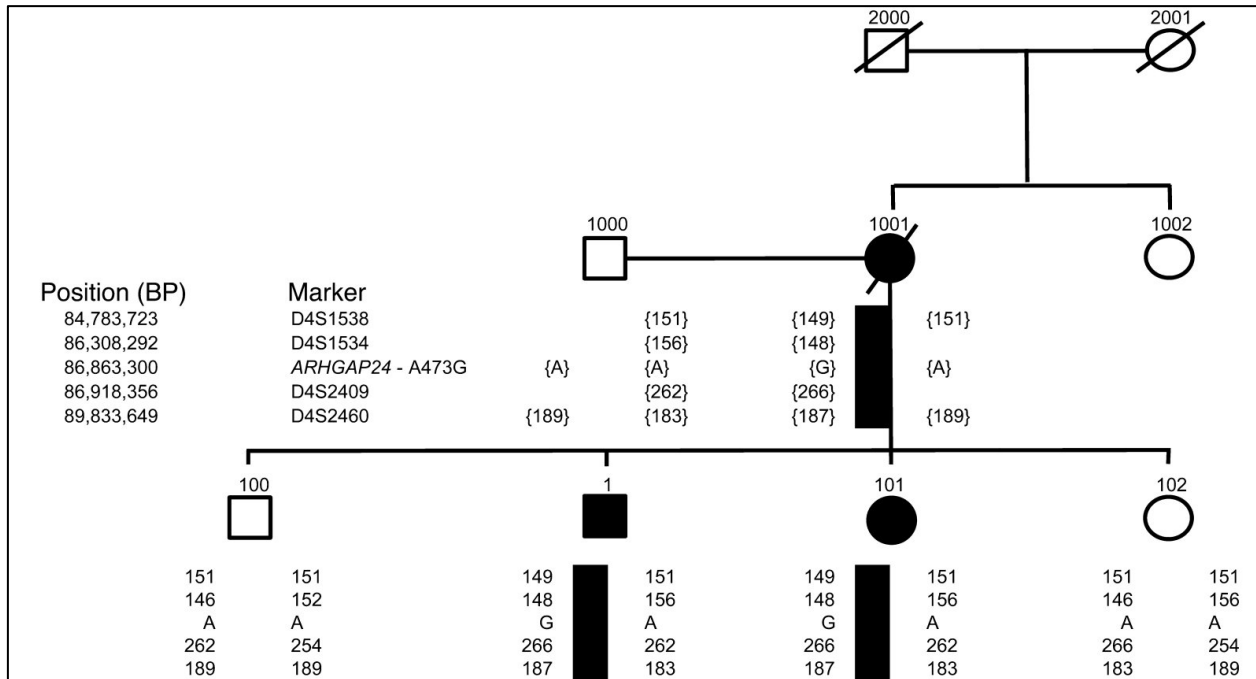


Figure 2.7 Individuals with end-stage kidney disease are denoted by black symbols

Deceased family members are represented by diagonal lines. Flanking MSM analysis shows that the unaffected siblings have a distinct haplotype that is different from that of the affected individuals. The columns of numbers and letters under each symbol refer to the alleles that individual carries at the given genetic markers. Where these numbers are within brackets, the haplotype is inferred. The solid black rectangle beneath individuals 1, 101, and 1001 represents the inherited disease haplotype.

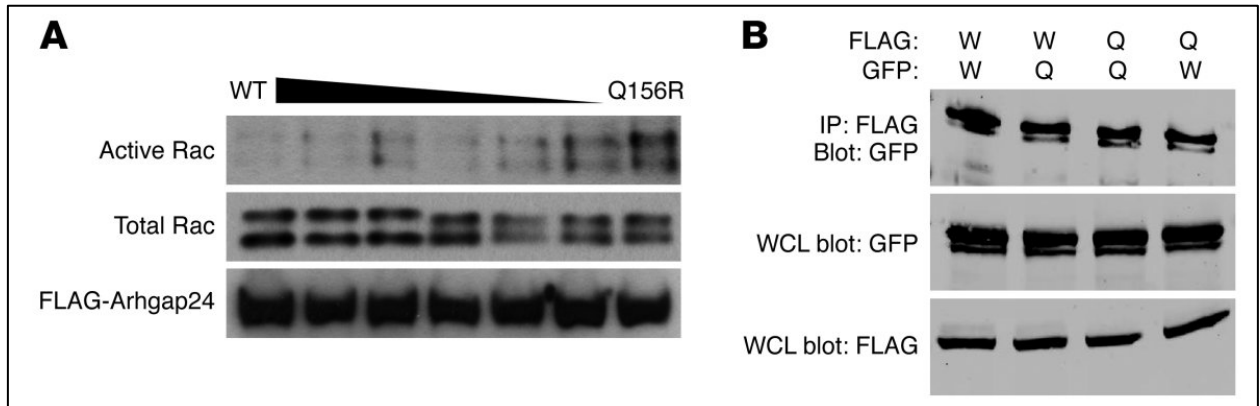


Figure 2.8 Arhgap24 Q158R has defective Rac1-GAP activity and dimerizes with the wild-type protein

(A) Wild-type FLAG-tagged Arhgap24 (first lane) transfected into HEK293 cells reduces active Rac1 levels compared with Q156R Arhgap24 (last lane). Titration of increasing proportions of Q156R Arhgap24 produces increased levels of active Rac1 (middle lanes). Total Rac1 and FLAG-Arhgap24 protein levels are similar across all lanes. Results are representative of 3 different experiments. (B) FLAG- or GFP-tagged wild-type (W) or Q158R Arhgap24 (Q) constructs were cotransfected into HEK293 cells. Cell lysates were immunoprecipitated with anti-FLAG antibody and then immunoblotted for GFP-tagged Arhgap24 to assess for protein dimerization. Whole cell lysates (WCLs) were immunoblotted for GFP and FLAG to ensure protein expression.

Chapter 3. Rac1 Activation in Podocytes Induces Rapid Foot Process Effacement and Proteinuria

3.1 Abstract

The kidney's vital filtration function depends on the structural integrity of the glomerulus, the proximal portion of the nephron. Within the glomerulus, the architecturally complex podocyte forms the final cellular barrier to filtration. Injury to the podocyte results in a morphologic change called foot process effacement and this is a ubiquitous feature of proteinuria. The exact nature of foot process effacement is not known but recently it has been proposed that this might reflect activation of the Rac1 GTPase. To test this hypothesis, we generated a podocyte specific, inducible transgenic mouse line that expressed constitutively active Rac1. We observed a rapid onset of proteinuria that began to remit spontaneously in one week. Using super resolution imaging, we verified that the induced transgene was expressed in damaged podocytes. The kinetics of this podocyte injury model differs from previously reported studies and highlights the complex balance of Rho-GTPase signaling that is required for proper regulation of the podocyte cytoskeleton.

3.2 Introduction

The structural integrity of the proximal portion of the nephron, the glomerulus, is vital to the kidney's filtration function. Within the glomerular capillary tuft, the kidney's filtration barrier is a biomechanical composite of fenestrated endothelial cells, a thick glomerular basement

membrane and complex visceral epithelial cells called podocytes. Podocytes lie on the outer aspect of glomerular capillaries and extend cytoplasmic processes (foot processes) that interdigitate with those from neighboring podocytes to form a mesh-like network that forms the final barrier to filtration. Podocyte foot processes are built around highly organized actin bundles that are reorganized during injury with flattening and simplification (“effacement”) of foot processes leading to spillage of serum proteins into the urine (proteinuria). Defects in actin regulatory proteins lead to irreversible podocyte injury and focal and segmental glomerulosclerosis (FSGS) in humans and in animal models [2].

Recent studies show that rather than being a static filter, the cytoskeleton and therefore the shape of the podocyte are both tightly regulated and dynamic [52]. Small GTPases of the Rho family (exemplified by RhoA, Cdc42, Rac1) are the central organizers of the actin cytoskeleton [48]. After receiving diverse signaling inputs, the Rho-family of small GTPases act through their effectors to polymerize and organize actin filaments into various configurations that deform the cell membrane and change cell shape. Of the three major Rho-family GTPases, Cdc42 has been shown to be critical for podocyte development, while both RhoA and Rac1 seem dispensable in early stages [28].

After this initial phase, RhoA and Rac1 seem to play more important roles in podocyte cell biology. In many biological systems, including podocytes, RhoA and Rac1 antagonize each other’s activation and function [50, 116]. Recent studies have shown that constitutive activation of RhoA causes podocyte foot process effacement and proteinuria after several weeks [49, 117], suggesting that inappropriate RhoA activation is pathogenic to podocytes. This is surprising

given that 1) activation of Rho family GTPases causes rapid cytoskeletal rearrangement *in vitro* [118, 119]; and 2) introduction of dominant-negative RhoA produces a similar phenotype [49].

On the other hand, it has been proposed that excessive Rac1 activation or inhibition of Rho activity might be the key step in podocyte injury. Synaptopodin, a podocyte actin-binding protein, reinforces RhoA signaling and suppresses Cdc42 signaling to promote proper cytoskeletal architecture [59, 120]. Genetic ablation of synaptopodin in mice results in increased susceptibility to proteinuria [60, 121]. Deletion of RhoGDI (a negative regulator of Rho-family GTPases) in mice results in foot process effacement and proteinuria that correlates with increased Rac1 activity [56]. Mutations in the GTPase activating protein Arhgap24 result in increased Rac1 activation *in vitro* and are correlated with podocyte injury and FSGS in patients [122].

The effects of Rac1 activation in podocytes have only been studied indirectly through the manipulation of upstream regulatory proteins [21, 56, 122, 123]. To test directly whether Rac activation induces podocyte foot process effacement, we generated a double transgenic system in mice in which GFP-tagged constitutively active Rac1 (Rac1Q61L) is expressed in podocytes after doxycycline (DOX) induction. We observed rapid onset of proteinuria within 2 days of DOX induction. The degree of proteinuria correlated with the levels of active Rac1 expression. However, proteinuria in this system was not durable and gradually decreased over the course of a month despite continuous exposure to DOX. Thus, activation of Rac1 in podocytes rapidly causes foot process effacement and proteinuria *in vivo*. These results are distinct from the effects of RhoA activation in podocytes and emphasize the complex interplay of small GTPase signaling in the regulation of podocyte shape and function.

3.3 Methods

3.3.1 Generation of EGFP_CA-Rac1 knock-in transgenic mice

We chose the X-linked *Hprt1* locus for targeting because it is a nonessential housekeeping gene that encodes a selectable marker [124, 125]. The pHPRT targeting vector was generated on a pBluescript SKII(-) backbone by PCR amplifying the left arm (5.1 kb fragment upstream of Exon 1) and right arm (2.1 kb fragment downstream of Exon 1) of the *Hprt1* gene from a bacterial artificial chromosome (RP24-335G16). The tetracycline responsive promoter element (TRE), EGFP, Rac1Q61L, and bovine growth hormone polyadenylation signal (bGH-polyA) sequences were amplified by PCR, and inserted sequentially into the pHPRT targeting vector. The KH2 ES cell line harboring the *Rosa26*-M2rtTA insertion was used for transfection. Cells with homologous recombination of the transgene into the *Hprt1* locus were selected based on their growth in the presence of 6-thioguanine, which is toxic to cells expressing functional *Hprt1*. Appropriate single copy insertion of the EGFP_CA-Rac1 transgene into the *Hprt1* locus was confirmed by PCR. Targeted ES cells were injected into blastocysts to generate chimeric mice. EGFP genotyping primers (a protocol from The Jackson Laboratory) were used for genotyping (Forward_oIMR0872 5'-AAGTTCATCTGCACCACCG-3', Reverse_oIMR1416 5'-TCCTTGAAGAAGATGGTGCG-3'; internal positive control Forward_oIMR7338 5'-CTAGGCCACAGAATTGAAAGATCT-3', Reverse_oIMR7339 5'-GTAGGTGGAAATTCTAGCATCATCC-3'). All animal experiments were conducted with approval of the Washington University Animal Studies Committee.

3.3.2 Mouse strains and transgene induction

The *Rosa26-rtTA* mouse strain was purchased from The Jackson Laboratory (#006965). The *NPHS2-rtTA* strain was obtained from Dr. Jeffrey Kopp at the NIH. The *Nphs1-rtTA-3G* strain will be described in detail elsewhere [126]. All mice used in this study were male and therefore carried a single copy of the EGFP_CA-Rac1 transgene. To induce transgene expression, regular chow was substituted with DOX-supplemented chow (2000ppm, TestDiet) for the indicated time periods.

3.3.3 Cell culture and cell based assays

Immortalized murine podocytes were maintained and differentiated as described previously [122]. For live cell imaging assays, podocytes were infected with lentiviral vectors encoding N-terminal EGFP tagged CA-Rac1 and CA-RhoA. An EGFP empty vector was used as control.

3.3.4 Antibodies

Antibodies for immunostaining included rabbit anti-podocin (Sigma Aldrich P0372, 1:400 dilution), goat anti-nephrin (R&D Systems AF3159, 1:100 dilution), rabbit anti-laminin β 2 (20) (1:1500 dilution) and chicken anti-GFP (Invitrogen A10262, 1:500 dilution). Antibodies used for immunoblotting were mouse anti-GFP (Clontech 632381, 1:10000 dilution), rabbit anti-ERK2 (Santa Cruz Biotechnology sc-154, 1:5000 dilution) and rabbit anti-podocin (Sigma-Aldrich P0372, 1:500 dilution). Fluorescently-conjugated secondary antibodies were purchased from Jackson ImmunoResearch, and the STORM antibodies were conjugated as described [127].

3.3.5 Immunofluorescence assays

Fresh kidney tissue was embedded in OCT compound and snap frozen on dry ice. 8 μm cryosections were applied to charged slides. Cultured podocytes were seeded onto collagen I coated coverslips. For immunofluorescence assays, the tissue sections or coverslips containing podocytes were fixed with 1% PFA in PBS for 5 minutes followed by blocking and permeabilization with 2% FBS in PBS with 0.1% saponin. Primary antibodies at the indicated dilutions were applied for 1 hour at room temperature. After extensive washes, fluorescently conjugated secondary antibodies were applied at 1:500 dilution for another hour at room temperature. After washing, the prepared slides were imaged on a Olympus FV-1000 spinning disc confocal microscope.

3.3.6 Albumin/creatinine assay

Mouse urine samples were collected at the indicated time points and urinary albumin (Bethyl, E90-134) and creatinine (BioAssay Systems, DICT-500) were quantified by ELISA according to the manufacturers' protocols.

3.3.7 Transmission Electron Microscopy

Portions of kidney cortex were fixed with 2% paraformaldehyde and 2% glutaraldehyde and processed for electron microscopy. Ultrathin sections were prepared and imaged by the Electron Microscopy Core Facility at Washington University.

3.3.8 STORM imaging and STORM-SEM correlation

Kidney tissues were fixed in 4% paraformaldehyde and cryoprotected in 30% sucrose. Tissues were then embedded in OCT compound and semi-thin sectioned at 100-200 nm thickness using an ultra cryomicrotome. These tissue sections were collected on a

carbon-coated #1 coverslip and fixed and stained as described previously [127]. Using a custom STORM microscope, 20,000 imaging cycles were collected and the resulting images were compiled to generate a composite multi-channel image as described earlier [128]. After STORM imaging, the coverslip was floated off and the sample was fixed with 2% glutaraldehyde. This sample was then processed for scanning electron microscopy (SEM). The images obtained from STORM and SEM were superimposed using Photoshop CS5.1.

3.3.9 Live cell imaging and kymograph analysis

Undifferentiated murine podocytes were transiently transfected using Amaxa Nucleofection (Lonza, Allendale, NJ) with plasmids encoding for constitutively active Rac1 or RhoA. Transfected podocytes were cultured on collagen I-coated glass-bottomed dishes overnight, and serum starved for 6 hours to arrest baseline membrane ruffling. Rac1 transfected podocytes were imaged in the serum starved state, while Rho transfected podocytes were imaged following the addition of 10% FBS 10 minutes prior to imaging to induce membrane ruffling. Sequential images were obtained by an Olympus FluoView FV1000 microscope every 10 seconds for a 20-minute duration, and movies assembled using Olympus Fluoview software. The ImageJ plug-in, Multiple Kymograph (<http://rsbweb.nih.gov/ij/>), was used to generate kymographs at 5 different locations of maximum membrane ruffling for each imaged cell [100]. 10 actin spikes were measured for each kymograph, and average length (ruffling index) was determined as previously described [100].

3.3.10 Rac1 pull-down assay

The GST-tagged Pak1-PBD was expressed in BL21(DE3) *E. coli* and purified using

glutathione-agarose beads. For the active Rac1 pull-down assay, whole kidney lysates were generated by homogenizing the kidneys in cell lysis buffer (50mM Tris-HCl, pH7.5, 150mM NaCl, 5mM MgCl₂, 10% Glycerol, 1% NP-40, 1mM DTT, 1mM PMSF, 10µg aprotinin, 10µg leupeptin; aprotinin, leupeptin, DTT and PMSF are fresh added), and isolating the supernatant. Equal volumes of the lysates were incubated with GST-PBD beads. Rac1-GTP bound to the beads (active Rac1) was eluted with Laemmli sample buffer and examined by western blot.

3.4 Results

3.4.1 Rho family GTPases induce distinct effects on the actin cytoskeleton in cultured murine podocytes

A network of highly organized actin cytoskeleton structures forms the structure of podocyte foot processes. During podocyte foot process effacement, these actin bundles are reorganized into broad membrane sheets that resemble lamellipodia seen in cultured cells. Numerous cell culture systems point to a critical role for Rho family GTPases in actin cytoskeleton remodeling with RhoA activation inducing actin bundling and Rac1 activation inducing lamellipodia [48]. Therefore, we hypothesized that the remodeling of the podocyte actin cytoskeleton seen during the process of effacement may represent an alteration in the balance between Rac1 and RhoA activities [122].

To test the effects of Rho GTPase activation on the podocyte actin cytoskeleton *in vitro*, we first transfected a murine immortalized podocyte cell line with enhanced green fluorescent protein (EGFP) fused to constitutively active versions of Rac1 (EGFP_CA-Rac1) and RhoA

(EGFP_CA-RhoA). Actin fibers and focal adhesions were visualized with phalloidin and vinculin respectively. Constitutively active Rho (CA-Rho) increased the number of stress fibers and focal adhesions in podocytes (Figure 3.1A). In contrast, CA-Rac1 expression in podocytes induced membrane spreading and lamellipodia formation resulting in large, round and flattened cells (Figure 3.1A).

Since foot process effacement might be an expression of podocyte motility [93], we next asked if these changes in cell morphology correlated with changes in podocyte membrane dynamics. Using live cell imaging, we quantitated membrane motility using kymograph analysis as described previously [122]. Podocytes expressing CA-Rac1 show increased membrane ruffling compared with wild type cells after serum starvation (Figure 3.1B, and Videos S1 and S2). Addition of serum induced membrane ruffling in wild type cells, and this was largely suppressed in podocytes expressing CA-RhoA (Figure 3.1C, and Videos S3 and S4). These experiments confirmed that activation of Rac1 and RhoA produce marked changes in the podocyte actin cytoskeleton and on membrane dynamics. Active Rac1 induced lamellipodia formation and increased membrane motility in podocytes, while active RhoA stabilized the cytoskeleton and suppressed membrane motility.

3.4.2 Generation of inducible EGFP CA-Rac1 transgenic mice

Our *in vitro* results suggested that Rac1 activation might have significant effects on podocyte morphology. This is in contrast to recent studies that showed RhoA activation could play a pathogenic role in podocytes *in vivo* [49, 117]. To test the effects of Rac1 activation in podocytes *in vivo*, we generated a transgenic mouse model that would allow for inducible

expression of EGFP_CA-Rac1. Using homologous recombination, we targeted the EGFP_CA-Rac1 transgene into the *Hprt1* locus in ES cells [124, 125] (Figure 3.2A) containing the tetracycline inducible transactivator (rtTA) inserted into the *Rosa26* locus (*Rosa-rtTA*) [129]. Cells with successful homologous recombination of the transgene for the *Hprt1* locus were selected based on their growth in the presence of 6-thioguanine, which is toxic to cells harboring a functional *Hprt1* allele. Targeted gene insertion was confirmed by PCR (Figs. 2 B and C) and recombinant ES cells were microinjected into blastocysts to generate chimeric mice.

To test inducible expression of the EGFP_CA-Rac1 transgene, mice were fed doxycycline (DOX) for one week, and multiple tissues were harvested and examined for EGFP expression by fluorescence microscopy (Figure 3-S1). DOX induced strong transgene expression in multiple tissues. However, we could not detect EGFP expression in podocytes by fluorescence microscopy. These experiments revealed that the *Rosa26-rtTA* allele was ineffective at driving efficient transgene expression in podocytes.

3.4.3 EGFP_CA-Rac1 expression in podocytes causes rapid onset but transient proteinuria

To induce podocyte-specific expression of the CA-Rac1 transgene, we crossed our mice with transgenic mice with the rtTA driven by the human podocin promoter (*NPHS2-rtTA*) [130]. In double transgenic mice (PODxRac1) fed DOX, EGFP expression was detectable as early as 4 days after induction. To validate the functionality of the CA-Rac1 transgene product, we used the p21 binding domain of PAK1 (PBD) to precipitate CA-Rac1 from whole kidney lysates of DOX-treated double transgenic mice (Figure 3.2D). EGFP_CA-Rac1 protein was easily detectable in the DOX-treated mice but was undetectable in the absence of DOX. Expression of

the transgene was barely detectable in the whole kidney lysate, which was not surprising given that podocytes constitute only a small fraction of cells in the kidney. Expression of the CA-Rac1 transgene in podocytes was confirmed by colocalization with the podocyte-specific marker (podocin) by immunofluorescence microscopy (Figure 3.3A). Surprisingly, the CA-Rac1 transgene was expressed in only a small fraction of podocytes, and this expression was variable between glomeruli and between mice.

After 2 days of induction with DOX, however, PODxRac1 mice developed significant proteinuria compared to single transgenic control mice. Proteinuria reached its peak on day 4 and then began to abate around 1 week post-induction (Figure 3.3B, and 3-S2). DOX treatment for up to one month did not result in progressive renal dysfunction or significant histologic alterations. Given the variable expression of the transgene, we assessed whether the level of proteinuria correlated with the level of expression (Figure 3.3C). The magnitude of proteinuria positively correlated with the frequency of EGFP-positive glomeruli. The kinetics of proteinuria, however, were similar among all PODxRac1 mice beginning around day 2 and abating after day 7 (Figure 3-S2). These experiments showed that podocyte-specific expression of CA-Rac1 induces rapid and transient proteinuria that correlated with the level of transgene expression.

3.4.4 *Nphs1*-rtTA-driven EGFP_CA-Rac1 expression in podocytes results in higher transgene expression and more severe proteinuria

We considered that the patchy and uneven expression of CA-Rac1 might be due to issues with silencing of the *NPHS2*-rtTA transgene. To circumvent this problem, a new transgenic mouse line (NEF) expressing a modified rtTA (rtTA-3G) under the control of the mouse nephrin

(*Nphs1*) promoter was generated [126] and bred to our CA-Rac1 mice. Examination of kidneys from double transgenic (NEFxBac1) mice after four days of DOX treatment showed a greater proportion of glomeruli and higher numbers of podocytes expressing the transgene compared to the PODxBac1 mice. Yet, the expression in podocytes was still not 100% (Figure 3.4A). This increased expression and distribution of the CA-Rac1 transgene correlated with a faster onset and higher levels of proteinuria (Figure 3.4B). In contrast to PODxBac1 mice, the proteinuria in NEFxBac1 mice persisted after one week of DOX treatment (Figure 3.4C, 3-S2). However, similar to PODxBac1 mice, proteinuria peaked at day 4 and gradually decreased over time (Figure 3.4C). After exposure to DOX for 28 days, we could not detect any EGFP expressing podocytes in kidney sections suggesting that the transgene-positive podocytes had been lost (Figure 3.5B).

3.4.5 EGFP CA-Rac1 induces foot process effacement, but without other histological changes in the glomerulus

The morphology of podocytes expressing CA-Rac1 was assessed by both light and electron microscopy. Glomeruli from DOX-induced Rac1 single transgenic mice and NEFxBac1 mice were unremarkable by light microscopy (Figure 3.5A). No obvious abnormalities were detected even after 1 month of continuous DOX induction. Transmission electron microscopy showed segmental effacement of podocyte foot processes in PODxBac1 glomeruli (Figure 3.6A) consistent with variable transgene expression. To test this, we used a super resolution fluorescence imaging method, Stochastic Optical Reconstruction Microscopy (STORM). STORM allows nanometer resolution of fluorescently tagged molecules such as labeled antibodies by

capturing thousands of sequential images of a specimen illuminated with a very low energy excitation source [127]. Sections of kidney tissue from NEF \times Rac1 mice on day 4 after DOX induction was stained with fluorescently tagged antibodies for EGFP (to localize CA-Rac1) and laminin β 2 (to detect the glomerular basement membrane) and examined by STORM. After STORM imaging, the same tissue sample was processed for freeze etch electron microscopy and the images were correlated (Figure 3.6 B and C). This showed that only the EGFP_CA-Rac1 expressing podocytes had effaced foot processes, while adjacent non-expressing podocytes had intact foot processes (Figure 3.6C). These studies provide an explanation for the segmental foot process effacement seen by TEM.

3.4.6 CA-Rac1 decreases podocin and nephrin levels via proteasomal degradation

During our examination of the kidney with immunofluorescence microscopy, we noted that in both POD \times Rac1 and NEF \times Rac1 mice CA-Rac1 expression was inversely correlated with podocin and nephrin level (Figure 3.7 A and B). Quantitative correlation of EGFP pixel intensity with that of podocin and nephrin showed a significant negative correlation (Figure 3.7 C, D, E and F). To test whether Rac1 activation cause a direct downregulation of podocin expression, cultured podocytes were transiently transfected with empty vector, EGFP_CA-Rac1 and EGFP_CA-RhoA, and podocin levels were analyzed by immunoblotting. Compared with the vector control, CA-Rac1 diminished podocin levels by about 50%, while CA-RhoA had no effect (Figure 3.7G). We measured the levels of podocin mRNA in these podocytes by quantitative PCR and found no significant difference, which suggested that the podocin decrease was not mediated by transcriptional downregulation (Figure 3-S3). The decrease in podocin levels could

be blocked by the proteasome inhibitor MG132, suggesting that Rac1 activation induces podocin degradation via a proteasomal pathway (Figure 3.7H).

3.4.7 CA-Rac1 expression stimulate membrane dynamics in podocytes *in vivo*

To further investigate that CA-Rac1 expressing podocytes *in vivo*, we used multiphoton intravital imaging (MPM) technique to directly assess podocyte membrane dynamics in live mice. Since CA-Rac1 is tagged with EGFP at the N-terminus and only some of the podocytes expressed this transgene after DOX induction, we could directly observe EGFP+ podocyte membrane dynamics. Dylight594-labeled lectin molecules were injected intravenously before imaging. Endothelial cells and Tubular epithelial cells can absorb lectin and be labeled in the red channel. During the imaging process, each frame was taken at 30-second time interval by using resonance scanner. We observed dramatic membrane dynamics in EGFP_CA-Rac1+ podocytes (Figure 3.8). Our result suggests that CA-Rac1 induce membrane ruffling in podocytes *in vivo*. The membrane ruffling is likely caused by actin cytoskeleton rearrangement induced by high Rac activity.

3.4.8 The shattered podocytes could from new interaction with the interstitial endothelium in the renal tubules

In our intravital imaging experiments, we observed EGFP+ cells that formed stable interaction with the renal tubules (Figure 3.9). Because the expression of rtTA transgene is restricted to podocytes [126], these cells could be podocytes that shattered from the glomerulus. Surprisingly, 3D images of these cells showed that they establish stable interactions with the epithelial cells in the tubules (Figure 3.9). Some of these cells extended protrusions that crossed

the basement membrane of the tubular epithelium and formed new interactions with the endothelial cells of the interstitial capillaries. This result suggests that high Rac activity could cause podocyte shattering from the glomerulus. However, shattered podocytes could form new connections with other endothelial cells outside the glomerulus.

3.5 Discussions

The structural integrity of the glomerular filtration barrier is essential for selective excretion of waste products and the retention of cells and large serum proteins within the circulation. The glomerular podocyte, with its arbor of interdigitating foot processes, is the critical final component of the kidney's filtration barrier. The elaborate actin-based cytoskeleton of the podocyte's foot process is simplified in many diseases in which serum proteins are lost into the urine. Since actin reorganization mediated by Rho family GTPases is a well-established mechanism for cell shape change, we and others have attempted to directly ask how specific Rho GTPase activation regulates podocyte morphology *in vivo*.

Previous studies used an approach similar to ours to study the role of RhoA in podocytes. Both constitutively active and dominant negative (DN) inducible RhoA transgenic mouse lines were generated [49, 118]. While both approaches resulted in podocyte dysfunction, the changes detected occurred relatively slowly, over weeks to months. Given how rapidly Rho family GTPases induce actin cytoskeletal changes *in vitro*, it raises the possibility that proteinuria in those systems is due to indirect effects of transgene expression in podocytes and not due to a direct signaling effect of RhoA. In addition, the mechanism of foot process effacement directed

by RhoA activation was not directly addressed in these studies.

In our mouse, expression of constitutively active Rac1 (CA-Rac1) produced rapid onset (~48 hours) proteinuria that correlated with the degree of transgene expression. While the *Nphs1*-rtTA transgene was expressed in a larger percentage of podocytes than the *NPHS2*-rtTA transgene, neither driver promoted expression in all of the cells. This was supported by our finding of segmental foot process effacement detected by electron microscopy. Using STORM imaging and freeze-etch electron microscopy correlation techniques, we confirmed that effaced foot processes correlated with GFP positive cells, while the foot processes of podocytes not expressing the transgene remained intact [128]. The rapid onset and dose-responsive nature of proteinuria induced by CA-Rac1 expression provides strong evidence for a direct signaling role for Rac1 activation in generating foot process effacement. This *in vivo* biologic correlate further supports the use of the membrane-ruffling assay in cultured podocytes as a useful reporter of podocyte injury *in vitro*. Our results demonstrate for the first time that Rac1 activation in podocytes can directly cause foot process effacement and proteinuria.

While onset of proteinuria in the CA-Rac1 expressing mice was rapid, the proteinuria induced was only transient. As GFP could not be detected in kidneys of mice treated long-term with DOX, we suspect that chronic Rac1 activation is toxic to podocytes. The efficiency of CA-Rac1 transgene expression differed between the two different rtTA driver lines and therefore incomplete CA-Rac1 expression is related in part to the efficiency of the promoter driving rtTA expression. It is well-known that epigenetic silencing can suppress transgene expression over time [131]. It is also possible that the incomplete expression of our CA-Rac1 transgene may be

related to other epigenetic factors that can affect expression of both the driver and CA-Rac1 transgenes.

We did not observe any progressive renal dysfunction or focal and segmental glomerulosclerosis (FSGS) in the CA-Rac1 expressing mice after prolonged DOX treatment, in contrast to the CA-RhoA transgenic mice [118]. This may be attributed to the low frequency of EGFP_CA-Rac1-expressing podocytes in our systems, since in a rat model of tunable podocyte loss, approximately 20 to 40% podocyte depletion was required before FSGS was consistently observed [26].

The presence of CA-Rac1 reduced podocin protein expression both *in vivo* and in cultured podocytes. This was mediated, at least in part, by proteasomal degradation as it could be blocked *in vitro* with proteasome inhibitors. Because we could not detect CA-Rac1-positive cells after extended DOX treatment, we suspect that the expressing podocytes were eliminated and replaced either by remaining podocytes or by a progenitor population [126, 132]. These compensatory mechanisms might explain the resolution of proteinuria over time in the CA-Rac1 expressing mice. Therefore, future studies should focus on the development of tools to detect activation of endogenous Rac1 and RhoA in podocytes. The balance and localization of the activity of these GTPases is likely to be tightly and dynamically regulated for proper podocyte function.

Acknowledgements

We are grateful for the help of Jacqueline Mudd from the Murine Embryonic Stem Cell Core of the Siteman Cancer Center in generating the recombinant embryonic stem cells. We thank Michael White from the Transgenic Knockout Microinjection Core of the Department of Pathology and Immunology for technical assistance in generating the chimeric mice and Jaclynn Lett for EM sample preparation and assistance with imaging (Microscopy and Digital Imaging Core in the Research Center for Auditory and Visual Studies, Department of Otolaryngology, Washington University School of Medicine; funded by NIH grant P30DC004665). We appreciate Rudolf Jaenisch for sharing the KH2 ES cell line and Takako Sasaki for providing the laminin β 2 antiserum. We also thank Jiancheng Hu for reagents and helpful discussions. This research was supported by the Howard Hughes Medical Institute and NIH grant R01DK058366 to A. S. Shaw and by NIH grant R21DK095419 to J. H. Miner.

* This chapter is adapted from Yu H, *et al.* Rac1 activation in podocyte induces rapid foot process effacement and proteinuria. *Mol Cell Biol.* 2013; 33(23): 4755-64.

3.6 Figures

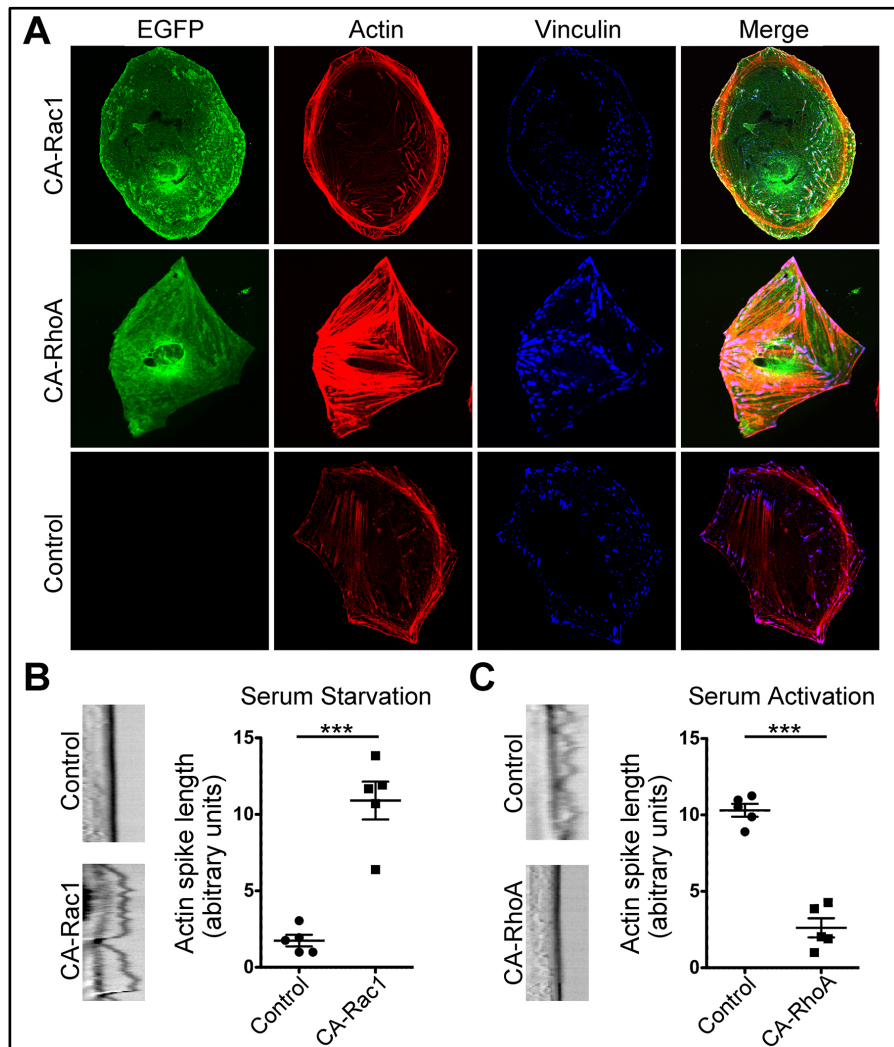


Figure 3.1 Constitutively active Rho family GTPases exert opposing effects on the actin cytoskeleton of podocytes

(A) Immunofluorescence imaging was performed on differentiated mouse podocytes that were stably transduced with EGFP_CA-Rac1 or EGFP_CA-RhoA (green). The filamentous actin network was delineated with phalloidin (red) and focal adhesions and contacts were identified with vinculin (blue). Compared to control, untransduced cells, EGFP_CA-Rac1 induced flattening of the cell and lamellipodia formation while EGFP_CA-RhoA induced numerous stress fibers and cell contraction. (B) EGFP_CA-RhoA suppresses serum-induced membrane ruffling in podocytes. Left panel, using kymographic analysis, under conditions of serum starvation, podocytes exhibit minimal membrane ruffling activity. Introduction of EGFP_CA-Rac1 significantly increases membrane dynamics and ruffling (***) $P < 0.0001$ by unpaired T-test). Right panel, exposing starved cells to serum also induces membrane ruffling which is suppressed by introduction of EGFP_CA-RhoA (***) $P < 0.0001$ by unpaired T-test).

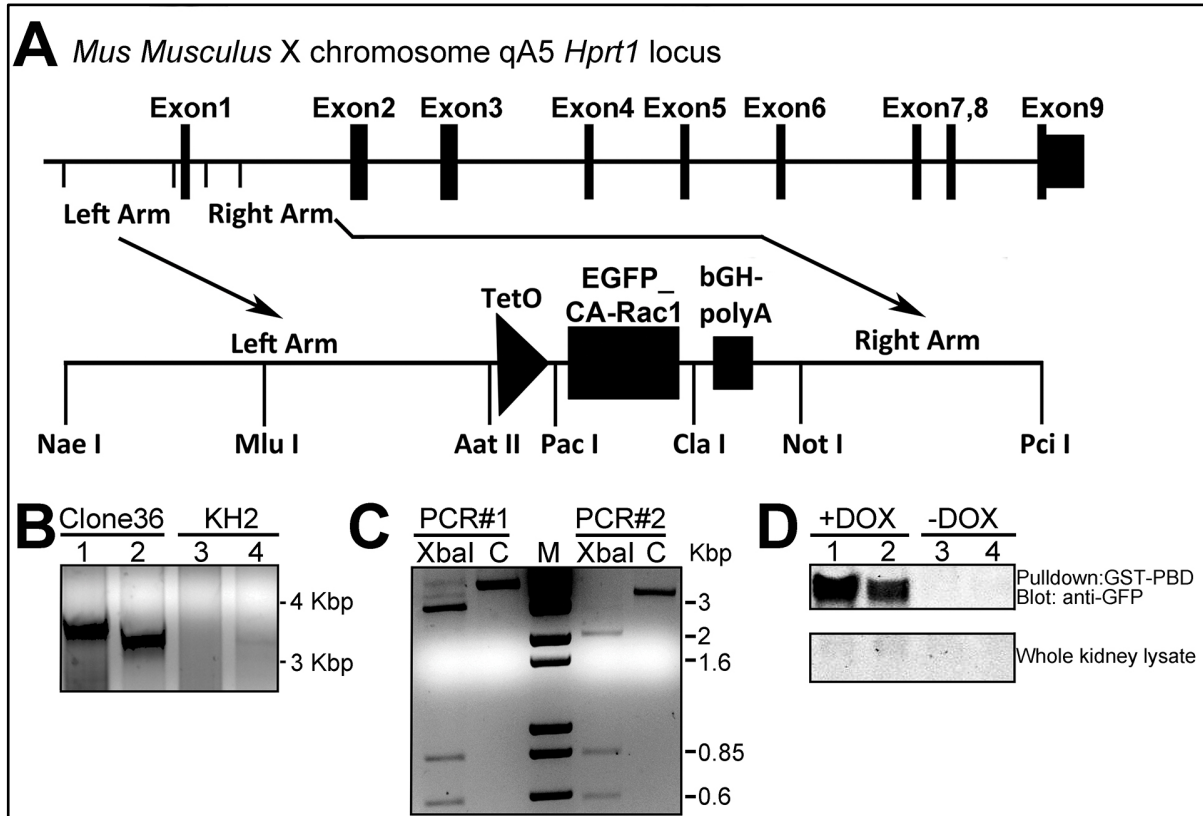


Figure 3.2 Generation of inducible EGFP_CA-Rac1 transgenic mice

(A) Strategy for targeted insertion of an inducible EGFP_CA-Rac1 into Exon 1 of the murine *Hprt1* locus on chromosome X. The tetracycline response element (TRE) allows for DOX inducible EGFP_CA-Rac1 expression when crossed to lineage-specific rtTA-transgenic mouse lines. (B) Confirmation of targeted insertion and verification of EGFP_CA-Rac1 activity in transgenic mice. Long genomic PCR for the 5' and 3' insertion sites confirmed homologous recombination in ES cell clone 36 (parental KH2 ES cells are used as the negative control). Lanes 1 and 3: Primer1 (in 5' EGFP transgene sequence) and Primer3 (400bp down stream of the 3' arm). Lanes 2 and 4: genomic PCR by Primer2 (in Rac1 transgene sequence) and Primer3. (C) *Xba*I digestion produced specific digestion bands (400bp and 600bp) that confirmed the specificity of the 5' and 3' targeted locus PCR products from Figure 3.2B. Two replicates are shown. (D) Transgenically expressed EGFP_CA-Rac1 is functionally active. EGFP_CA-Rac1 transgenic mice were crossed to *NPHS2*-rtTA inducer mice to generate PODxRac1 mice. EGFP_CA-Rac1 transgene was induced by feeding DOX to the mice. Transgenically expressed EGFP_CA-Rac1 binds to GST-PBD, which specifically recognizes the active conformation of Rac1. Transgenic EGFP_CA-Rac1 is not induced and is not present to bind to GST-PBD without DOX induction. Representative data from two induced and non-induced PODxRac1 mice are shown.

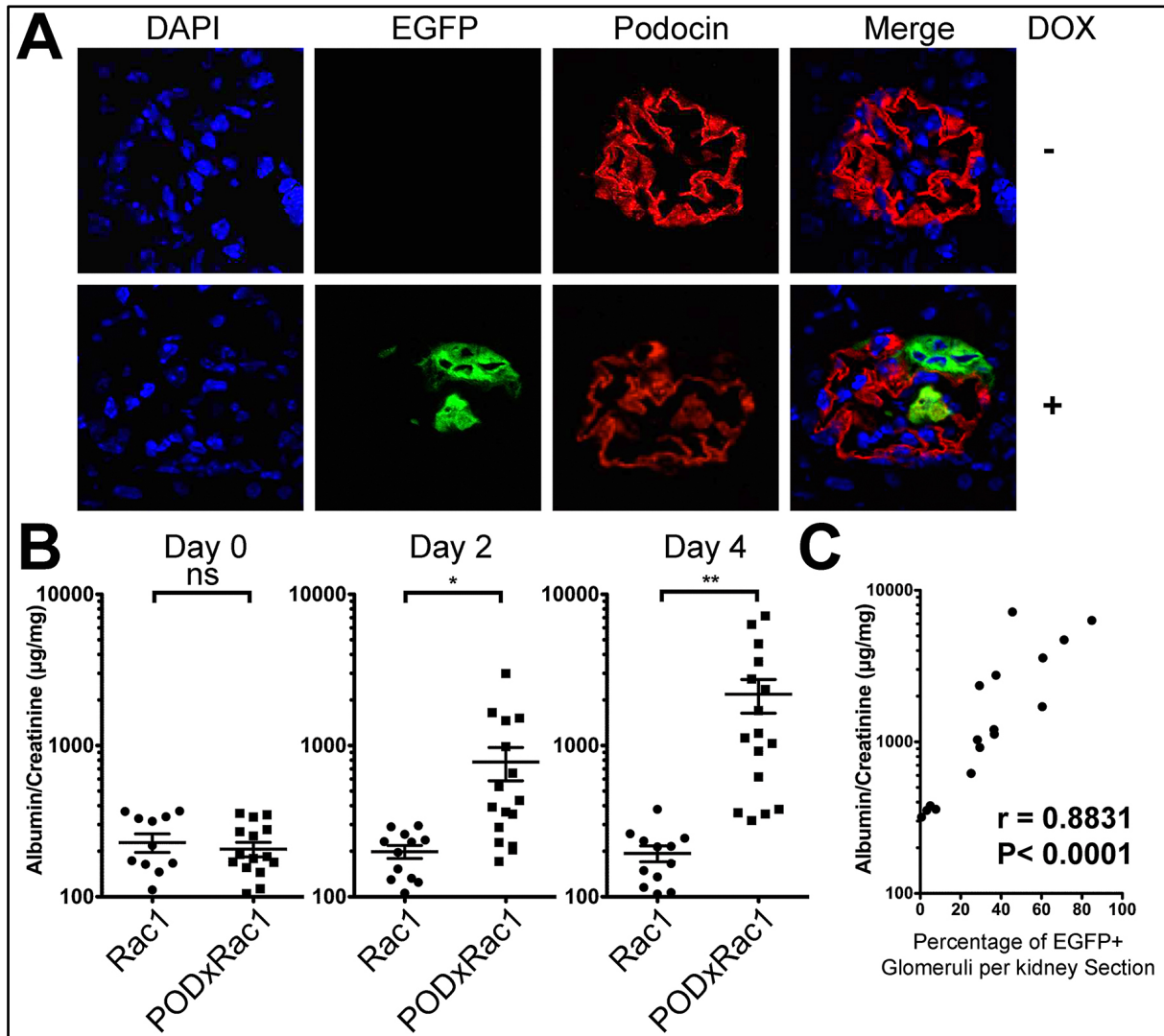


Figure 3.3 Podocyte specific expression of CA-Rac1 causes proteinuria

(A) Upper panels, without DOX induction, EGFP_CA-Rac1 is not expressed in PODxRac1 mice. Lower panels, after a 4-day DOX induction, EGFP_CA-Rac1 transgene (green) is specifically expressed in glomerular podocytes, confirmed by immunofluorescence colocalization with the podocyte marker, podocin (red). (B) DOX treatment induced fast onset of proteinuria in PODxRac1 mice. Urine samples were collected at the indicated timepoints from the single transgenic EGFP_CA-Rac1 and DOX induced double transgenic PODxRac1 mice at the indicated timepoints. Proteinuria was quantitated by measuring the albumin/Creatinine ratio (Al/Cr) for each sample. Each point represents the Al/Cr ratio from a single mouse measured at the indicated timepoints. (C) The frequency of EGFP+ glomeruli correlated positively with the level of proteinuria (Al/Cr ratio) (Pearson's $r=0.8831$, $P < 0.0001$).

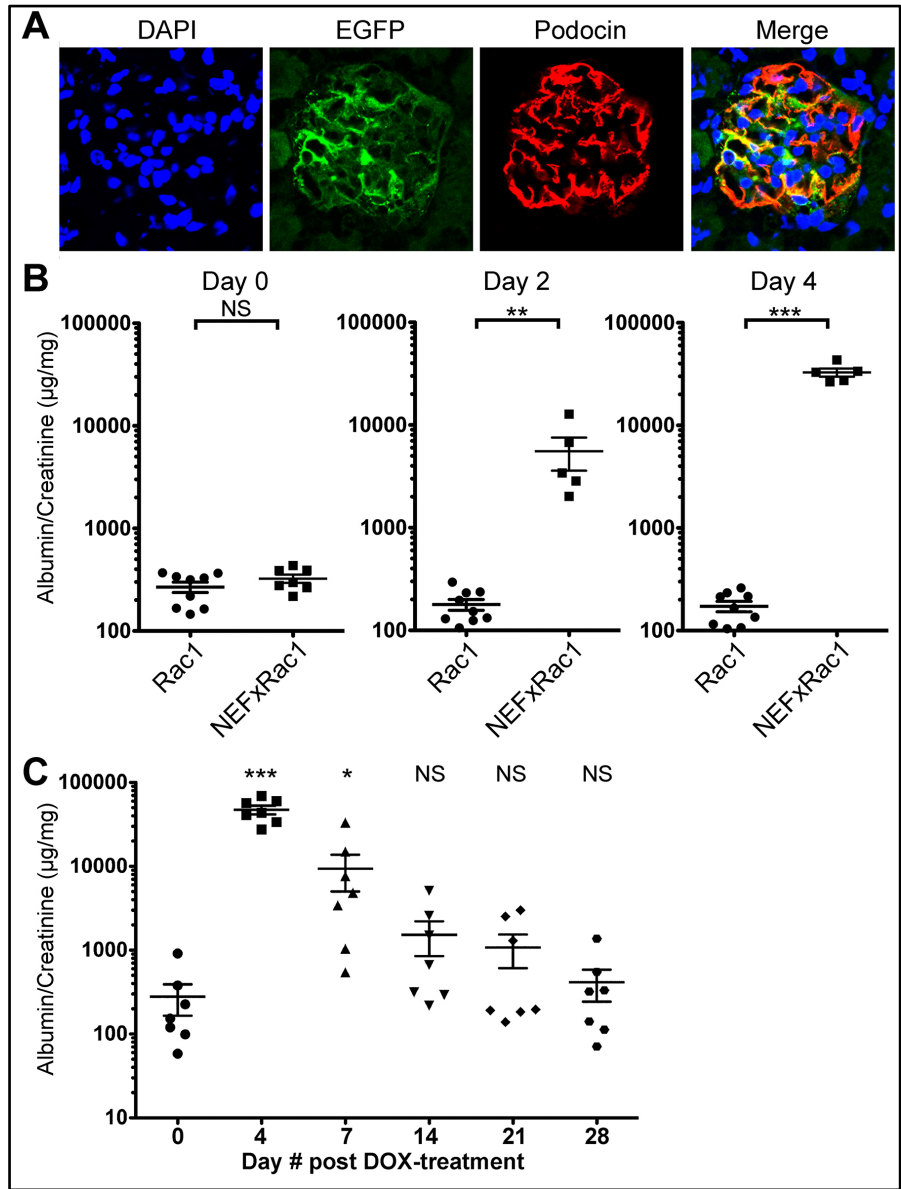


Figure 3.4 EGFP_CA-Rac1 expression driven by *Nphs1*-rtTA induces more robust transgene expression and transient proteinuria

(A) *Nphs1*-rtTA mice were generated and crossed to EGFP_CA-Rac1 transgenic mice to generate NEFxCrac1 mice. After 4 days of DOX treatment, there was robust expression of the EGFP_CA-Rac1 transgene (green) in podocytes, labeled with the podocyte marker, podocin (red). (B) As before, NEFxCrac1 mice were treated with DOX for various time periods and proteinuria was measured in the collected urine samples. Compared to the single transgenic (EGFP_CA-Rac1 only) control, NEFxCrac1 mice exhibit significant proteinuria as early as 2 days after induction. Each point represents the AI/Cr ratio from a single mouse measured at the indicated timepoints. (C) Similar to PODxRac1 mice, the proteinuria in NEFxCrac1 mice peaks around day 4 and then returns to baseline in 28 days. Each point represents the AI/Cr ratio from a single mouse measured at the indicated time points.

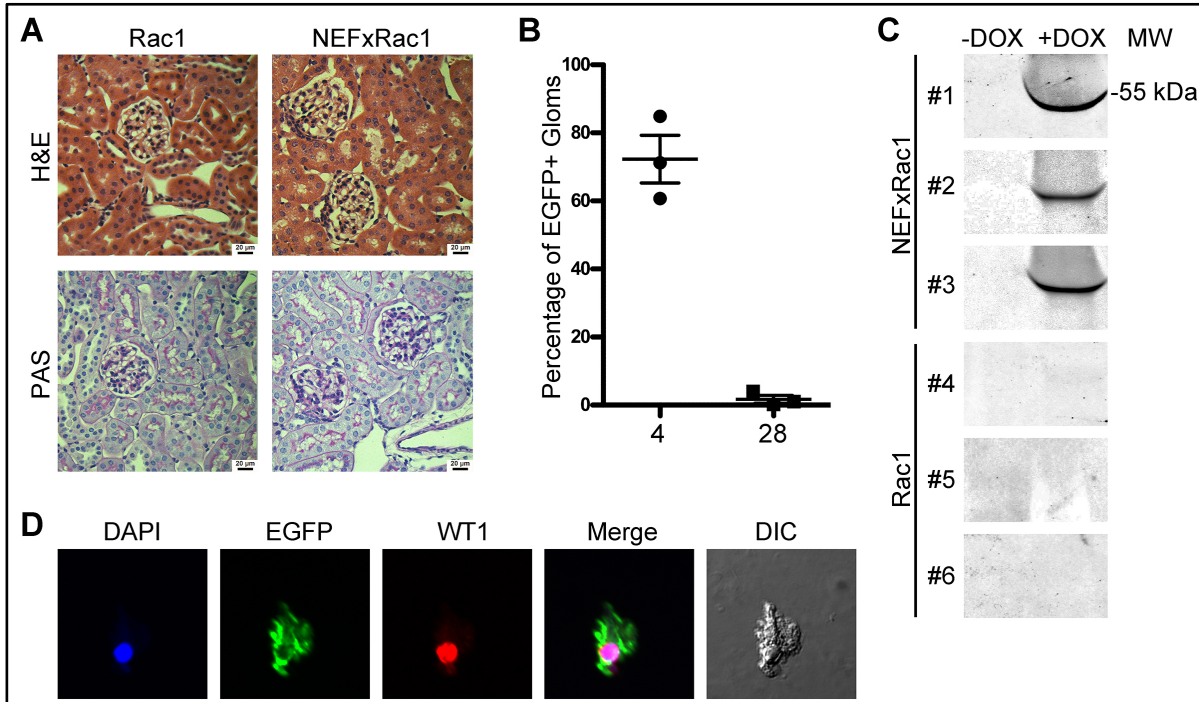


Figure 3.5 No obvious pathological changes were detected in histological analysis, and the transgene positive podocytes were lost after prolonged DOX treatment

(A) hematoxylin and eosin (H&E) and periodic acid-Schiff (PAS) stained kidney sections from NEFxFac1 mice induced with DOX for 4 days. The control kidney samples are shown on the left, and the NEFxFac1 tissues are shown on the right. (B) The kidney samples were harvested from 3 NEFxFac1 treated by DOX for 4 days or 28 days. For each kidney sections, the percentage of EGFP+ positive glomeruli was counted.

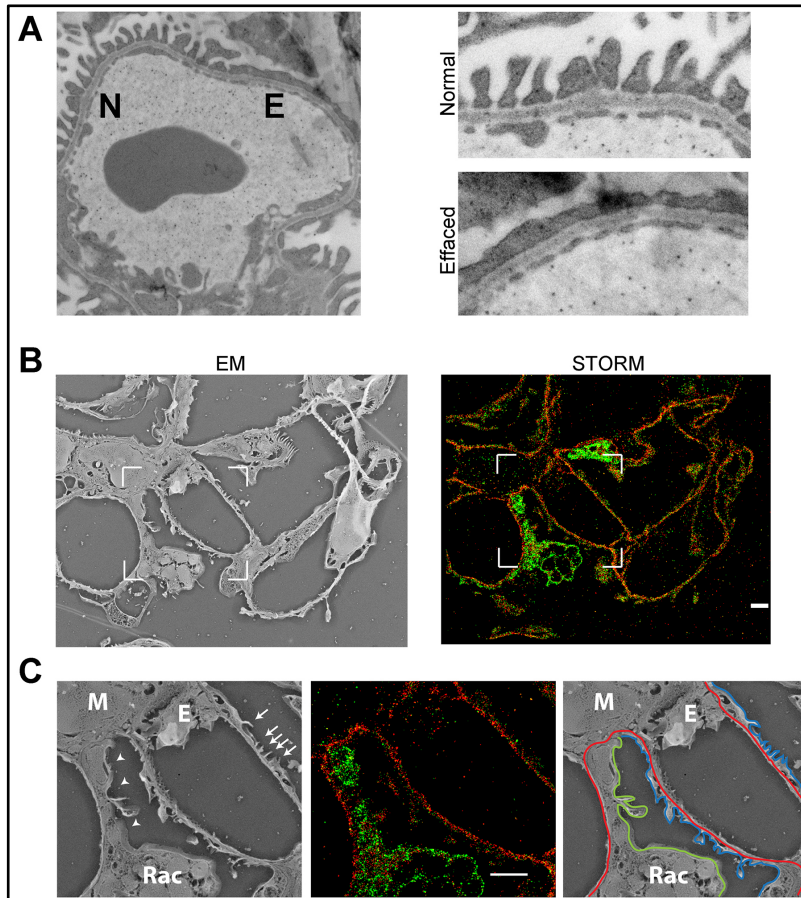


Figure 3.6 EGFP_CA-Rac1 expression in podocytes is associated with foot process effacement *in vivo*

(A) Left panel, examination of kidney tissues from DOX treated PODxRac1 mice by transmission electron microscopy demonstrates segmental effacement (E) of podocyte foot processes while the foot processes of neighboring podocytes are intact and appear normal (N). The panels on the right demonstrate the same areas at higher magnification. (B) Scanning electron microscopy (SEM, left panel) and STORM (right panel) imaging techniques were performed on the same glomerulus from a NEFxRac1 mouse treated with DOX for 4 days. For STORM imaging, the sample was stained for laminin β 2 (red) and EGFP (green) to label EGFP_CA-Rac1 expressing podocytes. The boxed area is examined in detail in Figure 3.4C. (C) Correlation of STORM and SEM images identifies that EGFP-CA-Rac1 expressing podocyte have effaced foot processes while neighboring, non-transgene expressing podocytes retain intact foot processes. The left panel shows capillary loops with effaced foot processes (arrowheads) and intact foot processes (arrows). The middle panel presents the STORM imaging of the same area with laminin β 2 (red) and EGFP (green). The right panel shows a schematized representation of the STORM data overlaid on the SEM image. The glomerular basement membrane marked by laminin 2 is outlined in red. The EGFP_CA-Rac1 podocyte with its effaced foot processes is outlined in green. The intact foot processes of non-transgene expressing podocytes are outlined in blue. (M-mesangial cell, E-endothelial cell)

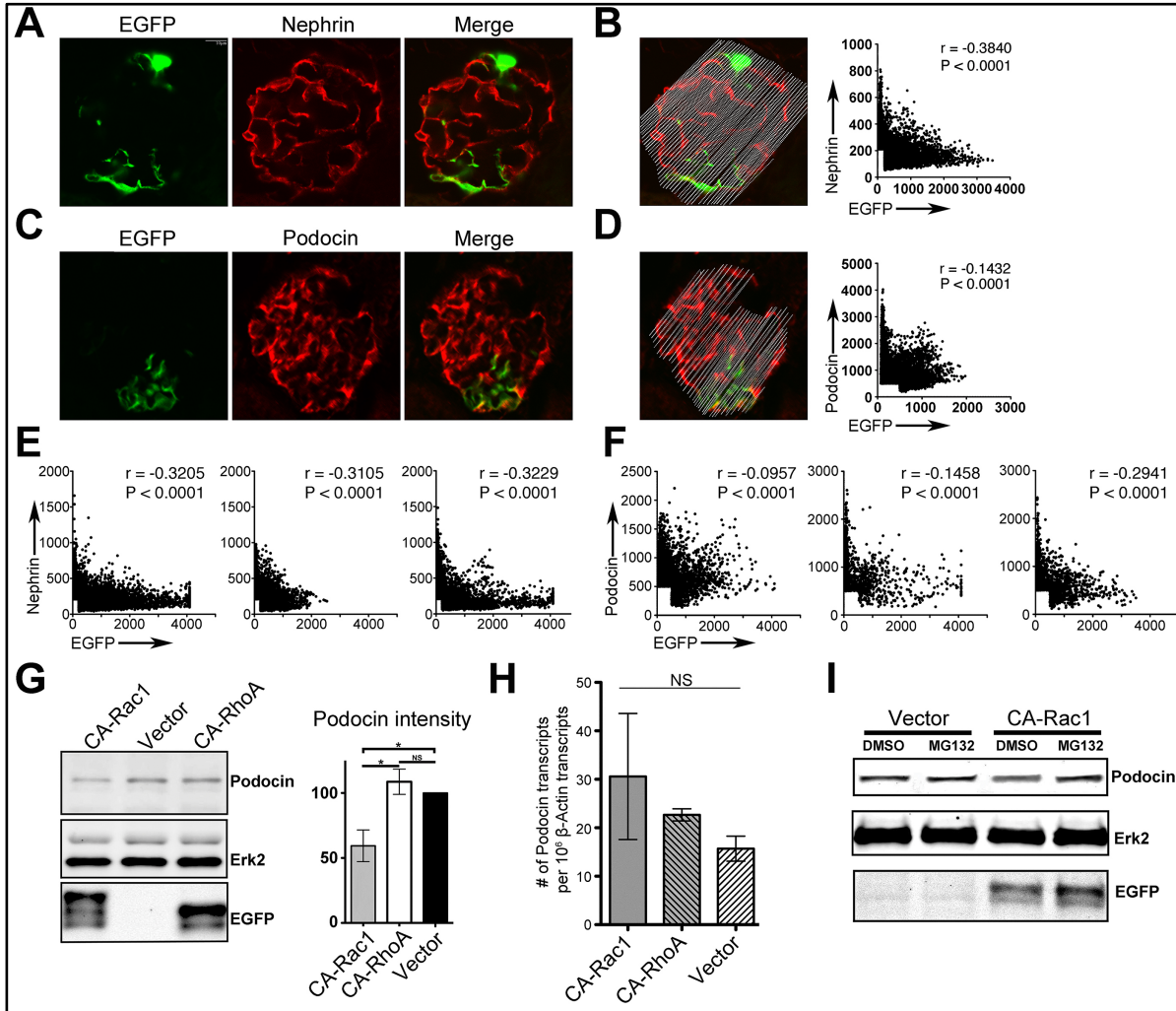


Figure 3.7 EGFP_CA-Rac1 expression correlates with reduced expression of podocin and nephrin

A NEFxCrac1 mouse was induced with DOX for 4 days and glomeruli were stained for nephrin (A) and podocin (C), both shown in red. There is decreased expression of nephrin and podocin in podocytes expressing the EGFP_CA-Rac1 transgene. Quantitation of pixel intensity across the glomerulus demonstrates separation of nephrin (B, Pearson's $r = -0.3840$, $P < 0.0001$) and podocin (D, Pearson's $r = -0.1432$, $P < 0.0001$) signals compared to EGFP_CA-Rac1 signals. Additional measurement of three other glomeruli are shown in (E, nephrin) and (F, podocin). (G) EGFP_CA-Rac1, but not EGFP_CA-RhoA expression in cultured podocytes reduces podocin protein levels. Left panel, cultured podocytes were electroporated with EGFP_CA-Rac1 or EGFP_CA-RhoA expression plasmids. Protein lysates were immunoblotted for podocin, Erk2 and EGFP. Compared to the empty vector control and EGFP_CA-RhoA, EGFP_CA-Rac1 reduced podocin protein levels. Right panel, densitometric quantitation of three independent experiments normalized to Erk2 levels. * $P < 0.05$ by unpaired t-test. (H) The reduction of podocin levels can be rescued by treatment with the proteasomal inhibitor MG132, but not with vehicle (DMSO) alone.

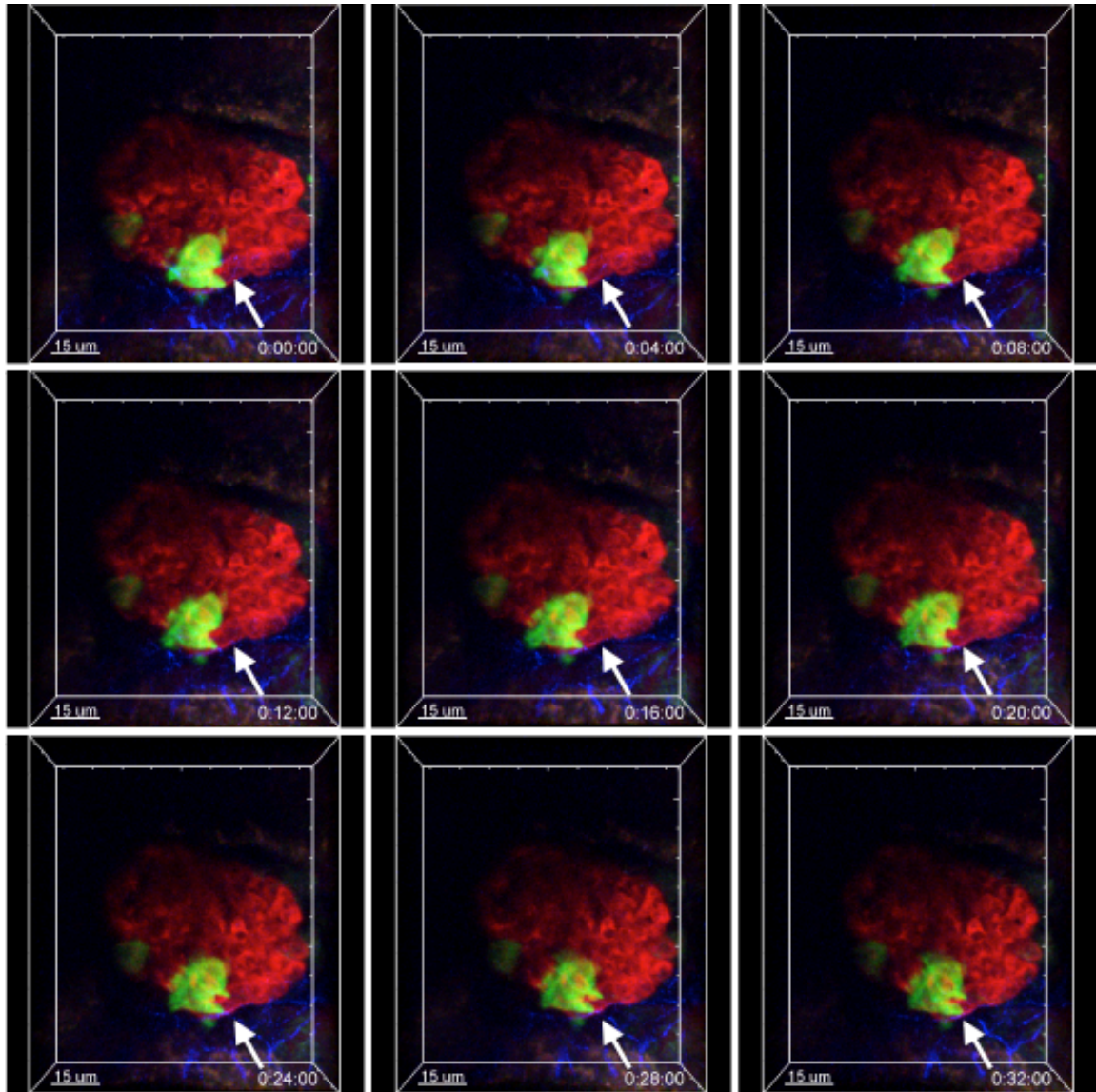


Figure 3.8 Time-lapse intravital MPM imaging of DOX induced NEF \times Rac1 mice

Here shows nine images of the same glomerulus in 32 minutes of intravital MPM imaging experiment. The green channel is EGFP_CA-Rac1 positive podocytes. The red channel shows the capillaries in the glomerulus. The blue channel shows second harmonic signal from collagen matrix. The white arrow shows the membrane dynamics of the podocytes over time.

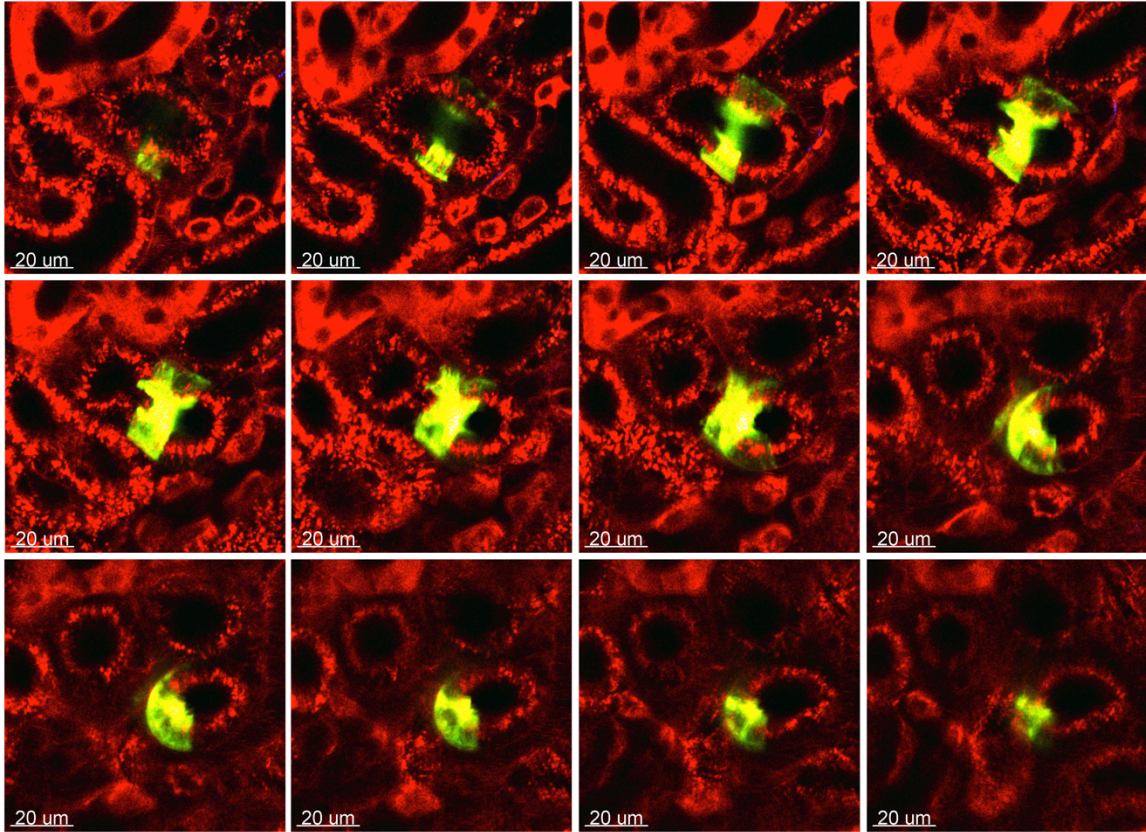


Figure 3.9 Z-stack images of EGFP_CA-Rac1+ podocyte that attach to the epithelium of the renal tubules

The green channel is EGFP_CA-Rac1 positive podocytes. The red channel shows the tubular epithelium and interstitial capillaries that absorbed Dylight594-labelled lectin. The images were generated from a 3D image file.

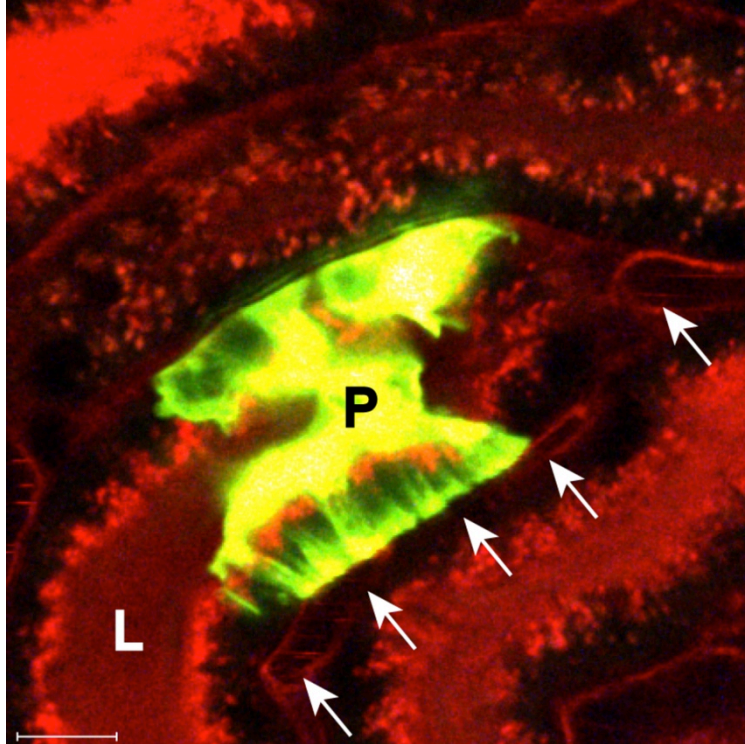


Figure 3.10 EGFP_CA-Rac1+ podocytes extended protrusions that penetrates the tubular epithelium and touched the basal side of the interstitial endothelial cells

The green channel is EGFP_CA-Rac1 positive podocytes. The red channel shows the tubular epithelium and interstitial capillaries that absorbed Dylight594-labelled lectin. The arrows show an interstitial capillary. L: the lumen of a renal tubule. P: podocytes that express EGFP_CA-Rac1.

Chapter 4. A Role for Genetic Susceptibility in Sporadic Focal Segmental

Glomerulosclerosis

4.1 Abstract

Focal segmental glomerulosclerosis (FSGS), a disease of kidney podocytes is a significant cause of chronic kidney disease. FSGS can be caused by multiple factors including genetics, medication toxicity, obesity, inflammation and viral infection. In the fraction of FSGS subjects with a family history, highly penetrant disease genes have been identified. The identification of APOL1 as a susceptibility factor for FSGS in African Americans with HIV suggests that genetic factors may play a broader role in enhancing susceptibility to FSGS. Here we used sequencing to investigate whether genetics plays a role in the majority of FSGS cases called primary or sporadic FSGS where medications and viruses have been ruled out as causes. We identified 16 potential new FSGS genes and found that over 46% of FSGS subjects may carry susceptibility genetic variants. Using a novel mouse method based on the manipulation of a murine embryonic stem cell line with a genetic background susceptible to FSGS, we validated three of the top four FSGS candidate genes. Our work supports the feasibility of studying the role of genetic background in the susceptibility to disease in humans.

4.2 Introduction

The glomerulus of the kidney is a specialized capillary bed that generates an ultrafiltrate that after modification by the kidney tubule system becomes urine. Diseases of the glomerulus often lead to chronic kidney disease, a major health care problem affecting between 5-10% of the adult population in developed countries [3]. Treatment options are limited, in part owing to the poor understanding of the pathogenesis of disease. Better insights into the root cause of disease offer hope for eventual improvement of this situation.

One of the most common glomerular syndromes is focal segmental glomerulosclerosis (FSGS). The pathologic change of FSGS is a scar that develops focally (in some but not all glomeruli) and segmentally (in only part of a glomerulus). While originally considered a disease, FSGS is now thought to consist of a variety of different syndromes. These include primary (idiopathic) FSGS that is thought to be caused by a circulating factor and secondary FSGS, which may be caused by viruses, medications and genetic mutations. The most common form of secondary FSGS follows glomerular hyperfiltration arising from mismatch between metabolic load and glomerular capacity, associated with obesity, low birth weight, reduced renal mass as well other causes. Genetic mutations can be sufficient by themselves to cause disease (Mendelian), or can increase susceptibility to FSGS by potentiating the effects of environmental factors.

The glomerulus is composed of three different cell types: endothelial cells, mesangial cells and epithelial cells known as podocytes. The podocyte is an unusual cell that covers the outside of the capillary wall and interdigitates with other podocytes to create small slits that allow the

passage of fluid and small solutes into urinary space. It is now clear that podocyte dysfunction is responsible for FSGS as well as other glomerular diseases such as minimal change disease, membranous glomerulopathy and congenital nephrotic syndrome. Current models suggest that increased podocyte loss is the primary lesion in FSGS [24, 26, 133, 134].

Over the last 10 years, highly penetrant disease genes has been identified in the fraction of FSGS subjects with a family history [135–137]. However, they do not explain the majority of the disease population, which are non-familial. In terms of number of people affected, the most significant genetic contributor to FSGS susceptibility identified to date is *APOL1*. FSGS associated alleles of *APOL1*, called G1 and G2, are common in West African populations, possibly as a consequence of providing resistance to trypanosomiasis [19, 138, 139]. The presence of two variant alleles significantly increases the risk of arterionephrosclerosis (hypertensive nephropathy) (Odds Ratio (OR) = 7), FSGS (OR = 17) or HIV associated nephropathy (OR = 29) in African [19, 20]. Approximately 13% of African Americans carry two variant alleles and are at increased risk for chronic kidney disease. As these variants are absent from individuals lacking any African ancestry, they are not documented to play a role in FSGS susceptibility in other ancestries, and by themselves largely explain the increased frequency of FSGS among African-Americans. Despite this, mechanisms by which *APOL1* variants cause or predispose to glomerular damage remain unknown.

Here, we used high-throughput sequencing of FSGS subjects to investigate whether genetics plays a broader role in the majority of FSGS cases that cannot be explained by the familial FSGS genes. Since FSGS is considered to be a disease of podocytes, we focused our

sequencing analysis on 2500 genes that are highly and/or specifically expressed in podocytes. DNA from 214 FSGS subjects including 192 sporadic cases and 22 familial cases were sequenced (Table 4.1). DNA samples of FSGS subjects were mostly from a multi-center NIH study of biopsy-confirmed FSGS [20], but also included some subjects diagnosed with FSGS by kidney biopsy at Washington University. All subjects provided informed consent for genetic studies. Control subjects sequenced for an autism study were used as controls [66]. Because the controls were of European ancestry, we focused on FSGS subjects of similar genetic ancestry.

A major challenge of large scale sequencing studies will be to develop strategies that will allow for candidate susceptibility genes identified through association studies to be experimentally validated as functionally relevant to disease. Since there is no *in vitro* assay for podocyte injury leading to FSGS, validating candidate genes here requires the use of an animal model. We developed a system based on embryonic stem (ES) cells from a susceptible background for FSGS that allows for efficient method for targeted delivery of shRNAs, and that uses a method to generate mice that are close to 100% derived from the ES cells eliminating the need for breeding. Scaling up our system will allow for large numbers of candidate genes constituting the network of FSGS genes to be validated which will provide critical insight into the pathogenesis of this disease syndrome. In addition, our experimental approach should be broadly applicable to studying other oligogenic diseases.

4.3 Methods

4.3.1 Exon capture and sequencing

Sample preparation and sequencing were carried out using standard protocols for targeted capture and Illumina sequencing. In brief, genomic DNA was fragmented to 150-200bp using a Covaris E220 focused ultra-sonicator. The ends of the fragmented DNA were repaired using a mixture of T4 DNA polymerase, Klenow polymerase and T4 polynucleotide kinase. Subsequently, adapters for Illumina sequencing were ligated onto the fragments. These libraries were then hybridized to biotinylated DNA probes from regions of interest (manufactured by MyGenostics, Baltimore, MD). After washing away DNA libraries that bound non-specifically to the probes, DNA of interest was recovered using Dynabeads® MyOne™ Streptavidin T1 (Life Technologies). Resulting DNA libraries were amplified, if needed, to provide enough products for sequencing on an Illumina HiSeq 2500.

4.3.2 Variant calling and data quality control

We performed alignment of the raw sequencing data and variant calling according to GATK best practices with BWA/Picard/GATK software pipeline of the Broad Institute. To insure that we are working with equally well-covered loci in both cases and controls we have performed a QC separately on cases and controls genotypes applying following filters: (1) Keep only SNPs; (2) Keep variants that PASS all GATK quality filters; (3) Keep genotypes with $DP > 10, GQ > 30, AB$ for hets $0.3 < AB < 0.7$, for homozygous alternative $AB < 0.3$; (4) Keep variants with less than 5% of missing genotypes. After applying these filters we have combined variants from cases and controls keeping only those variants with less than 5% of missing genotypes in both cases and controls. Our final dataset contained 16108 SNPs in 1874 genes.

4.3.3 Principle component analysis and case-control matching

PCA was performed with Eigenstrat software on the common (MAF>5%) variants found in autosomes only. We computed a Euclidian distance from each point on the PCA plot to the origin and plotted distributions of this parameter for both cases and controls. Using 3-sigma rule to remove the samples that appeared to be outlying from the distribution. This resulted in 30 samples of mixed Hispanic ancestry to be removed from initial data.

Sample statistics and case-control matching metrics were computed using Plink-seq. We have used number of variants called per sample, number of heterozygous genotypes per sample and number of genotypes with minor allele per sample as a metrics representing genetic background of the cohort. We established similarity between the genetic background of cases and controls by matching mean and variance of case and control distributions for every metric. We tested the validity of this approach by running Fisher's exact test on the common variation and QQ-plot of the p-values showed no inflation confirming absence of the population stratification in the case-control dataset (Supplementary Figure 4.1).

4.3.4 Mouse strains and antibodies

Cd2ap^{+/-} mice were generated in our previous study [77]. *Synpo*^{-/-} mice were obtained from Peter Mundel's laboratory [140]. The *Nphs1-rtTA3G (NEFTA)* strain was a gift from Dr. Jeffrey Miner's laboratory [126]. *Dlg5*^{+/-} strain was a gift from Dr. Valori Vasiokin's lab [141]. All mouse strains were genotyped by published protocol. All animal experiments were conducted with the approval of the Washington University Animal Studies Committee. The antibodies used for immunoblotting were mouse anti-XFP (632381; dilution, 1:10,000; Clontech), rabbit anti-ERK2

(sc-154; dilution, 1:5,000; Santa Cruz Biotechnology), mouse anti- β -actin (A2228; dilution, 1:10000, Sigma), and rabbit anti-CD2AP (generated in our previous study, dilution, 1:10000)

4.3.5 Generation of a male *Cd2ap*^{+/-}, *Synpo*^{+/-}, *NEFTA*+ ES cell line

To generate a male ES cell line that was sensitized to FSGS, we bred *Cd2ap*^{+/-}, *Synpo*^{-/-} males with *NEFTA*+ females. The females were superovulated using standard methods. After mating, the embryos were isolated at the eight-cell stage (morulae), and cultured overnight in KSOM (Millipore MR-121-D) micro-drops overlaid with mineral oil at 5% CO₂ and 37C. Blastocysts were transferred one per well, into 48 well plates with gamma-irradiated MEF feeders and standard ESC Medium that contains 15% ES qualified fetal bovine serum (SH30070.03E, Hyclone). The inner cell mass (ICM) was allowed to grow out. The ICM outgrowth was trypsinized after 5-7 days depends on the size and shape of the outgrowth, and cultured until ES colonies were identified. The colonies were expanded, frozen back and genotyped by using standard methods.

4.3.6 Generation of miR30-shRNA knock-in transgenic mice

In our previous studies, we developed a method to integrate a single copy of transgene into *Hprt1* locus, and use 6-thioguanine to select for ES clones with homologous recombination [142]. Based on this method, we further developed a double selection method, which significantly improve the chance of obtaining a positive ES clone.

A PGK-Puro cassette was inserted between the left and right arm of the pHPRT targeting vector. The miR30-based shRNA-expressing transgene that was driven by the tetracycline-responsive promoter (TRE) was inserted between the left arm and the PGK-Puro

cassette. Linearized targeting vector was transfected into ES cells that were growing at extension phase. At 24 hours post transfection, the ES cells were treated by 1µg/mL puromycin for 48 hours. Then the survived ES cells were passaged once. After 48 hours, the ES cells were treated by 6-thioguanine for 48 hours. Survived ES cell colonies were picked, expanded, and examined by genomic PCR across the right arm (Forward primer: 5'-CAAGCCCGGTGCCTGATCTAGATCATAATC-3'; Reverse primer: 5'-CTGTAAAGGTCTCTGAACTACCAATTGCAC-3'). Positive ES cells were then stocked for injection.

4.3.7 Laser assisted microinjection

The ES cells were maintained at extension phase before the injection. Eight ES cells were injected into a recipient embryo at eight-cell stage by following a standard protocol published previously [143]. Since the ES cell line produces mice with agouti coat color, albino B6 (C57BL/6J-*Tyr^{c-2J}*) mice were used as host embryos for direct evaluation of chimerism by coat color.

4.3.8 Cell culture and lentivirus infection

Immortalized murine podocytes were maintained and differentiated as described previously [122]. To examine the knockdown efficiency of Cd2ap-sh877, podocytes were infected with lentiviral vectors encoding miR30-sh877. A control lentiviral vector encoding miR30-FF3 that targets fire fly luciferase cDNA was used as a control. The CD2AP expression was examined by immunoblotting of the whole cell lysates.

4.3.9 Design and validation of the miR30-shRNA constructs for genes of interest

The shRNA oligo sequences were picked using an online algorithm (<http://katahdin.cshl.org/siRNA/RNAi.cgi?type=shRNA>) as described [144]. The miR30-shRNA backbone was sub-cloned by PCR from pPRIME-CMV-GFP-FF3 (<https://www.addgene.org/11663/>) and inserted into pcDNA3.1-Zeo(+) vector to generate pcMIR vector. To examine the knockdown efficiency, the miR30-shRNA construct and its artificial target (Figure 4-S3B) were co-transfected into HEK293T cells at molar ratio 5:1. The expression of EGFP in whole cell lysates was examined by immunoblotting.

4.3.10 Albumin-creatinine assay

Mouse urine samples were collected at the time points indicated in the figures, and urinary albumin (E90-134; Bethyl) and creatinine (DICT-500; BioAssay Systems) were quantified by enzyme-linked immunosorbent assays (ELISA) according to the manufacturers' protocols.

4.3.11 Transmission electron microscopy

Portions of kidney cortex were fixed with 2% paraformaldehyde and 2% glutaraldehyde. Specimen processing, ultrathin sectioning, and imaging were performed by the Electron Microscopy (EM) Core Facility at Washington University.

4.4 Results

4.4.1 Identification of podocyte genes for sequencing

To identify susceptibility genes for FSGS, we designed a custom exome capture reagent that focused on genes that were highly expressed in podocytes and/or previously implicated in FSGS. We began with five genes reported in OMIM in which heterozygous mutation confers risk

to idiopathic FSGS: *TRPC6* [17, 145], , *INF2* [13], *APOL1* [19], *ACTN4* [8], and *CD2AP* (Kim et al., 2003). Pathway analysis was performed to identify ~200 genes that are functionally linked to known FSGS genes and other syndromic or recessive genes. 677 genes were added based on their high expression in microdissected human glomeruli [147] and 1600 were the human orthologs of the most highly expressed genes identified by DNA microarrays in mouse podocytes [122, 148, 149]. Our total capture, which we term the “podocyte exome”, included about 2500 genes comprising a total of 7Mb. (Figure 4.1A).

4.4.2 Variant association analysis of FSGS patients of European ancestry using Next Generation sequencing

DNA from 225 biopsy confirmed FSGS patients that were of European ancestry was sequenced. Patient DNA samples were mostly from a multi-center NIH study of FSGS [150], but also included some FSGS patients diagnosed at Washington University; all subjects provided informed consent for genetic testing. The patient population included mostly sporadic but also some cases of familial FSGS patients. Patients sequenced for an autism study, lacking evaluation for kidney phenotypes were used as controls [66]. Because the controls were of European ancestry, our plan was to focus on FSGS patients of similar genetic ancestry. The podocyte exome was captured from the FSGS patients and sequenced using standard technologies with an average coverage of 200X.

Since the FSGS patient sequences were generated using a different platform and sequenced at a different institution than were the controls, we needed to validate that the two data sets were comparable as this is critical for unbiased analysis. After eliminating two case

samples with <20x average coverage, data from all case and control samples were processed in a single batch with raw data was aligned to the human genome using the BWA/Picard pipeline at the Broad Institute and subsequent variant calling was performed using GATK Unified Genotyper (Figure. 4.1B) [64, 151, 152].

The depth of coverage of protein coding exons targeted by both capture reagents was compared between cases and controls; only those exons covered adequately (>20X) in both cases and controls were advanced into the analysis stage. In summary, 16784 exons and 2769942 base pairs were confidently covered in both case and control cohorts, resulting in 16,008 SNPs and 1724 genes analyzed in the final dataset. The SNP calls were equally represented in cases and controls (GQ>30 and rate of missing genotypes less than 5% in each cohort) (Figure 4.1C).

Next, principal component analysis (PCA) was performed to define an appropriately ancestry matched case-control sample set (Figure 4.2A,B). Thirty patient samples were removed because a mixture of Hispanic ancestry was detected. Three more samples were removed because the call-rate of SNPs was less than 95%. The number of SNPs, heterozygous genotypes, and genotypes containing an alternative allele per sample were similar between cases and controls. This reassured us that we could move forward with association analysis (Figure 4.2C,D,E). Our final dataset contained 179 cases and 378 controls of European-American ancestry as determined by PCA (Table 4.1). Accuracy of this analysis strategy was further confirmed by resequencing key SNPs using Sanger sequencing.

4.4.3 Identification of new candidate genes by testing single variant associations

An association test examining single variants (minor allele frequency (MAF) >1%) was performed using Fisher's exact test. Ten common variants from nine different genes were significantly enriched in cases versus controls with p-value < 0.001 and odds ratios > 4 (Table 4.2). These variants were found only in the sporadic cases and the controls. No common variant was identified in the familial cases. Four cases carried a single copy of the *APOL1* G1 variant (G1); this allele is present in 29% of African Americans but only 0.03% of European Americans and confers FSGS susceptibility when two *APOL1* risk alleles are present [150]. A search of the NHLBI-Exome Sequencing Project database showed that four other single variants enriched in our cohort (*WNK4*, *KANK1*, *IL36G*, *ARHGEF17*) had MAFs that were more common in African Americans. These variants were distributed across many patients, and no variant was linked to other common African SNPs. The specific enrichment for African SNPs in some of our European ancestry patients largely explains the high odds ratios that were calculated for these variants and suggest that some of the risk variants could be ancestral variants.

4.4.4 Identification of new candidate genes by rare variant analysis

Rare variants (MAF < 1%) were analyzed by using tests that compare the total numbers of rare variants between cases and controls. We used three such tests: the burden test [153], the variable threshold test [154] and the C-alpha test [155]. Because the effect sizes of genetic variants differ, the accuracy of each method can vary depending on the specific situation. Using a p-value < 0.001 as a cutoff, we identified 11 genes as potential FSGS susceptibility genes (Table 4.3): *WNK4*, *APOL1*, *DLG5*, *GCC1*, *XYLT1*, *KAT2B*, *BPTF*, *COL4A4*, *NID1*, *EPHX1* and *EPHB6*. Two of these genes, *WNK4* and *APOL1* were also identified by common variant analysis.

In support of our approach, *COL4A4*, identified by rare variant analysis, was recently identified as an FSGS susceptibility gene [156]. With the exception of *APOL1* and *COL4A4*, none of the identified genes has been previously identified as FSGS susceptibility genes. Thus, we identified 16 potential new FSGS genes.

4.4.5 Analysis of known familial FSGS genes

Family studies have identified about 20 genes as the cause of familial FSGS [157, 158]. To determine, whether these genes are also involved in sporadic FSGS, we assessed the frequencies of rare deleterious (missense/nonsense) coding variants in 20 of these genes in cases and controls (Table 4.4). Among cases, 46/179 subjects (32%) had at least one rare variant in these genes compared to 13/378 controls (3.4%, p value = $4.7e-14$) (Table 4.1 and 4.5). The distribution of variants between familial and sporadic cases was similar and consistent with previous studies that about 30% of steroid resistant nephrotic syndrome cases have a variant in a known disease gene [159]. There was also a difference in the total number of unique rare variants identified in cases (59 variants in 179 cases) versus controls (15 variants in 378 controls). The significance of this finding was tested using a permutation analysis of groups of 20 genes randomly chosen from our dataset. This showed, however, that 27% of random sets of 20 genes had a p -value that was similar to or below $4.7e-14$, suggesting the presence of novel FSGS genes with strong genetic effects in our dataset.

4.4.6 Development of a sensitized mouse system to identify potential FSGS disease causing genes

The FSGS syndrome likely involves diverse injury pathways and so no single in vitro

system is available to test whether a particular gene variant might induce FSGS. We therefore developed a genetic system in mouse, to examine the function of candidate genes in vivo in the kidney. Our strategy involved knocking down the expression of candidate genes in a mouse genetic background that is prone to develop FSGS. Previously, we showed that mice that are heterozygous for two podocyte genes, *Cd2ap* and *Synpo* (encoding synaptopodin), developed FSGS with an incomplete penetrance (~25%), with albuminuria, a sign of podocyte dysfunction not apparent until animals are about six months of age [21]. We reasoned that if impairing the function of a candidate gene worsened the phenotype on this transgenic background, by either enhancing the penetrance or leading to an earlier onset of disease, it would validate the specific candidate gene.

We generated ES cells from mice that were *Cd2ap*^{+/-} *Synpo*^{+/-} using standard methods (Figure 4.3A). To induce RNAi expression in a podocyte specific fashion, the ES cells also express a podocyte-specific and doxycycline-inducible trans-activator (*Nphs1*-rtTA3G) [126]. The rtTA3G is a synthetic transcription factor that binds and transactivates promoters that contain the bacterial tet-operator sequence [160]. After confirming the genotype of the ES cells (Figure 4.3B), we confirmed that the ES cells could generate mice with high-level chimerism using the traditional method of blastocyst injection. Using the method of laser-assisted microinjection into 8-cell embryos [143], we also validated that these ES cells could generate mice that were close to 100% derived from the ES cells as assessed by coat color (Figure 4.3C). As expected based on the genotype (Huber et al., 2006), about 50% of the mice generated from these ES cells developed mild proteinuria after three to four months of age (Figure 4.3D).

We then used homologous recombination to integrate a single copy of the RNAi transgene into the mouse *Hprt1* locus to eliminate variability that could result from the random integration of an RNAi transgene [142]. The *Hprt1* locus is on the X chromosome and because the ES cells were male, targeting of the transgene results in complete loss of the *Hprt1* gene resulting in resistance to 6-thioguanine (6-TG) toxicity (Figure 4.4A). This method was efficient as over 90% of the ES cell colonies that survived selection had a correctly targeted recombination event (data not shown).

We validated the system by testing an RNAi for *Cd2ap*. Mice that are *Cd2ap*^{+/-} exhibit normal renal function and have normal lifespans, but mice that completely lack *Cd2ap* expression develop severe proteinuria shortly after birth [77]. To control shRNA expression by doxycycline, shRNA oligos were embedded into the miR30 backbone that allows for RNA polymerase II transcription [161]. We tested multiple *Cd2ap* specific RNAi's *in vitro* for their ability to inhibit *Cd2ap* expression (Figure 4.4B and 4.5A) and the best one (sh877) was targeted into the *Hprt1* locus of our ES cell line (Figure 4.5B). An RNAi targeting the firefly luciferase gene was used as a control. Laser-assisted microinjection generated 16 animals that were nearly 100% derived from the ES cell based on the completely agouti coat-color.

When the chimeric mice were two weeks of age, half were given doxycycline (DOX) in the drinking water to induce shRNA transgene expression. Four weeks later, oodocyte function was assessed by monitoring albumin leakage into the urine by measuring the ratio of albumin to creatinine ratio. All of the DOX treated mice developed proteinuria with an average albumin/creatinine ratio that was almost 150 fold higher than in the control animals (1.5×10^5

compared to 1.0×10^3) (Figure 4.4C). The proteinuria was sustained during eight weeks of DOX treatment and was reversible, as proteinuria abated when DOX was removed (Figure 4.5D). Histological analysis also confirmed the presence of proteinuria, as protein casts were consistently present in tubules (Figure 4.4D). Electron microscopic examination of the kidney showed widespread foot process effacement, another marker of proteinuria (Figure 4.4E). Control RNAi mice targeting firefly luciferase showed no proteinuria after DOX treatment (Figure 4.4F). This verified that our RNAi strategy could be used to test candidate FSGS genes.

4.4.7 Testing candidate FSGS genes using the novel mouse genetic system

To validate our system, we chose four genes, *WNK4*, *DLG5*, *ARHGEF17* and *KANK1*. *WNK4* was chosen as it was identified by single variant analysis and by all three rare variant tests. *ARHGEF17* and *KANK1* were identified by single variant analysis but not by rare variant analysis. *DLG5* was identified by all three rare variant tests but not by single variant analysis. Because the mouse ortholog for human *KANK1* is unclear, we targeted *Kank2* in addition to *Kank1*.

Multiple shRNAs were generated for all five candidate genes and their efficacy was first tested in vitro (Figure 4.6A, and 4.7A,B). Validated shRNAs were then ligated into targeting constructs that were transfected into ES cells. After selection for loss of *Hprt1*, mice were genotyped by PCR to confirm homologous recombination. Two independent clones for each candidate gene were selected for microinjection and 15-30 mice were generated by laser-assisted injection for each clone. Coat color verified that the chimerism for each animal was close to 100%.

At two weeks of age, half of each cohort was given DOX in the drinking water to induce expression of the transgene. Proteinuria was assessed at four weeks and eight weeks after DOX treatment, at which time mice were sacrificed for histological and electron microscopic examination (Figure 4.6B~F). Induction of both the *Wnk4*, *Arhgef17* and *Kank2* RNAi transgenes induced substantial proteinuria four weeks after induction with doxycycline with a level of proteinuria that was between 150-200 fold higher than the controls. For both lines of mice, proteinuria was attenuated after eight weeks (Figure 4.6B, D, E). The *Kank1* RNAi mice showed only modest proteinuria at the four-week time point but proteinuria increased significantly after that (Figure 4.6C).

In contrast, *Dlg5* RNAi mice did not develop significant proteinuria at any time up to 12 weeks after induction (Figure 4.6G and 4.7C). We validated this result by breeding *Dlg5*^{+/-} mice to our sensitized background (*Cd2ap*^{+/-}, *Synpo*^{+/-}). Up to six months of age, no significant difference was detected between triple heterozygous mice (*Dlg5*^{+/-}*Cd2ap*^{+/-}, *Synpo*^{+/-}) and double heterozygous (*Cd2ap*^{+/-}, *Synpo*^{+/-}) littermates (Figure 4.6F). This suggested that *Dlg5* is not an FSGS susceptibility gene or that it may not be epistatic with *Cd2ap* and *Synpo* in podocytes. As expected, electron microscopic examination of the kidneys showed podocyte foot process effacement from *Arhgef17*, *Kank1*, *Kank2* and *Wnk4* RNAi mice, but not in *Dlg5* RNAi mice (Figure 4.7D).

4.5 Discussions

We added *KANK1*, *WNK4* and *ARHGEF17* to the list of 20 known FSGS genes and

reanalyzed the differences between cases and controls. Addition of these three genes increased the p-value to $1.6e-23$. Testing random sets of 23 genes by permutation analysis in cases and controls showed that only 0.04% of random sets equaled or matched the p-value for these 23 genes. This supports the idea that genetic variants in a specific subset of genes may function more broadly to create a susceptible background for the development of sporadic FSGS.

The role of genetics in the pathogenesis of FSGS was thought to be restricted to those with a family history. Familial studies have identified ~20 FSGS disease genes with specific variants that are highly penetrant in these families. The identification of *APOL1* as a sensitizing factor for FSGS in African Americans with HIV demonstrated that genetic factors may also play a role in enhancing susceptibility to FSGS by environmental factors [19, 20]. Here we found that DNA variants in a set of 23 or more genes may play a role in over 46% of non-familial FSGS cases presumably by enhancing podocyte susceptibility to injury. The role of genetics in sporadic cases is likely much weaker than in the familial cases. Common variants were found exclusively in the sporadic cases and in addition, a significant fraction of sporadic cases had more than one variant, a feature that was not seen in any of the controls or the familial cases. Our analysis was likely facilitated by our focus on podocyte-specific genes that we reasoned would have a higher likelihood to be involved in FSGS and by our RNAi mouse model that allowed us to begin validating these genes. Since oligogenic genetic effects and environmental factors are likely to be broadly involved in disease susceptibility, our methods could be widely applicable to the study of other rare and common diseases.

Acknowledgement

This project was supported by grants from NIDDK (A.S.S., J.H.M., M.K., M.G.S.), HHMI (A.S.S.), and the Intramural Research Programs of NIDDK (J.B.K.) and NCI (C.A.W). We thank Dr. V. Vasioukhin for sharing *Dlg5*^{+/-} mice, overexpression and RNAi lentiviral plasmids, and histology staining of *Dlg5*^{-/-} kidney with us and Dr. Channing Der for sharing *Arhgef17* cDNA construct with us. We also thank R. Kopan and members of the Shaw lab for critical discussions.

4.6 Tables and Figures

Table 4.1 Distribution of single and rare variants in FSGS subjects and controls

A total of 192 sporadic and 22 familial FSGS cases were sequenced. 157 sporadic and 22 familial FSGS cases remained after quality control and were compared to 378 controls. The number of subjects with predicted deleterious variants in 20 known FSGS genes, single variants in the top 9 genes from the common variant analysis and the top 11 genes from rare variant analyses. The total number of subjects with variants in 20 known FSGS genes + the three genes that were validated are also shown.

	Sporadic FSGS	Familial FSGS	Total # of Patients	Total # of Controls
Total number of samples sequenced	192	22	214	378
Number of samples that passed QC	157	22	179	378
Number of patients with deleterious variants in 20 known FSGS genes*	40	6	46	13
Number of patients with single variants in 9 genes**	28	0	28	14
Number of patients with rare deleterious variants in 11 genes***	112	4	116	134
Number of patients with variants in 3 validated genes****	32	1	33	8
Number of patients with variants in 20+3 genes	72	7	79	21
Percentage of patients with variants in 20+3 genes	46%	32%	44%	6%
* The list of 20 known genes is in the Supplemental Table 2				
** Genes identified by common variant analysis (Figure 1A)				
*** Genes identified by 3 rare variant analyses (Figure 1B)				
**** Genes validated by our mouse model (<i>ARHGEF17</i> , <i>KANK1</i> and <i>WNK4</i>)				

Table 4.2 Potential FSGS susceptibility genes identified by common variant analyses

15 potential susceptibility genes identified by common variant analysis. The frequency of common variants (MAF > 1%) was assessed in cases versus controls and high scoring variants with odds ratios greater than 2.5 are shown here ranked by p value. For each common variant, the chromosome position, gene name, reference and alternative base pair, overall mean allele frequency, number of alternative alleles in cases versus controls, total number of genotypes in cases, the allele frequency in European vs African Americans from the ESP database, the p value and the odds ratio and the Polyphen prediction score are shown.

CHROM.POS	GENE_NAME	REF	ALT	MAF	MINA	MINU	REFA	ESP_EA	ESP_AA	ANNOTATION	P	OR
chr17:40947320	WNK4	C	T	5.4E-03	6	0	172	1.3E-03	4.95E-01	MISSENSE	1.0E-03	28.2
chr9:710966	KANK1	G	A	2.1E-02	15	8	166	8.0E-03	4.95E-01	MISSENSE	1.1E-03	4.1
chr2:113737630	IL36G	C	A	4.8E-03	5	0	137	1.0E-03	1.23E-01	MISSENSE	1.5E-03	29.9
chr11:73020633	ARHGEF17	G	C	4.5E-03	5	0	168	2.0E-03	2.53E-01	MISSENSE	2.8E-03	24.7
chr17:40939855	WNK4	G	T	4.5E-03	5	0	172	1.2E-03	2.07E-01	MISSENSE	3.2E-03	23.9
chr22:36661906	APOL1	A	G	4.5E-03	5	0	174	3.4E-04	2.26E-01	MISSENSE	3.2E-03	23.8
chr10:123843946	TACC2	C	T	4.5E-03	5	0	173	1.0E-03	1.01E-01	MISSENSE	3.3E-03	23.6
chr8:144994916	PLEC	C	T	4.5E-03	5	0	174	2.5E-03	2.06E-01	MISSENSE	3.3E-03	23.6
chr16:30999434	HSD3B7	T	C	1.6E-02	12	6	168	9.5E-03	2.89E-01	MISSENSE	3.5E-03	4.3
chr8:68204202	ARFGEF1	C	A	6.3E-03	6	1	167	8.4E-03	9.08E-04	MISSENSE	4.7E-03	13.4

CHROM.POS - the chromosome position of a common variant
REF - reference allele
ALT - alternative allele (variant)
MAF - mean allele frequency
MINA - number of alternative alleles in cases
MINU - number of alternative alleles in controls
REFA - number of reference genotypes in cases,
ESP_EA - the allele frequency in European Americans in the NHLBI-Exome Sequencing Project
ESP_AA - the allele frequency in African Americans in the NHLBI-Exome Sequencing Project
OR - allelic odds ratio
Bold - genes that are identified by both Fisher's test (Table 2) and at least one of the three rare variant test

Table 4.3 Potential FSGS susceptibility genes identified by rare variant analyses

11 genes identified by rare variant analyses. Rare missense, and nonsense variants (MAF < 1%) were pooled together for rare variant analysis using the burden, variable threshold and C-alpha tests. The top genes (p-value < 0.001) identified for each test are shown ordered by p value. Genes that were also identified by single gene analysis using Fisher's exact test are shown in bold.

C-alpha	P (C-alpha)	Variable Threshold	P (Variable Threshold)	Burden	P (Burden)
XYLT1	1.74E-04	COL4A4	6.76E-05	DLG5	1.65E-04
APOL1	3.4E-04	DLG5	7.7E-05	COL4A4	1.8E-04
KAT2B	4.37E-04	WNK4	3.10E-04	WNK4	2.89E-04
WNK4	7.6E-04	GCC1	4.8E-04	NID1	3.9E-04
BPTF	7.68E-04			EPHX1	5.42E-04
				GCC1	6.2E-04
				XYLT1	6.97E-04
				EPHB6	7.7E-04

Bold - genes that are identified by both Fisher's test (Table 2) and at least one of the three rare variant test
 VT - variable threshold
 Genes that are identified by 2 rare variant tests
 Genes that are identified by all 3 rare variant tests

Table 4.4 The list of 20 known FSGS genes

GENE NAME			
ACE	CD2AP	INF2	PAX2
ACTN4	COL4A3	LAMB2	PLCE1
ANLN	COL4A4	MYO1E	TCC21B
APOL1	ECT2	NPHS1	TRPC6
ARHGAP24	ENPEP	NPHS2	WT1

Table 4.5 The list of rare deleterious variants identified in 20 known FSGS genes in the FSGS subjects that we sequenced

CHROM.POS	GENE NAME	MINA	MINU	OBSA	OBSU	Mutation Type
chr17:61557751	ACE	1	0	183	380	NON_SYNONYMOUS_CODING
chr17:61559844	ACE	1	0	173	379	NON_SYNONYMOUS_CODING
chr17:61562654	ACE	1	1	182	380	NON_SYNONYMOUS_CODING
chr17:61570992	ACE	1	0	181	379	NON_SYNONYMOUS_CODING
chr19:39198786	ACTN4	1	0	181	380	NON_SYNONYMOUS_CODING
chr19:39220016	ACTN4	1	1	181	343	NON_SYNONYMOUS_CODING
chr7:36438949	ANLN	1	0	172	380	NON_SYNONYMOUS_CODING
chr7:36445826	ANLN	1	1	176	380	NON_SYNONYMOUS_CODING
chr22:36661814	APOL1	1	0	182	380	NON_SYNONYMOUS_CODING
chr22:36661906	APOL1	4	0	182	380	NON_SYNONYMOUS_CODING
chr22:36661940	APOL1	2	0	182	380	NON_SYNONYMOUS_CODING
chr4:86491702	ARHGAP24	1	0	179	380	NON_SYNONYMOUS_CODING
chr4:86491814	ARHGAP24	2	0	181	380	STOP_GAINED
chr4:86852097	ARHGAP24	2	3	170	380	NON_SYNONYMOUS_CODING
chr2:228118867	COL4A3	2	1	177	380	NON_SYNONYMOUS_CODING
chr2:228173675	COL4A3	1	0	142	380	NON_SYNONYMOUS_CODING
chr2:227872069	COL4A4	1	0	182	380	NON_SYNONYMOUS_CODING
chr2:227872777	COL4A4	1	0	181	378	NON_SYNONYMOUS_CODING
chr2:227872887	COL4A4	1	0	182	377	NON_SYNONYMOUS_CODING
chr2:227876939	COL4A4	1	0	182	380	NON_SYNONYMOUS_CODING
chr2:227917111	COL4A4	1	0	155	380	NON_SYNONYMOUS_CODING
chr2:227942712	COL4A4	1	0	142	375	NON_SYNONYMOUS_CODING
chr2:228012183	COL4A4	1	0	179	380	NON_SYNONYMOUS_CODING
chr3:172482204	ECT2	1	1	179	380	NON_SYNONYMOUS_CODING
chr4:111397664	ENPEP	2	0	184	380	NON_SYNONYMOUS_CODING
chr14:105169653	INF2	1	0	176	380	NON_SYNONYMOUS_CODING
chr14:105169717	INF2	1	0	180	380	NON_SYNONYMOUS_CODING
chr14:105169782	INF2	1	0	175	378	NON_SYNONYMOUS_CODING
chr14:105180960	INF2	1	0	175	345	NON_SYNONYMOUS_CODING
chr3:49158893	LAMB2	1	0	183	380	NON_SYNONYMOUS_CODING
chr3:49159265	LAMB2	1	0	183	380	NON_SYNONYMOUS_CODING
chr3:49159603	LAMB2	1	0	183	380	NON_SYNONYMOUS_CODING
chr3:49160746	LAMB2	1	0	183	380	NON_SYNONYMOUS_CODING
chr3:49161062	LAMB2	1	0	179	380	NON_SYNONYMOUS_CODING
chr3:49170064	LAMB2	2	2	175	370	NON_SYNONYMOUS_CODING
chr15:59487752	MYO1E	2	1	179	380	NON_SYNONYMOUS_CODING
chr15:59494583	MYO1E	1	1	146	380	NON_SYNONYMOUS_CODING
chr15:59497600	MYO1E	1	1	165	380	NON_SYNONYMOUS_CODING
chr15:59497622	MYO1E	3	1	172	380	NON_SYNONYMOUS_CODING
chr15:59564514	MYO1E	1	0	164	380	NON_SYNONYMOUS_CODING
chr19:36321981	NPHS1	1	0	182	380	NON_SYNONYMOUS_CODING
chr19:36322018	NPHS1	1	0	182	380	NON_SYNONYMOUS_CODING
chr10:102509533	PAX2	2	0	176	378	NON_SYNONYMOUS_CODING
chr10:95931011	PLCE1	1	1	182	380	NON_SYNONYMOUS_CODING
chr10:96005767	PLCE1	1	0	182	380	NON_SYNONYMOUS_CODING
chr11:32450067	WT1	1	1	184	379	NON_SYNONYMOUS_CODING

CHROM.POS - the chromosome position of a common variant
MINA - number of alternative alleles in cases
MINU - number of alternative alleles in controls
OBSA -
OBSU -

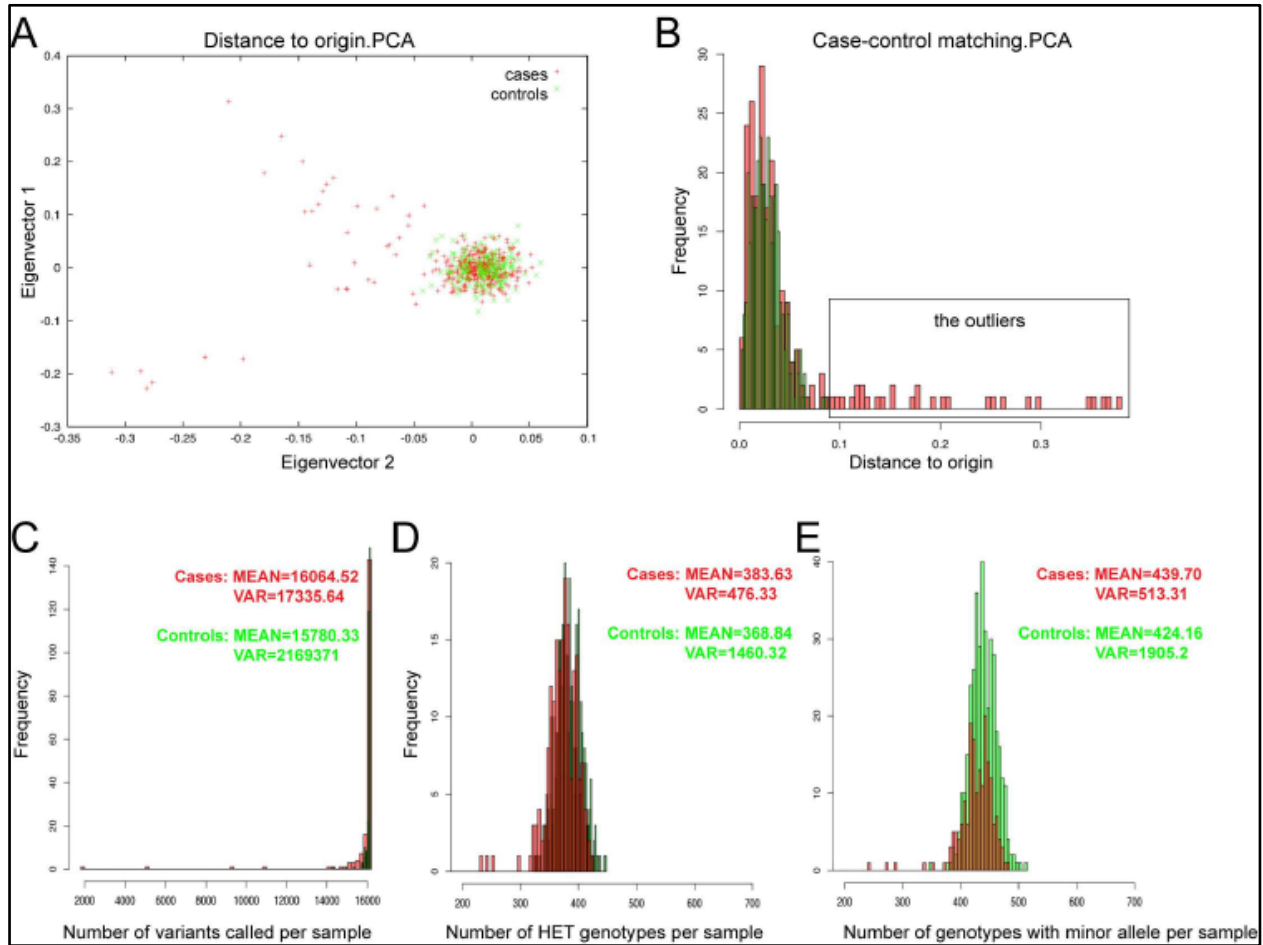


Figure 4.1 Comparability of variant calls between cases and controls

(A) Principal component analysis (PCA) of variants between cases (+) and controls (x) shows close similarity of ancestry. (B) The PCA data shown in A is depicted as distance from the origin. The 30 case sample with a distance of greater than 0.09 from the origin, suggesting substantial admixture with non-European populations, were removed from further analysis. (C) The number of total variants per sample were similar between cases and controls. (D) The number of heterozygous (HET) genotypes was similar between cases and controls. (E) The number of heterozygous or homozygous genotypes containing an alternative allele was similar between cases and controls.

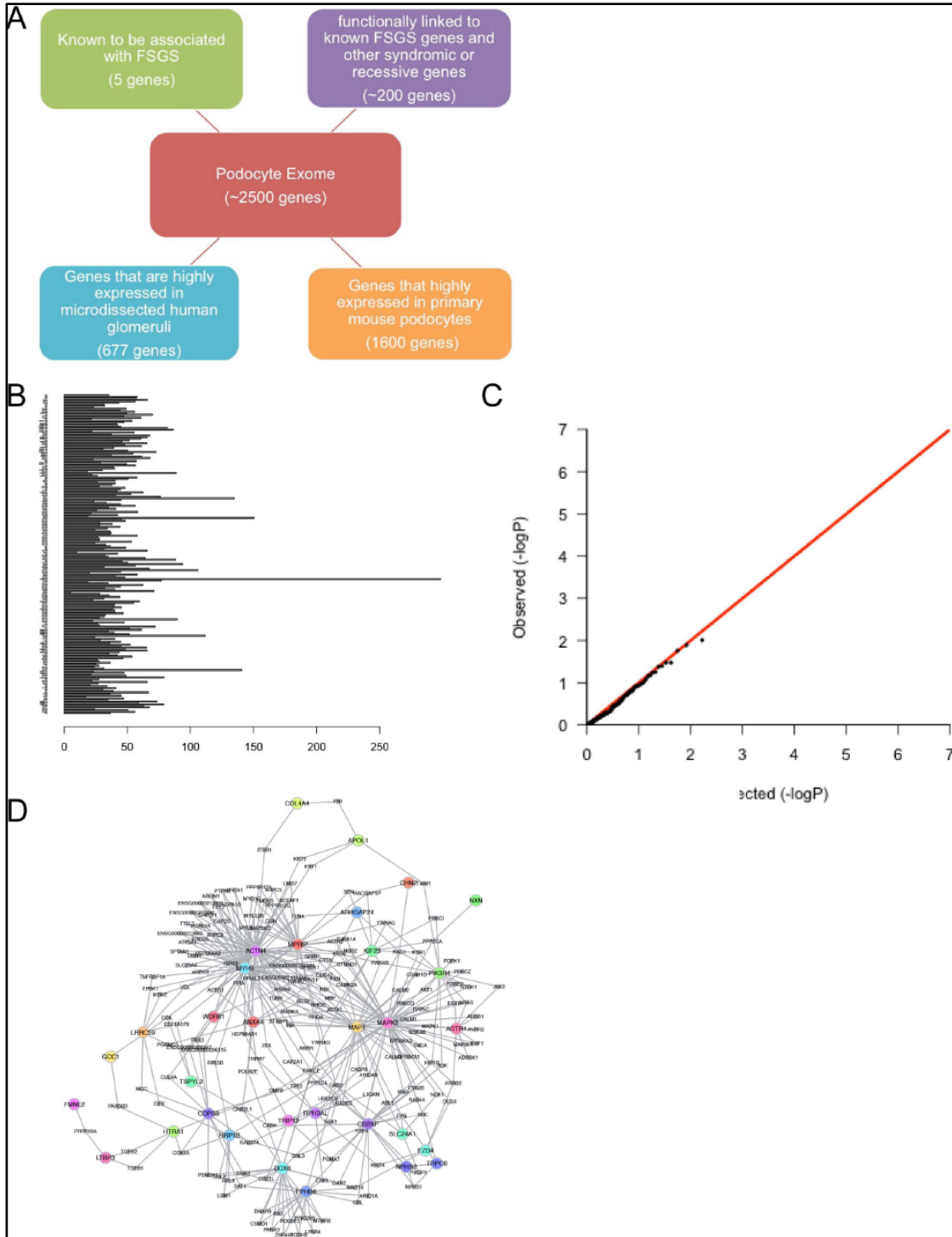


Figure 4.2 Supplementary figure for Figure 4.1

(A) 2500 genes were clustered and defined as “podocyte exome”. (B) Average sequencing coverage for all patients in FSGS cases. Each bar represents the coverage of a patient DNA sample we sequenced. (C) PCA Plot. (D) Dapple analysis for the interaction network of all gene identified by common and rare analyses.

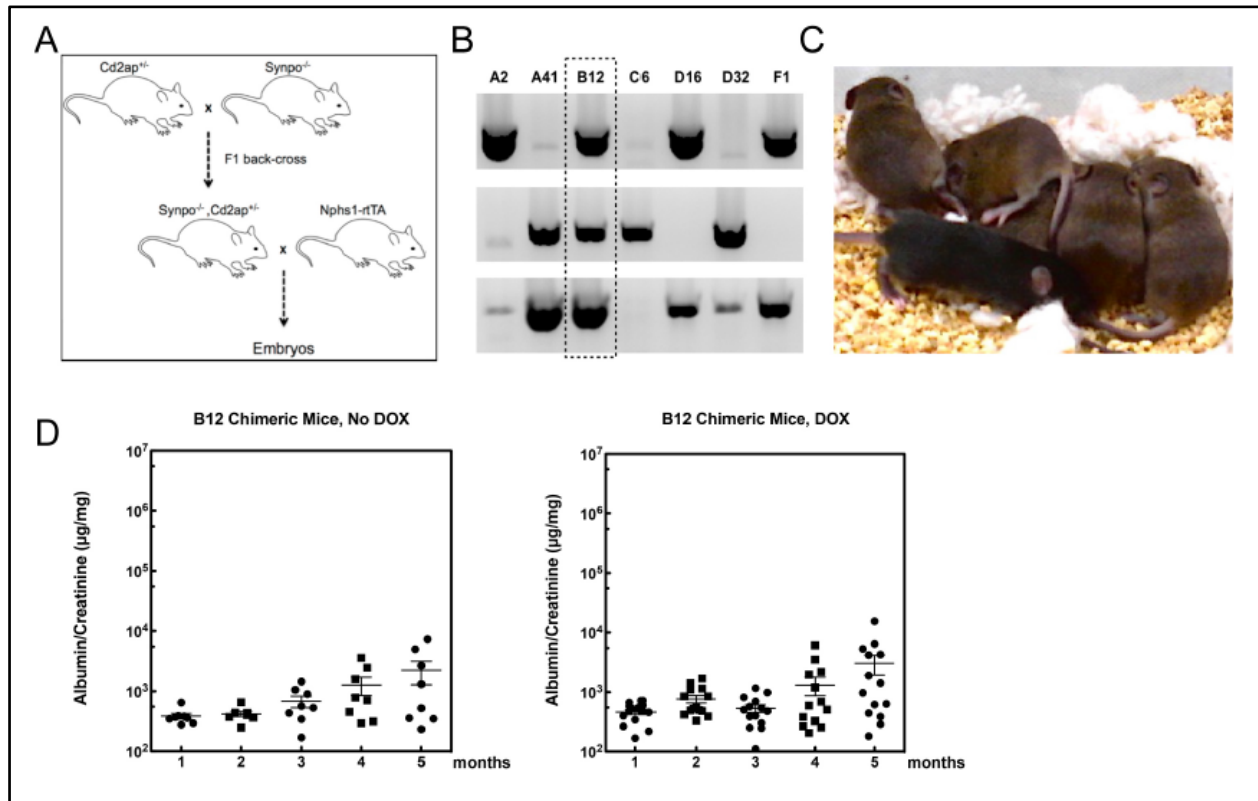


Figure 4.3 Generating an ES cell line with an FSGS susceptibility genetic background
 (A) Male *Synpo*^{-/-}, *Cd2ap*^{+/-} and female *Nphs1-rtTA*3G mice were bred together to isolate blastocyst. ES cell lines were derived from these blastocysts. The chance of deriving a male ES cell line that is *Synpo*^{+/-}, *Cd2ap*^{+/-}, *Nphs1-rtTA*3G is 1/16. (B) Genomic PCR confirms B12 ES cell line is male, *Cd2ap*^{+/-} and *Nphs1-rtTA*3G. *Synpo* +/- was also confirmed (data not shown). (C) Mice were generated using laser assisted injection from B12 ES cell line were monitored for the development of proteinuria by measuring the urine albumin/creatinine ratio. Approximately 50% of mice generated from these ES cells treated with or without doxycycline (administered from 2 weeks of age) slowly developed proteinuria over a period of 3-5 months.

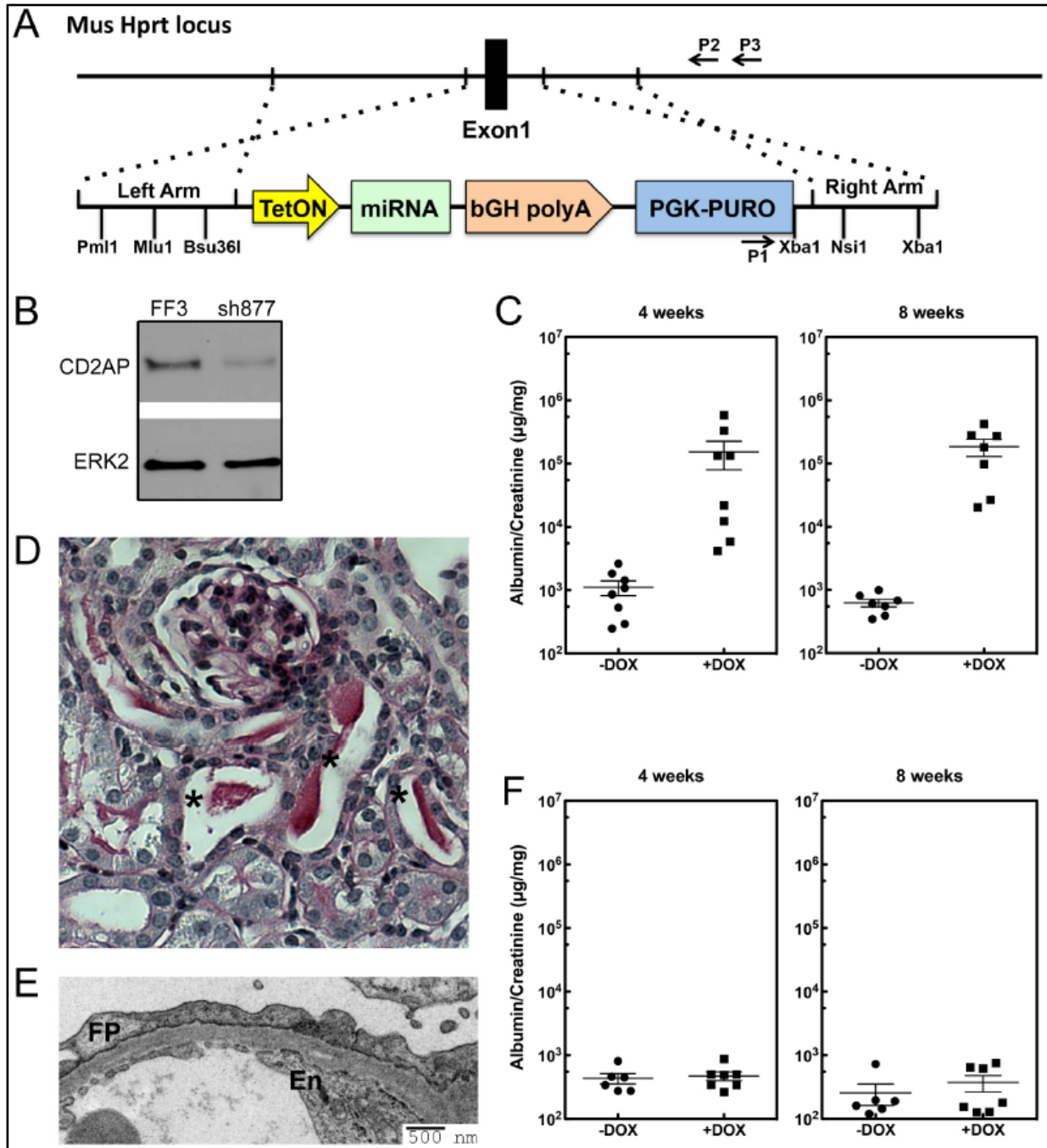


Figure 4.4 Generating a system to validate candidate FSGS genes

(A) The targeting strategy used to integrate a miR30-shRNA transgene into *Hprt1* locus is shown. A targeting vector with the miR30 transgene and a *PGK*-puromycin cassette was generated with left and right homology arms containing sequences that flank exon1 of the *Hprt1* gene on the X chromosome. Primers (P1, P2, and P3) for PCR validation of homologous recombination are shown. (B) The knockdown efficiency of a miR30 shRNA for *Cd2ap* (sh877) is shown. A podocyte cell line was transduced with a lentivirus containing the *Cd2ap* shRNA was blotted for *Cd2ap* expression. *Erk2* was used as a protein loading control. Transduction with an shRNA

targetting firefly luciferase (FF3) serves as a negative control. (C) Mice generated with ES cells with the *Cd2ap* shRNA recombined in the *Hprt1* locus were treated with and without doxycycline for four or eight weeks and urine was analyzed by measuring the urine albumin/creatinine ratio. (D) By light microscopy, Doxycycline treated *Cd2ap*-RNAi mice manifested proteinaceous tubular casts (asterisks). (E) By electron microscopy, doxycycline dependent foot process effacement was present in *Cd2ap*-RNAi mice, while podocyte cytoarchitecture is preserved in control mice. (F) Control FF3-RNAi mice were treated with and without doxycycline for four and eight weeks and urine analyzed by measuring the albumin/creatinine ratio.

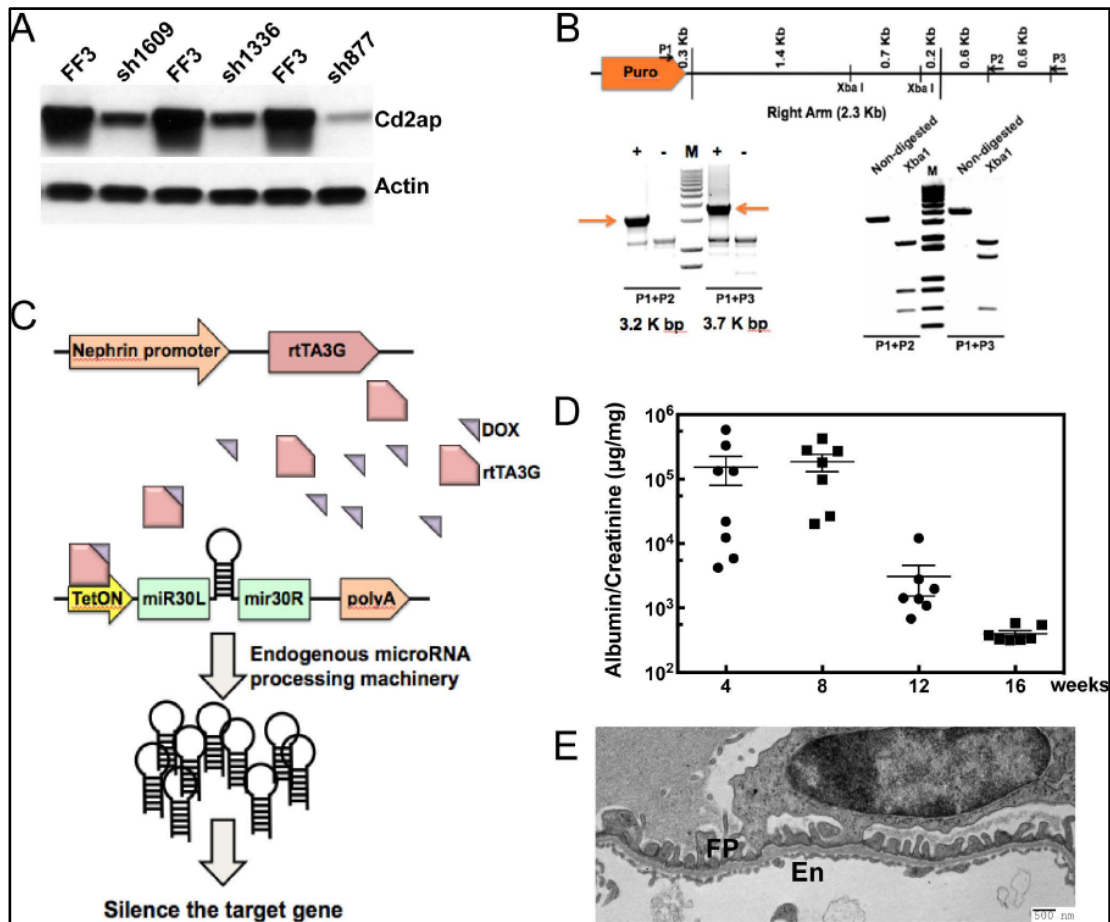
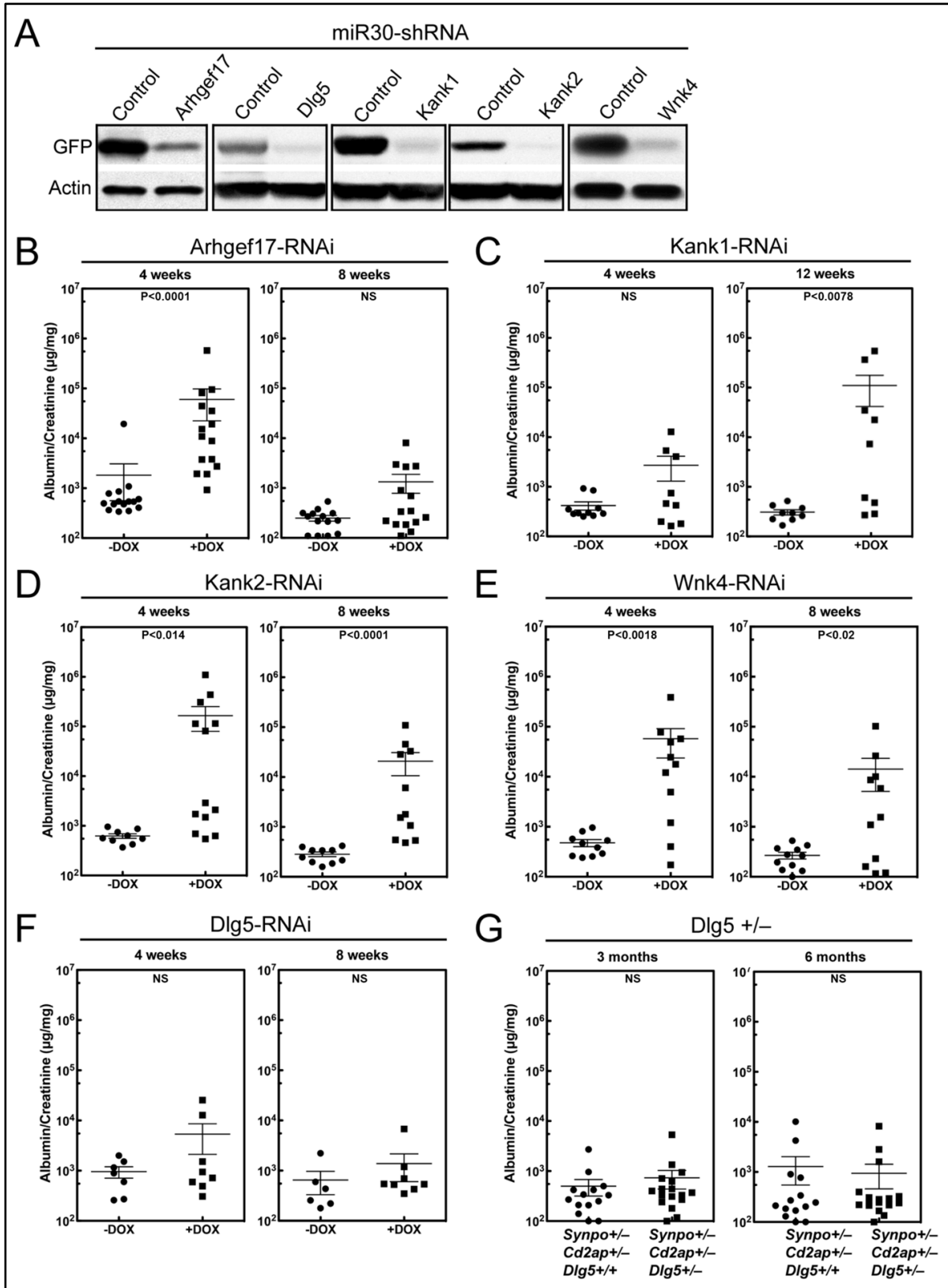


Figure 4.5 Supplemental figure for Figure 4.4

(A) The efficiency of 3 miR30-shRNAs that targets Cd2ap. A mouse CD2AP-EGFP construct was co-expressed with different miR30-shRNA constructs in HEK293 cells. The expression level of CD2AP-EGFP was detected by immunoblotting. Actin immunoblotting was used as loading control. FF3, A miR30-shRNA that targets fire fly luciferase was used as control. The design of genomic PCR and the example of results that validate homologous recombination in ES clones. Forward primer (P1: 5'-CAAGCCCGGTGCCTGATCTAG ATCATAATC-3') was designed at the end of puromycin resistant cassette. Two reverse primers were designed outside the Right Arm. (P2: 5'-CTGTAAAGGTCTCTGAACTACCAATTGCAC-3', and P3: 5'-GAGACTAAGGCAGGAGGATTCCAGGTTT-3'). (B) PCR validation of homologous recombination. The arrows point to the specific PCR products for the PCR reactions by using P1+P2 and P1+P3, and the PCR products were confirmed by restriction digestion with desired sizes of digested DNA fragments. (C) The system of podocyte-specific, DOX-inducible RNAi. (D) *Cd2ap*-RNAi mice showed DOX-dependent proteinuria. The DOX treatment was stopped after 8 weeks. The urine samples were collected at 4, 8, 12 and 16-week time points. Albumin/creatinine ratio was measured and plotted. (E) Untreated *Cd2ap*-RNAi mice showed normal foot processes.



(A) To select the best shRNA construct, multiple shRNAs were tested for *Arhgef17*, *Dlg5*, *Kank1*, *Kank2* and *Wnk4* by inhibiting expression of a construct containing the GFP-tagged target sequence in 293 cells (Figure 4-S3A). GFP immunoblotting was used to determine the best shRNA for each gene. (B-E) Mice were generated by laser-assisted microinjection of ES cells with the specific shRNAs for the indicated genes. After treatment with or without doxycycline to induce expression of the transgene, urine albumin/creatinine ratio was measured after 4 and 8 weeks. As shown, shRNA knockdown of *Arhgef17*, *Kank1*, *Kank2*, and *Wnk4* increased proteinuria at 4 and 8 weeks, (F-G) By contrast, neither *Dlg5* shRNA knockdown nor a *Dlg5*^{+/-} mouse on a susceptible genetic background (*Cdap*^{+/-} and *Synpo*^{+/-}) increased albuminuria.

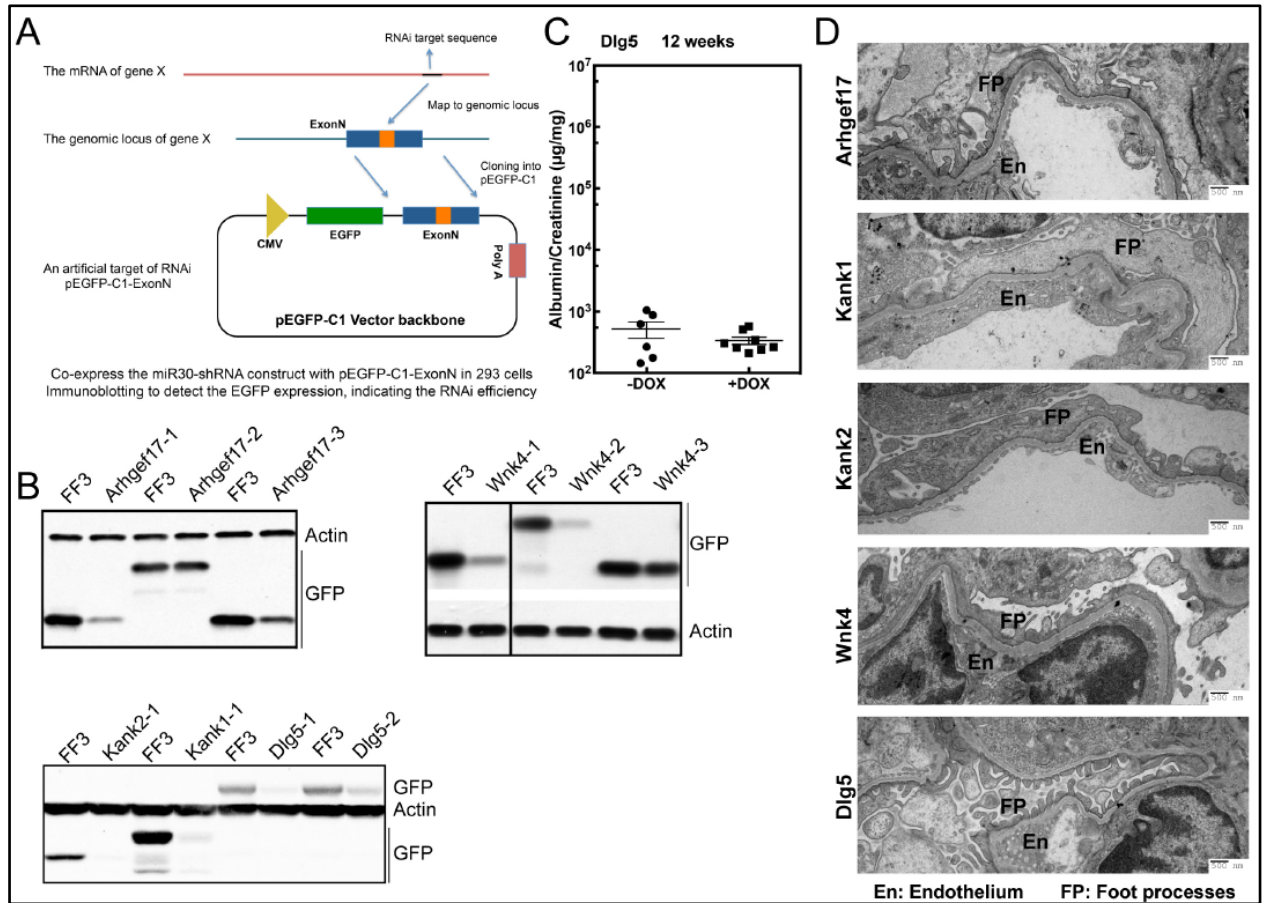


Figure 4.7 Supplemental figure for Figure 4.6

(A) The system was developed to test the RNAi efficiency of a given miR30-shRNA. The ExonX targeted by the shRNA is amplified by genomic PCR and inserted to the 3' end of EGFP sequence of pEGFP-C1 vector. The pEGFP-C1-ExonX became an artificial target for the shRNA. The pEGFP-C1-ExonX and miR30-shRNA constructs were co-expressed in 293 cells, and the expression level of EGFP was detected by immunoblotting. (B) Immunoblotting results for each miR30-shRNA oligo designed for the candidate genes. The FF3 miR30-shRNA was used as control for each miR30-shRNA oligos. Actin immunoblotting was used as loading control. The expression of EGFP was used as an indicator of the RNAi efficiency, the miR30-shRNA oligo that had the best RNAi efficiency was inserted into pHPRT vector to generate RNAi ES cells and mice. (C) *Dig5*-RNAi mice showed no proteinuria after 12 weeks of DOX treatment. (D) Electron microscopy of each RNAi mice showed the foot process effacement.

Chapter 5. Conclusions and Future Directions

5.1 Conclusions

5.1.1 The balance between Rho and Rac activity maintains the morphology and function of the podocyte.

To form properly interdigitated foot processes, podocytes established organized actin cytoskeleton. In the foot processes, actin polymerize into at least two different structures that are observed by transmission electron microscopy, the dense actin bundle and the loose cortical actin network. *In vitro*, active Rho promotes the actin bundle formation, while active Rac promotes the branched actin network. Podocytes regulate the spatial balance of Rac and Rho activities. The active Rho could maintain the thick actin bundles along with other actin bundling proteins such as alpha-actinin4 and INF2, while active Rac could keep the actin network next to the slit diaphragm.

Over-active Rac or Rho in podocytes could cause transient or permanent damages. Transgenic mice that express the constitutively active mutant of either Rac (CA-Rac) or Rho (CA-Rho) are lethal in embryonic stage, which indicates the high toxicity of both constitutively active mutants [162]. Inducible expression of CA-Rho in podocytes cause slow onset of proteinuria and permanent FSGS [49]. In contrast, our research showed that inducible expression of CA-Rac1 caused much faster onset of proteinuria, which can be detected as early as 2 days post doxycycline treatment. This observation supports the hypothesis that foot process

effacement is analogous to lamellipodia. Our result also supports that loss of podocyte foot processes is a direct cause of albumin leakage. Long-term expression of CA-Rac1 could lead to chronic damage such as glomerulosclerosis.

Podocytes express high level of ARHGAP24, a Rho-activated Rac/Cdc42 GAP. We identified this gene initially by comparing expression profiles of differentiated versus undifferentiated mouse podocytes, and later we found mutations of this gene associated with familial FSGS. This protein is also called “FilGAP”, because it binds to filamin A, a protein that dimerizes and binds to branched actin filaments [94, 114]. Thus, ARHGAP24 could work as a barrier between the cortical actin network and the actin bundles to keep the active Rac from the center of the foot processes.

5.1.2 The genetic susceptibility could explain over 46% of the non-familial FSGS subjects.

Our genetic study and podocyte-specific RNAi mouse model identified and validated genetic susceptibility to FSGS in non-familial FSGS cases. FSGS was thought mainly caused by environmental factors such as virus infection, and chemical toxins [3]. Studies of familial FSGS cases have identified about 20 FSGS susceptibility genes, but only a few of them were recently found mutated in non-familial cases. Here we identified another 16 genes that could potentially involve in the susceptibility of non-familial FSGS. We validated 4 genes in our podocyte-specific RNAi mouse model, *ARHGEF17*, *KANK1*, *KANK2* and *WNK4*. We also observe that variants of different genes presents in the same non-familial FSGS subjects but not in familial FSGS subjects. This observation suggests that a combination of low penetrant genetic risks could cause susceptibility to FSGS, which was first shown by our bigenic mouse models [21]. The

oligogenic genetic factors of non-familial FSGS was not considered as important risk factors before, but our research suggests that non-familial FSGS could be caused by oligogenic genetic factors plus an environmental trigger, such as virus infection, chemical toxicity, and a circulating factor in the serum.

5.1.3 Actin Cytoskeleton pathway is the major pathway of susceptibility to FSGS.

Among the known FSGS genes and the susceptibility genes that we identified from our sequencing approach, we found that a large proportion of these genes are involved in regulation of actin cytoskeleton. In the 20 known FSGS genes (Table 4.4), 9 genes either directly interact with actin filaments (*INF2*, *ACTN4*, *MYO1E* and *CD2AP*), or regulate the activity of Rho family GTPases (*ARHGAP24*, *ECT2*, *NPHS1*, *NPHS2*, and *TRPC6*). 3 genes (*COL4A3*, *COL4A4*, and *LAMB2*) are extracellular matrix genes that connect to intracellular actin network through integrins and focal complexes. Thus over half of the familial FSGS genes influence the actin cytoskeleton. The secretion of extracellular matrix proteins is also regulated by actin cytoskeleton. In the susceptibility genes we validated, 3 out of 4 regulate the actin through Rho family GTPases, *KANK1* [163], *KANK2* [164] and *ARHGEF17* [165]. The enrichment of mutants in actin-associated and actin-regulatory genes in FSGS patients support the hypothesis the natural susceptibility to FSGS comes from a weakly organized actin cytoskeleton in the podocytes. Previous mouse model and human genetic studies also support this hypothesis. *Cd2ap* deficient mice develop normal foot processes in the beginning and do not have any protein leakage before 14 days of age. However, after 14 days post natal, *Cd2ap* deficient mice start to exhibit foot process effacement and proteinuria. In children, *NPHS2* mutations account

for about 30% of steroid-resistant nephrotic syndrome [159], which also have proteinuria and foot process effacement. These patients have normal kidney function and foot processes before the syndrome starts. Thus the genetic lesion of *NPHS2* might also lead to an actin network that is susceptible to damage. Minimal change disease and steroid-sensitive nephrotic syndrome, however, show transient proteinuria and foot process effacement, because the actin structure in the podocytes could recover from the diseases to regenerate foot processes.

5.1.4 Elevated Rac signal could cause podocyte shattering and shattered podocytes could still be functional to certain extent.

We detected EGFP_CA-Rac1+ podocytes in the urine of DOX induced NEF/Rac1 mice. Using intravital multi-photon microscopy (MPM), we observed that EGFP_CA-Rac1+ podocytes enhanced membrane ruffling in the glomerulus and that some EGFP_CA-Rac1+ podocytes attached to the renal tubules. These results indicate that abnormal activation of Rac in podocytes could lead to increased membrane activity, decreased adherence, and podocyte loss. Pathological changes that lead to Rac activation in podocytes could also initiate similar response. At physiological condition, the crosstalk between podocytes and glomerular endothelial cells could suppress the Rac activity, and could also maintain the normal foot process structure and adherence. It is well studied that VEGF secreted by podocytes play an important role in maintaining the endothelium, but which cytokine is maintaining low Rac in podocytes is still not known. Damaging factors that increase Rac activity could compensate this physiological signal, and could cause podocyte shattering into the urine.

The process that shattered podocyte established new interaction with the renal tubules

after was overlooked before, because this event is very rare, and hard to detect by conventional histological techniques. We uncovered this process by intravital MPM experiments. This observation suggests that the defects caused by high Rac activity can be compensated and that shattered podocytes are at least partially functional. How the Rac phenotype is compromised and whether this process has physiological or pathological contribution are interesting questions to answer.

5.2 Future Directions

5.2.1 The temporal change of Rho GTPase activity during podocyte damage.

Given the central role of Rho GTPase signaling in maintaining the normal actin cytoskeleton structure in the podocyte, it is intriguing to know how small GTPases are activated in different podocyte damage models. Do they share similar mechanism? Which GTPase contribute the most to podocyte damage? Intravital imaging is a good approach to investigate these questions. However, new mouse models with novel Rho GTPase sensors are required. The bioluminescence resonance energy transfer is a promising candidate sensor technique to investigate dynamic signaling of small GTPases *in vivo*.

5.2.2 The function of *ARHGEF17*, *KANK1*, *KANK2* and *WNK4* in maintaining podocyte function.

In our sequencing study, we identified multiple candidate genes that could be potential susceptibility gene and validated that decreased expression of *ARHGEF17*, *KANK1*, *KANK2* and *WNK4* in podocytes could cause proteinuria in *Cd2ap/Synpo* double heterozygous background. It remains unknown how these genes maintain normal podocyte function. Loss of function of

these risk genes might not directly cause podocyte damage, and which environmental factor trigger FSGS under these susceptible background is also an open question.

5.2.4 Can podocytes de-differentiate and become other cell types after they leave the glomerulus?

Using intravital MPM imaging, we observed that podocytes could interact with other cells outside the glomerulus. Is this phenomenon common in other models of podocyte damage? Are these interactions transient? Can podocytes pass the tubular epithelium and enter the interstitial space? Can they de-differentiate into mesenchymal cells? To answer these questions, lineage-tracing experiments are required.

References

1. Basgen JM, Steffes MW, Stillman a E, Mauer SM (1994) Estimating glomerular number in situ using magnetic resonance imaging and biopsy. *Kidney Int* 45:1668–72.
2. Greka A, Mundel P (2012) Cell biology and pathology of podocytes. *Annu Rev Physiol* 74:299–323. doi: 10.1146/annurev-physiol-020911-153238
3. D'Agati VD, Kaskel FJ, Falk RJ (2011) Focal Segmental Glomerulosclerosis. *N Engl J Med* 365:2398–2411. doi: 10.1056/NEJMra1106556
4. Fahr T (1925) Pathologische Anatomie des Morbus Brightii. *Handb der Spez Pathol Anat und Histol* 6:156–472. doi: 10.1007/978-3-7091-3054-4
5. AR R (1957) A hitherto undescribed vulnerability of the juxtamedullary glomeruli in the lipid nephrosis. *Bull Johns Hopkins Hosp* 100:173–175.
6. Stokes MB, Valeri AM, Markowitz GS, D'Agati VD (2006) Cellular focal segmental glomerulosclerosis: Clinical and pathologic features. *Kidney Int* 70:1783–1792. doi: 10.1038/sj.ki.5001903
7. D'Agati V (2003) Pathologic classification of focal segmental glomerulosclerosis. *Semin Nephrol* 23:117–134. doi: 10.1053/snep.2003.50012
8. Kaplan JM, Kim SH, North KN, et al. (2000) Mutations in ACTN4, encoding alpha-actinin-4, cause familial focal segmental glomerulosclerosis. *Nat Genet* 24:251–6. doi: 10.1038/73456
9. Gbadegesin RA, Hall G, Adeyemo A, et al. (2014) Mutations in the Gene That Encodes the F-Actin Binding Protein Anillin Cause FSGS. *J Am Soc Nephrol ASN*.2013090976–. doi: 10.1681/ASN.2013090976
10. Kim JM, Wu H, Green G, et al. (2003) CD2-associated protein haploinsufficiency is linked to glomerular disease susceptibility. *Science* 300:1298–300. doi: 10.1126/science.1081068
11. Gigante M, Pontrelli P, Montemurno E, et al. (2009) CD2AP mutations are associated with sporadic nephrotic syndrome and focal segmental glomerulosclerosis (FSGS). *Nephrol Dial Transplant* 24:1858–64. doi: 10.1093/ndt/gfn712
12. Löwik MM, Groenen PJTA, Pronk I, et al. (2007) Focal segmental glomerulosclerosis in a patient homozygous for a CD2AP mutation. *Kidney Int* 72:1198–203. doi: 10.1038/sj.ki.5002469
13. Brown EJ, Schlöndorff JS, Becker DJ, et al. (2010) Mutations in the formin gene INF2 cause focal segmental glomerulosclerosis. *Nat Genet* 42:72–6. doi: 10.1038/ng.505
14. Kopp JB, Smith MW, Nelson GW, et al. (2008) MYH9 is a major-effect risk gene for focal segmental glomerulosclerosis. *Nat Genet* 40:1175–84. doi: 10.1038/ng.226
15. Kao WHL, Klag MJ, Meoni LA, et al. (2008) MYH9 is associated with nondiabetic end-stage renal disease in African Americans. *Nat Genet* 40:1185–92. doi: 10.1038/ng.232
16. Boute N, Gribouval O, Roselli S, et al. (2000) NPHS2, encoding the glomerular protein podocin, is mutated in autosomal recessive steroid-resistant nephrotic syndrome. *Nat Genet* 24:349–54. doi: 10.1038/74166
17. Winn MP, Conlon PJ, Lynn KL, et al. (2005) A mutation in the TRPC6 cation channel causes familial focal segmental glomerulosclerosis. *Science* 308:1801–1804. doi: 10.1126/science.1106215

18. Reiser J, Polu KR, Möller CC, et al. (2005) TRPC6 is a glomerular slit diaphragm-associated channel required for normal renal function. *Nat Genet* 37:739–44. doi: 10.1038/ng1592
19. Genovese G, Friedman DJ, Ross MD, et al. (2010) Association of trypanolytic ApoL1 variants with kidney disease in African Americans. *Science* 329:841–5. doi: 10.1126/science.1193032
20. Kopp JB, Nelson GW, Sampath K, et al. (2011) APOL1 Genetic Variants in Focal Segmental Glomerulosclerosis and HIV-Associated Nephropathy. *J Am Soc Nephrol* 22:2129–2137. doi: 10.1681/ASN.2011040388
21. Huber TB, Kwoh C, Wu H, et al. (2006) Bigenic mouse models of focal segmental glomerulosclerosis involving pairwise interaction of CD2AP, Fyn, and synaptopodin. *J Clin Invest* 116:1337–1345. doi: 10.1172/JCI27400
22. Zheng Z, Schmidt-Ott KM, Chua S, et al. (2005) A Mendelian locus on chromosome 16 determines susceptibility to doxorubicin nephropathy in the mouse. *Proc Natl Acad Sci U S A* 102:2502–2507. doi: 10.1073/pnas.0409786102
23. Papeta N, Zheng Z, Schon EA, et al. (2010) Prkdc participates in mitochondrial genome maintenance and prevents Adriamycin-induced nephropathy in mice. *J Clin Invest* 120:4055–64. doi: 10.1172/JCI43721
24. Wiggins RC (2007) The spectrum of podocytopathies: a unifying view of glomerular diseases. *Kidney Int* 71:1205–14. doi: 10.1038/sj.ki.5002222
25. Wiggins JE, Goyal M, Sanden SK, et al. (2005) Podocyte hypertrophy, “adaptation,” and “decompensation” associated with glomerular enlargement and glomerulosclerosis in the aging rat: prevention by calorie restriction. *J Am Soc Nephrol* 16:2953–66. doi: 10.1681/ASN.2005050488
26. Wharram BL, Goyal M, Wiggins JE, et al. (2005) Podocyte depletion causes glomerulosclerosis: diphtheria toxin-induced podocyte depletion in rats expressing human diphtheria toxin receptor transgene. *J Am Soc Nephrol* 16:2941–2952. doi: 10.1681/ASN.2005010055
27. Burnette DT, Shao L, Ott C, et al. (2014) A contractile and counterbalancing adhesion system controls the 3D shape of crawling cells. *J Cell Biol* 205:83–96. doi: 10.1083/jcb.201311104
28. Faul C, Asanuma K, Yanagida-Asanuma E, et al. (2007) Actin up: regulation of podocyte structure and function by components of the actin cytoskeleton. *Trends Cell Biol* 17:428–437. doi: S0962-8924(07)00167-5 [pii] 10.1016/j.tcb.2007.06.006
29. Ichimura K, Kurihara H, Sakai T (2003) Actin Filament Organization of Foot Processes in Rat Podocytes. *J Histochem Cytochem* 51:1589–1600. doi: 10.1177/002215540305101203
30. Huber TB, Benzing T (2005) The slit diaphragm: a signaling platform to regulate podocyte function. *Curr Opin Nephrol Hypertens* 14:211–216. doi: 10.1097/01.mnh.0000165885.85803.a8
31. Verma R, Kovari I, Soofi A, et al. (2006) Nephrin ectodomain engagement results in Src kinase activation, nephrin phosphorylation, Nck recruitment, and actin polymerization. *J Clin Invest* 116:1346–1359. doi: 10.1172/JCI27414

32. Shih NY, Li J, Cotran R, et al. (2001) CD2AP localizes to the slit diaphragm and binds to nephrin via a novel C-terminal domain. *Am J Pathol* 159:2303–2308. doi: 10.1016/S0002-9440(10)63080-5
33. Jones N, Blasutig IM, Eremina V, et al. (2006) Nck adaptor proteins link nephrin to the actin cytoskeleton of kidney podocytes. *Nature* 440:818–823. doi: 10.1038/nature04662
34. Welsch T, Endlich N, Kriz W, Endlich K (2001) CD2AP and p130Cas localize to different F-actin structures in podocytes. *Am J Physiol Renal Physiol* 281:F769–F777.
35. Bruck S, Huber TB, Ingham RJ, et al. (2006) Identification of a novel inhibitory actin-capping protein binding motif in CD2-associated protein. *J Biol Chem* 281:19196–19203. doi: 10.1074/jbc.M600166200
36. Edwards M, Zwolak A, Schafer DA, et al. (2014) Capping protein regulators fine-tune actin assembly dynamics. *Nat Rev Mol Cell Biol* 15:677–689. doi: 10.1038/nrm3869
37. Zhao J, Bruck S, Cemerski S, et al. (2012) CD2AP Links Cortactin and Capping Protein at the Cell Periphery to Facilitate Lamellipodia Formation. *Mol Cell Biol*. doi: 10.1128/MCB.00734-12
38. Rivero-Lezcano OM, Marcilla A, Sameshima JH, Robbins KC (1995) Wiskott-Aldrich syndrome protein physically associates with Nck through Src homology 3 domains. *Mol Cell Biol* 15:5725–5731.
39. Naumanen P, Lappalainen P, Hotulainen P (2008) Mechanisms of actin stress fibre assembly. *J. Microsc.* pp 446–454
40. Sun H, Schlondorff J, Higgs HN, Pollak MR (2013) Inverted Formin 2 Regulates Actin Dynamics by Antagonizing Rho/Diaphanous-related Formin Signaling. *J Am Soc Nephrol* 1–13. doi: 10.1681/ASN.2012080834
41. Vicente-Manzanares M, Ma X, Adelstein RS, Horwitz AR (2009) Non-muscle myosin II takes centre stage in cell adhesion and migration. *Nat Rev Mol Cell Biol* 10:778–790. doi: 10.1038/nrm2786
42. Beall B, Chalovich JM (2001) Fesselin, a synaptopodin-like protein, stimulates actin nucleation and polymerization. *Biochemistry* 40:14252–14259. doi: 10.1021/bi011806u
43. Wong JS, Iorns E, Rheault MN, et al. (2011) Rescue of tropomyosin deficiency in *Drosophila* and human cancer cells by synaptopodin reveals a role of tropomyosin α in RhoA stabilization. *EMBO J* 31:1028–1040. doi: 10.1038/emboj.2011.464
44. Hood JD, Cheresh DA (2002) Role of integrins in cell invasion and migration. *Nat Rev Cancer* 2:91–100. doi: 10.1038/nrc727
45. Miner JH, Li C (2000) Defective glomerulogenesis in the absence of laminin alpha5 demonstrates a developmental role for the kidney glomerular basement membrane. *Dev Biol* 217:278–289. doi: 10.1006/dbio.1999.9546
46. Schordan S, Schordan E, Endlich K, Endlich N (2011) AlphaV-integrins mediate the mechanoprotective action of osteopontin in podocytes. *Am J Physiol Renal Physiol* 300:F119–F132. doi: 10.1152/ajprenal.00143.2010
47. Wozniak MA, Modzelewska K, Kwong L, Keely PJ (2004) Focal adhesion regulation of cell behavior. *Biochim Biophys Acta* 1692:103–119. doi: 10.1016/j.bbamcr.2004.04.007

48. Hall A (1998) Rho GTPases and the actin cytoskeleton. *Science* (80-) 279:509–514.
49. Zhu L, Jiang R, Aoudjit L, et al. (2011) Activation of RhoA in podocytes induces focal segmental glomerulosclerosis. *J Am Soc Nephrol* 22:1621–1630. doi: 10.1681/ASN.2010111146
50. Scott RP, Hawley SP, Ruston J, et al. (2012) Podocyte-specific loss of Cdc42 leads to congenital nephropathy. *J Am Soc Nephrol* 23:1149–1154. doi: 10.1681/ASN.2011121206
51. Babelova A, Jansen F, Sander K, et al. (2013) Activation of Rac-1 and RhoA contributes to podocyte injury in chronic kidney disease. *PLoS One*. doi: 10.1371/journal.pone.0080328
52. Blattner SM, Hodgins JB, Nishio M, et al. (2013) Divergent functions of the Rho GTPases Rac1 and Cdc42 in podocyte injury. *Kidney Int*. doi: 10.1038/ki.2013.175
53. Jaffe AB, Hall A (2005) Rho GTPases: biochemistry and biology. *Annu Rev Cell Dev Biol* 21:247–269. doi: 10.1146/annurev.cellbio.21.020604.150721
54. Boulter E, Garcia-Mata R, Guilluy C, et al. (2010) Regulation of Rho GTPase crosstalk, degradation and activity by RhoGDI1. *Nat Cell Biol* 12:477–483. doi: 10.1038/ncb2049
55. Garcia-Mata R, Boulter E, BurrIDGE K (2011) The “invisible hand”: regulation of RHO GTPases by RHOGDIs. *Nat Rev Mol Cell Biol* 12:493–504. doi: 10.1038/nrm3153
56. Shibata S, Nagase M, Yoshida S, et al. (2008) Modification of mineralocorticoid receptor function by Rac1 GTPase: implication in proteinuric kidney disease. *Nat Med* 14:1370–1376. doi: nm.1879 [pii] 10.1038/nm.1879
57. Zhu J, Sun N, Aoudjit L, et al. (2008) Nephrin mediates actin reorganization via phosphoinositide 3-kinase in podocytes. *Kidney Int* 73:556–566. doi: 10.1038/sj.ki.5002691
58. Uhlen M, Oksvold P, Fagerberg L, et al. (2010) Towards a knowledge-based Human Protein Atlas. *Nat Biotechnol* 28:1248–1250. doi: 10.1038/nbt1210-1248
59. Asanuma K, Yanagida-Asanuma E, Faul C, et al. (2006) Synaptopodin orchestrates actin organization and cell motility via regulation of RhoA signalling. *Nat Cell Biol* 8:485–491. doi: ncb1400 [pii] 10.1038/ncb1400
60. Yanagida-Asanuma E, Asanuma K, Kim K, et al. (2007) Synaptopodin protects against proteinuria by disrupting Cdc42:IRSp53:Mena signaling complexes in kidney podocytes. *Am J Pathol* 171:415–427. doi: 10.2353/ajpath.2007.070075
61. Tian D, Jacobo SM, Billing D, et al. (2010) Antagonistic regulation of actin dynamics and cell motility by TRPC5 and TRPC6 channels. *Sci Signal* 3:ra77. doi: 3/145/ra77 [pii] 10.1126/scisignal.2001200
62. Bunney TD, Katan M (2006) Phospholipase C epsilon: linking second messengers and small GTPases. *Trends Cell Biol* 16:640–648. doi: 10.1016/j.tcb.2006.10.007
63. Metzker ML (2010) Sequencing technologies - the next generation. *Nat Rev Genet* 11:31–46. doi: 10.1038/nrg2626
64. DePristo MA, Banks E, Poplin R, et al. (2011) A framework for variation discovery and genotyping using next-generation DNA sequencing data. *Nat Genet* 43:491–498. doi: 10.1038/ng.806
65. Vogelstein B, Papadopoulos N, Velculescu VE, et al. (2013) Cancer genome landscapes. *Science* 339:1546–58. doi: 10.1126/science.1235122

66. Neale BM, Kou Y, Liu L, et al. (2012) Patterns and rates of exonic de novo mutations in autism spectrum disorders. *Nature* 485:242–5. doi: 10.1038/nature11011
67. Nejentsev S, Walker N, Riches D, et al. (2009) Rare variants of IFIH1, a gene implicated in antiviral responses, protect against type 1 diabetes. *Science* 324:387–389. doi: 10.1126/science.1167728
68. Ashraf S, Gee HY, Woerner S, et al. (2013) ADCK4 mutations promote steroid-Resistant nephrotic syndrome through CoQ10 biosynthesis disruption. *J Clin Invest* 123:5179–5189. doi: 10.1172/JCI69000
69. Gee HY, Saisawat P, Ashraf S, et al. (2013) ARHGDI1 mutations cause nephrotic syndrome via defective RHO GTPase signaling. *J Clin Invest* 123:3243–3253. doi: 10.1172/JCI69134
70. Gee HY, Ashraf S, Wan X, et al. (2014) Mutations in EMP2 cause childhood-onset Nephrotic syndrome. *Am J Hum Genet* 94:884–890. doi: 10.1016/j.ajhg.2014.04.010
71. Köttgen A, Glazer NL, Dehghan A, et al. (2009) Multiple loci associated with indices of renal function and chronic kidney disease. *Nat Genet* 41:712–717. doi: 10.1038/ng.377
72. Köttgen A, Pattaro C, Böger CA, et al. (2010) New loci associated with kidney function and chronic kidney disease. *Nat Genet* 42:376–384. doi: 10.1038/ng.568
73. Putaala H, Soininen R, Kilpelainen P, et al. (2001) The murine nephrin gene is specifically expressed in kidney, brain and pancreas: inactivation of the gene leads to massive proteinuria and neonatal death. *Hum Mol Genet* 10:1–8.
74. Mollet G, Ratelade J, Boyer O, et al. (2009) Podocin inactivation in mature kidneys causes focal segmental glomerulosclerosis and nephrotic syndrome. *J Am Soc Nephrol* 20:2181–2189. doi: 10.1681/ASN.2009040379
75. Donoviel DB, Freed DD, Vogel H, et al. (2001) Proteinuria and perinatal lethality in mice lacking NEPH1, a novel protein with homology to NEPHRIN. *Mol Cell Biol* 21:4829–4836. doi: 10.1128/MCB.21.14.4829-4836.2001
76. Michaud J-L, Lemieux LI, Dubé M, et al. (2003) Focal and segmental glomerulosclerosis in mice with podocyte-specific expression of mutant alpha-actinin-4. *J Am Soc Nephrol* 14:1200–1211. doi: 10.1097/01.ASN.0000059864.88610.5E
77. Shih NY, Li J, Karpitskii V, et al. (1999) Congenital nephrotic syndrome in mice lacking CD2-associated protein. *Science* (80-) 286:312–315. doi: 7865 [pii]
78. Eckel J, Lavin PJ, Finch EA, et al. (2011) TRPC6 enhances angiotensin II-induced albuminuria. *J Am Soc Nephrol* 22:526–535. doi: 10.1681/ASN.2010050522
79. Johnstone DB, Zhang J, George B, et al. (2011) Podocyte-specific deletion of Myh9 encoding nonmuscle myosin heavy chain 2A predisposes mice to glomerulopathy. *Mol Cell Biol* 31:2162–2170. doi: 10.1128/MCB.05234-11
80. Göppert-Mayer M (1931) Über Elementarakte mit zwei Quantensprüngen. *Ann Phys* 401:273–294. doi: 10.1002/andp.19314010303
81. Denk W, Strickler JH, Webb WW (1990) Two-photon laser scanning fluorescence microscopy. *Science* 248:73–76. doi: 10.1126/science.2321027
82. Zipfel WR, Williams RM, Webb WW (2003) Nonlinear magic: multiphoton microscopy in the biosciences. *Nat Biotechnol* 21:1369–1377. doi: 10.1038/nbt899

83. Williams RM, Zipfel WR, Webb WW (2001) Multiphoton microscopy in biological research. *Curr Opin Chem Biol* 5:603–608. doi: 10.1016/S1367-5931(00)00241-6
84. Zipfel WR, Williams RM, Christie R, et al. (2003) Live tissue intrinsic emission microscopy using multiphoton-excited native fluorescence and second harmonic generation. *Proc Natl Acad Sci U S A* 100:7075–7080. doi: 10.1073/pnas.0832308100
85. Hackl MJ, Burford JL, Villanueva K, et al. (2013) Tracking the fate of glomerular epithelial cells in vivo using serial multiphoton imaging in new mouse models with fluorescent lineage tags. *Nat Med* 19:1661–1666. doi: 10.1038/nm.3405
86. Endlich N, Simon O, Göpferich A, et al. (2013) Two-Photon Microscopy Reveals Stationary Podocytes in Living Zebrafish Larvae. *J Am Soc Nephrol* 681–686. doi: 10.1681/ASN.2013020178
87. Burford JL, Villanueva K, Lam L, et al. (2014) Intravital imaging of podocyte calcium in glomerular injury and disease. *J Clin Invest* 124:2050–2058. doi: 10.1172/JCI71702
88. Pavenstädt H, Kriz W, Kretzler M (2003) Cell biology of the glomerular podocyte. *Physiol Rev* 83:253–307. doi: 10.1152/physrev.00020.2002
89. Kriz W (2005) TRPC6 - A new podocyte gene involved in focal segmental glomerulosclerosis. *Trends Mol Med* 11:527–530. doi: 10.1016/j.molmed.2005.10.001
90. Tybulewicz VLJ, Henderson RB (2009) Rho family GTPases and their regulators in lymphocytes. *Nat Rev Immunol* 9:630–644. doi: 10.1038/nri2606
91. Tryggvason K, Patrakka J, Wartiovaara J (2006) Hereditary proteinuria syndromes and mechanisms of proteinuria. *N Engl J Med* 354:1387–1401. doi: 10.1056/NEJMra052131
92. D'Agati VD (2008) Podocyte injury in focal segmental glomerulosclerosis: Lessons from animal models (a play in five acts). *Kidney Int* 73:399–406. doi: 10.1038/sj.ki.5002655
93. Mundel P, Reiser J (2010) Proteinuria: an enzymatic disease of the podocyte? *Kidney Int* 77:571–580. doi: 10.1038/ki.2009.424
94. Ohta Y, Hartwig JH, Stossel TP (2006) FilGAP, a Rho- and ROCK-regulated GAP for Rac binds filamin A to control actin remodelling. *Nat Cell Biol* 8:803–814. doi: 10.1038/ncb1437
95. Mundel P, Reiser J, Zúñiga Mejía Borja A, et al. (1997) Rearrangements of the cytoskeleton and cell contacts induce process formation during differentiation of conditionally immortalized mouse podocyte cell lines. *Exp Cell Res* 236:248–258. doi: 10.1006/excr.1997.3739
96. Akilesh S, Huber TB, Wu H, et al. (2008) Podocytes use FcRn to clear IgG from the glomerular basement membrane. *Proc Natl Acad Sci U S A* 105:967–972. doi: 10.1073/pnas.0711515105
97. Takemoto M, Asker N, Gerhardt H, et al. (2002) A new method for large scale isolation of kidney glomeruli from mice. *Am J Pathol* 161:799–805. doi: 10.1016/S0002-9440(10)64239-3
98. Takemoto M, He L, Norlin J, et al. (2006) Large-scale identification of genes implicated in kidney glomerulus development and function. *EMBO J* 25:1160–1174. doi: 10.1038/sj.emboj.7601014
99. Mundel P, Gilbert P, Kriz W (1991) Podocytes in glomerulus of rat kidney express a characteristic 44 KD protein. *J Histochem Cytochem* 39:1047–1056. doi: 10.1177/39.8.1856454

100. Abràmoff MD, Magalhães PJ, Ram SJ (2004) Image processing with imageJ. *Biophotonics Int* 11:36–41. doi: 10.1117/1.3589100
101. Moeller MJ, Soofi A, Braun GS, et al. (2004) Protocadherin FAT1 binds Ena/VASP proteins and is necessary for actin dynamics and cell polarization. *EMBO J* 23:3769–3779. doi: 10.1038/sj.emboj.7600380
102. Rottner K, Hall A, Small J V. (1999) Interplay between Rac and Rho in the control of substrate contact dynamics. *Curr Biol* 9:640–648. doi: 10.1016/S0960-9822(99)80286-3
103. Tcherkezian J, Lamarche-Vane N (2007) Current knowledge of the large RhoGAP family of proteins. *Biol Cell* 99:67–86. doi: 10.1042/BC20060086
104. Burridge K, Wennerberg K (2004) Rho and Rac Take Center Stage. *Cell* 116:167–179. doi: 10.1016/S0092-8674(04)00003-0
105. Sander EE, Ten Klooster JP, Van Delft S, et al. (1999) Rac downregulates Rho activity: Reciprocal balance between both GTPases determines cellular morphology and migratory behavior. *J Cell Biol* 147:1009–1021. doi: 10.1083/jcb.147.5.1009
106. Sanz-Moreno V, Gadea G, Ahn J, et al. (2008) Rac Activation and Inactivation Control Plasticity of Tumor Cell Movement. *Cell* 135:510–523. doi: 10.1016/j.cell.2008.09.043
107. Faul C, Donnelly M, Merscher-Gomez S, et al. (2008) The actin cytoskeleton of kidney podocytes is a direct target of the antiproteinuric effect of cyclosporine A. *Nat Med* 14:931–938. doi: 10.1038/nm.1857
108. Rao TK, Friedman EA, Nicastrì AD (1987) The types of renal disease in the acquired immunodeficiency syndrome. *N Engl J Med* 316:1062–1068. doi: 10.1056/NEJM198704233161705
109. Lu TC, He JC, Wang ZH, et al. (2008) HIV-1 Nef disrupts the podocyte actin cytoskeleton by interacting with diaphanous interacting protein. *J Biol Chem* 283:8173–8182. doi: 10.1074/jbc.M708920200
110. Fackler OT, Luo W, Geyer M, et al. (1999) Activation of Vav by Nef induces cytoskeletal rearrangements and downstream effector functions. *Mol Cell* 3:729–739. doi: 10.1016/S1097-2765(01)80005-8
111. Sunamoto M, Husain M, He JC, et al. (2003) Critical role for Nef in HIV-1-induced podocyte dedifferentiation. *Kidney Int* 64:1695–1701. doi: 10.1046/j.1523-1755.2003.00283.x
112. Boulter E, Garcia-Mata R, Guilluy C, et al. (2010) Regulation of Rho GTPase crosstalk, degradation and activity by RhoGDI1. *Nat Cell Biol* 12:477–483. doi: ncb2049 [pii] 10.1038/ncb2049
113. Togawa A, Miyoshi J, Ishizaki H, et al. (1999) Progressive impairment of kidneys and reproductive organs in mice lacking Rho GDI α . *Oncogene* 18:5373–5380. doi: 10.1038/sj.onc.1202921
114. Nakamura F, Heikkinen O, Pentikäinen OT, et al. (2009) Molecular basis of filamin A-FilGAP interaction and its impairment in congenital disorders associated with Filamin A mutations. *PLoS One*. doi: 10.1371/journal.pone.0004928
115. Nakamura F, Osborn TM, Hartemink CA, et al. (2007) Structural basis of filamin A functions. *J Cell Biol* 179:1011–1025. doi: 10.1083/jcb.200707073

116. Burridge K, Doughman R (2006) Front and back by Rho and Rac. *Nat Cell Biol* 8:781–782. doi: 10.1038/ncb0806-781
117. Wildenberg GA, Dohn MR, Carnahan RH, et al. (2006) p120-catenin and p190RhoGAP regulate cell-cell adhesion by coordinating antagonism between Rac and Rho. *Cell* 127:1027–1039. doi: 10.1016/j.cell.2006.09.046
118. Wang L, Ellis MJ, Gomez JA, et al. (2012) Mechanisms of the proteinuria induced by Rho GTPases. *Kidney Int* 81:1075–1085. doi: 10.1038/ki.2011.472
119. Pertz O, Hodgson L, Klemke RL, Hahn KM (2006) Spatiotemporal dynamics of RhoA activity in migrating cells. *Nature* 440:1069–1072. doi: 10.1038/nature04665
120. Kraynov VS, Chamberlain C, Bokoch GM, et al. (2000) Localized Rac activation dynamics visualized in living cells. *Science* (80-) 290:333–337.
121. Asanuma K, Kim K, Oh J, et al. (2005) Synaptopodin regulates the actin-bundling activity of alpha-actinin in an isoform-specific manner. *J Clin Invest* 115:1188–1198. doi: 10.1172/JCI23371
122. Akilesh S, Suleiman H, Yu H, et al. (2011) Arhgap24 inactivates Rac1 in mouse podocytes, and a mutant form is associated with familial focal segmental glomerulosclerosis. *J Clin Invest* 121:4127–37. doi: 10.1172/JCI46458
123. Gupta IR, Baldwin C, Auguste D, et al. (2013) ARHGDI1: a novel gene implicated in nephrotic syndrome. *J Med Genet* 50:330–338. doi: 10.1136/jmedgenet-2012-101442
124. Doetschman T, Gregg RG, Maeda N, et al. (1987) Targetted correction of a mutant HPRT gene in mouse embryonic stem cells. *Nature* 330:576–578. doi: 10.1038/330576a0
125. Hooper M, Hardy K, Handyside A, et al. (1987) HPRT-deficient (Lesch-Nyhan) mouse embryos derived from germline colonization by cultured cells. *Nature* 326:292–295. doi: 10.1038/326292a0
126. Lin X, Suh JH, Go G, Miner JH (2014) Feasibility of repairing glomerular basement membrane defects in Alport syndrome. *J Am Soc Nephrol* 25:687–92. doi: 10.1681/ASN.2013070798
127. Bates M, Huang B, Dempsey GT, Zhuang X (2007) Multicolor super-resolution imaging with photo-switchable fluorescent probes. *Science* (80-) 317:1749–1753. doi: 10.1126/science.1146598
128. Suleiman H, Zhang L, Roth R, et al. (2013) Nanoscale protein architecture of the kidney glomerular basement membrane. *Elife*. doi: 10.7554/eLife.01149
129. Beard C, Hochedlinger K, Plath K, et al. (2006) Efficient method to generate single-copy transgenic mice by site-specific integration in embryonic stem cells. *Genesis* 44:23–28. doi: 10.1002/gene.20180
130. Shigehara T, Zaragoza C, Kitiyakara C, et al. (2003) Inducible podocyte-specific gene expression in transgenic mice. *J Am Soc Nephrol* 14:1998–2003.
131. Whitelaw E, Sutherland H, Kearns M, et al. (2001) Epigenetic effects on transgene expression. *Methods Mol Biol* 158:351–368. doi: 10.1385/1-59259-220-1:351
132. Appel D, Kershaw DB, Smeets B, et al. (2009) Recruitment of podocytes from glomerular parietal epithelial cells. *J Am Soc Nephrol* 20:333–343. doi: 10.1681/ASN.2008070795

133. Kim YH, Goyal M, Kurnit D, et al. (2001) Podocyte depletion and glomerulosclerosis have a direct relationship in the PAN-treated rat. *Kidney Int* 60:957–968. doi: 10.1046/j.1523-1755.2001.060003957.x
134. Wickman L, Afshinnia F, Wang SQ, et al. (2013) Urine podocyte mRNAs, proteinuria, and progression in human glomerular diseases. *J Am Soc Nephrol* 24:2081–95. doi: 10.1681/ASN.2013020173
135. Pollak MR (2002) Inherited podocytopathies: FSGS and nephrotic syndrome from a genetic viewpoint. *J Am Soc Nephrol* 13:3016–3023. doi: 10.1097/01.ASN.0000039569.34360.5E
136. Barua M, Brown EJ, Charoonratana VT, et al. (2013) Mutations in the INF2 gene account for a significant proportion of familial but not sporadic focal and segmental glomerulosclerosis. *Kidney Int* 83:316–22. doi: 10.1038/ki.2012.349
137. Laurin L-P, Lu M, Mottl AK, et al. (2014) Podocyte-associated gene mutation screening in a heterogeneous cohort of patients with sporadic focal segmental glomerulosclerosis. *Nephrol Dial Transplant* gft532–. doi: 10.1093/ndt/gft532
138. Friedman DJ, Kozlitina J, Genovese G, et al. (2011) Population-based risk assessment of APOL1 on renal disease. *J Am Soc Nephrol* 22:2098–105. doi: 10.1681/ASN.2011050519
139. Thomson R, Genovese G, Canon C, et al. (2014) Evolution of the primate trypanolytic factor APOL1. *Proc Natl Acad Sci U S A* 111:E2130–9. doi: 10.1073/pnas.1400699111
140. Deller T, Korte M, Chabanis S, et al. (2003) Synaptopodin-deficient mice lack a spine apparatus and show deficits in synaptic plasticity. *Proc Natl Acad Sci U S A* 100:10494–10499. doi: 10.1073/pnas.1832384100
141. Nechiporuk T, Fernandez TE, Vasioukhin V (2007) Failure of Epithelial Tube Maintenance Causes Hydrocephalus and Renal Cysts in Dlg5^{-/-} Mice. *Dev Cell* 13:338–350. doi: 10.1016/j.devcel.2007.07.017
142. Yu H, Suleiman H, Kim AHJ, et al. (2013) Rac1 activation in podocytes induces rapid foot process effacement and proteinuria. *Mol Cell Biol* 33:4755–64. doi: 10.1128/MCB.00730-13
143. Poueymirou WT, Auerbach W, Friendewey D, et al. (2006) F0 generation mice fully derived from gene-targeted embryonic stem cells allowing immediate phenotypic analyses. *Nat Biotechnol* 25:91–99. doi: 10.1038/nbt1263
144. Stegmeier F, Hu G, Rickles RJ, et al. (2005) A lentiviral microRNA-based system for single-copy polymerase II-regulated RNA interference in mammalian cells. *Proc Natl Acad Sci U S A* 102:13212–7. doi: 10.1073/pnas.0506306102
145. Reiser J, Polu KR, Moller CC, et al. (2005) TRPC6 is a glomerular slit diaphragm-associated channel required for normal renal function. *Nat Genet* 37:739–744. doi: 10.1038/ng1592
146. Kim JM, Wu H, Green G, et al. (2003) CD2-associated protein haploinsufficiency is linked to glomerular disease susceptibility. *Science* (80-) 300:1298–1300. doi: 10.1126/science.1081068 300/5623/1298 [pii]
147. Lindenmeyer MT, Eichinger F, Sen K, et al. (2010) Systematic analysis of a novel human renal glomerulus-enriched gene expression dataset. *PLoS One* 5:e11545. doi: 10.1371/journal.pone.0011545

148. Boerries M, Grahammer F, Eiselein S, et al. (2013) Molecular fingerprinting of the podocyte reveals novel gene and protein regulatory networks. *Kidney Int* 83:1052–64. doi: 10.1038/ki.2012.487
149. Brunskill EW, Georgas K, Rumballe B, et al. (2011) Defining the molecular character of the developing and adult kidney podocyte. *PLoS One* 6:e24640. doi: 10.1371/journal.pone.0024640
150. Kopp JB, Nelson GW, Sampath K, et al. (2011) APOL1 genetic variants in focal segmental glomerulosclerosis and HIV-associated nephropathy. *J Am Soc Nephrol* 22:2129–37. doi: 10.1681/ASN.2011040388
151. Li H, Durbin R (2009) Fast and accurate short read alignment with Burrows-Wheeler transform. *Bioinformatics* 25:1754–1760. doi: 10.1093/bioinformatics/btp324
152. Van der Auwera GA, Carneiro MO, Hartl C, et al. (2013) From fastQ data to high-confidence variant calls: The genome analysis toolkit best practices pipeline. *Curr Protoc Bioinforma*. doi: 10.1002/0471250953.bi11110s43
153. Li B, Leal SM (2009) Discovery of rare variants via sequencing: implications for the design of complex trait association studies. *PLoS Genet* 5:e1000481. doi: 10.1371/journal.pgen.1000481
154. Price AL, Kryukov G V, de Bakker PIW, et al. (2010) Pooled association tests for rare variants in exon-resequencing studies. *Am J Hum Genet* 86:832–8. doi: 10.1016/j.ajhg.2010.04.005
155. Neale BM, Rivas MA, Voight BF, et al. (2011) Testing for an unusual distribution of rare variants. *PLoS Genet* 7:e1001322. doi: 10.1371/journal.pgen.1001322
156. Voskarides K, Damianou L, Neocleous V, et al. (2007) COL4A3/COL4A4 mutations producing focal segmental glomerulosclerosis and renal failure in thin basement membrane nephropathy. *J Am Soc Nephrol* 18:3004–3016. doi: 10.1681/ASN.2007040444
157. Agrawal S, Prakash S, Sharma RK (2014) Genetic aspects of familial focal segmental glomerulosclerosis. *Clin Queries Nephrol*. doi: 10.1016/j.cqn.2014.06.001
158. Rood IM, Deegens JKJ, Wetzels JFM (2012) Genetic causes of focal segmental glomerulosclerosis: implications for clinical practise. *Nephrol Dial Transplant*. doi: 10.1093/ndt/gfr771
159. Sadowski CE, Lovric S, Ashraf S, et al. (2014) A Single-Gene Cause in 29.5% of Cases of Steroid-Resistant Nephrotic Syndrome. *J Am Soc Nephrol ASN.2014050489–*. doi: 10.1681/ASN.2014050489
160. Zhou X, Vink M, Klaver B, et al. (2006) Optimization of the Tet-On system for regulated gene expression through viral evolution. *Gene Ther* 13:1382–90. doi: 10.1038/sj.gt.3302780
161. Stegmeier F, Hu G, Rickles RJ, et al. (2005) A lentiviral microRNA-based system for single-copy polymerase II-regulated RNA interference in mammalian cells. *Proc Natl Acad Sci U S A* 102:13212–13217. doi: 0506306102 [pii] 10.1073/pnas.0506306102
162. Stappenbeck TS, Gordon JI (2000) Rac1 mutations produce aberrant epithelial differentiation in the developing and adult mouse small intestine. *Development* 127:2629–2642.

163. Kakinuma N, Roy BC, Zhu Y, et al. (2008) Kank regulates RhoA-dependent formation of actin stress fibers and cell migration via 14-3-3 in PI3K-Akt signaling. *J Cell Biol* 181:537–49. doi: 10.1083/jcb.200707022
164. Zhu Y, Kakinuma N, Wang Y, Kiyama R (2008) Kank proteins: A new family of ankyrin-repeat domain-containing proteins. *Biochim Biophys Acta - Gen Subj* 1780:128–133. doi: 10.1016/j.bbagen.2007.09.017
165. Ngok SP, Geyer R, Kourtidis A, et al. (2013) TEM4 is a junctional Rho GEF required for cell-cell adhesion, monolayer integrity and barrier function. *J Cell Sci* 126:3271–7. doi: 10.1242/jcs.123869

Curriculum Vitae

Haiyang Yu

Address: Department of Pathology and Immunology, Campus Box 8118, Washington University,
660 South Euclid Avenue, Saint Louis, Missouri 63110, USA

Phone: (314) 397-6653

E-mail: hyu@go.wustl.edu

EDUCATION

- Ph.D. Molecular Cell Biology, Washington University in St. Louis, St. Louis, MO, USA (May. 2015)
- B.S. *Summa cum laude* - Biological Sciences, Nankai University, Tianjin, P.R. China (Jun. 2008)

RESEARCH EXPERIENCE

Jul. 2009 ~ 2015, thesis research supervised by Dr. Andrey Shaw.

- Validate rare genetic variants that associate with focal segmental glomerulosclerosis by an *in vivo* RNAi mouse model (Thesis project).
 - Explore how the balance between Rac and Rho activity influences the structure and function of podocytes.
 - Investigate the function of ARHGAP24 in podocytes.
 - Study the mechanism of allosteric activation of Raf kinases.
- Oct. 2006 ~ Jun. 2008, undergraduate research internship supervised by Dr. Jun Zhou
- Explore the mechanism of mitotic arrest induced by Eg5 inhibitors.
 - Use RT-PCR to measure the expression level of Eg5 in different pancreatic cancer cell lines

HONORS AND AWARDS

- Lucille P. Markey Special Emphasis Pathway in Human Pathobiology (internal training grant for graduate students), Washington University in St. Louis, 2011;
- Travel Support, ASN Annual Conference, Philadelphia, 2011;
- Transcontinental Young Travel Fund Award, FEBS Workshop, Oslo, Norway, 2010;
- Outstanding Graduate Award (*summa cum laude*), Nankai University, 2008;

- The Second-Class Fellowship, Nankai University, 2007;
- Novozymes-Teda Biotechnology Scholarship, Nankai University, 2007;
- Tri-A Outstanding Student of The City Award, Tianjin, 2006;
- Tri-A Outstanding Student Awards, Nankai University, twice in 2005 and in 2008;
- The First-Class Fellowships, Nankai University, twice in 2005 and in 2006.
-

PODIUM PRESENTATIONS

- **Yu H.**, and Shaw A.S., Validation of Rare Genetic Variants Associated with Focal Segmental Glomerulosclerosis by Using An ES Cell-Based RNAi mouse Model. American Society of Nephrology Kidney Week 2013 Annual Meeting, Atlanta, USA, 2013 Nov 9.
- **Yu H**, Suleiman H., Kim A.H.J., Miner J.H., Akilesh S., and Shaw A.S., Rac1 Activation in Podocytes Induces Rapid Foot Process Effacement and Proteinuria. American Society of Nephrology Kidney Week 2013 Annual Conference, Atlanta, USA, 2013 Nov 9.
- **Yu H.**, Sampson M. G., Kretzler M., Miner M. J., Kopp J. B. Shaw A. S. Identification and Validation of New Risk genes in European-American Population by Exome-sequencing and RNAi-Based Mouse Model for Focal Segmental Glomerulosclerosis. American Society of Nephrology Kidney Week 2014 Annual Meeting, Philadelphia, USA, 2014 Nov 11.

PUBLICATIONS

- **Yu H.***, Artomov M.*, Stander M. C., Shamsan G., Sampson M. G., White M.J., Kretzler M., Miner M. J., Winkler C. A., Mitra R. D., Kopp J. B., Daly M. J.#, Shaw A. S. Sequence and validation of susceptibility genes for human Focal Segmental Glomerulosclerosis. Submitted (* Co-first authorship)
- **Yu H.**, Suleiman H., Kim A.H.J., Miner J.H., Dani A., Shaw A.S. and Akilesh S., Rac1 activation in podocyte induces rapid foot process effacement and proteinuria. *Mol Cell Biol.* 2013; 33(23): 4755-64.
- Hu J., Stites E.C., **Yu H.**, Germino E.A., Shibatsu H.S., Stork P.J.S., Kornev A.P., Taylor S.S., and Shaw A.S., Allosteric activation of Functionally Asymmetric RAF kinases. *Cell* 2013; 154(5): 1036-46.
- Sun X.D., Shi X.J., Sun X.O., Luo Y., Wu J, Yao C., **Yu H.**, Li D., Liu M. and Zhou J., Dimethylenastron suppresses human pancreatic cancer cell migration and invasion in vitro via allosteric inhibition of mitotic kinesin Eg5. *Acta Pharmacol Sin.* 2011; 32(12): 1543-8.
- Akilesh S.*, Suleiman H.*, **Yu H.***, Stander M.C., Lavin P., Gbadegesin R., Antignac C., Pollak M.R., Kopp J.B., Winn M.P., Shaw A.S., Arhgap24 (FilGAP) inhibits Rac1 activity in mouse podocytes and is associated with familial focal segmental glomerulosclerosis. *J Clin Invest.* 2011; 121(10): 4127-37. (* Co-first authorship)
- Hu J., **Yu H.**, Kornev A.P., Zhao J., Filbert E.L., Taylor S.S. and Shaw A.S., A mutation that

blocks ATP binding creates a pseudokinase that stabilizes the scaffolding function of KSR1, CRAF and BRAF. Proc Natl Acad Sci U S A. 108(15): 6067-72.

- Liu M., **Yu H.**, Huo L., Liu J., Li M., and Zhou J., Validating the mitotic kinesin Eg5 as a therapeutic target in pancreatic cancer cells. Biochem Pharmacol. 2008 Jul 15; 76(2): 169-78.
- Sun L., Li D., Dong X, **Yu H.**, Dong J.T., Zhang C., Lu X., and Zhou J., Small-molecule inhibition of Aurora kinases triggers apoptosis in cancer cells independently of the spindle checkpoint. Biochem Pharmacol. 2008 Mar 1; 75(5): 1027-34.

PATENT

- Shaw A.S., Hu J., and **Yu H.**, Methods and uses of KSR kinase, and mutations thereof. Patent No. 8900845; issue date 12-02-2014.